REPUBLIC OF TURKEY
YILDIZ TECHNICAL UNIVERSITY
GRADUATE SCHOOL OF SCIENCE AND ENGINEERING

RECYCLING OF ZnS FROM WASTES AND ITS UTILIZATION AS AN ELECTRODE MATERIAL IN SUPERCAPACITORS

Ozan AYDIN

MASTER OF SCIENCE THESIS

Department of Metallurgical and Materials Engineering
Materials Program

Supervisor
Assist. Prof. Dr. Burak BİROL

Co-Supervisor
Assoc. Prof. Dr. Metin GENÇTEN

December, 2022

REPUBLIC OF TURKEY

YILDIZ TECHNICAL UNIVERSITY

GRADUATE SCHOOL OF SCIENCE AND ENGINEERING

ATIKLARDAN ZnS'ÜN GERİ DÖNÜŞÜMÜ VE SÜPERKAPASİTÖRLERDE ELEKTROT MALZEMESİ OLARAK KULLANIMININ ARAŞTIRILMASI

A thesis submitted by Ozan AYDİN in partial fulfillment of the requirements for the degree of MASTER OF SCIENCE is approved by the committee on 29.12.2022 in Department of Metallurgical and Materials Engineering, Materials Program.

Assist. Prof. Dr. Burak BİROL	Assoc Prof. Dr. Metin GENÇTEN
Yıldız Technical University	Yıldız Technical University
Supervisor	Co- supervisor

Approved By the Examining Committee

Assist. Prof. Dr. Burak BİROL, Supervisor
Yildiz Technical University _____

Assist. Prof. Dr. Rıdvan GECÜ, Member
Yildiz Technical University _____

Assoc. Prof. Dr. Mustafa BOYRAZLI, Member
Fırat University _____

I hereby declare that I have obtained the required legal permissions during data collection and exploitation procedures, that I have made the in-text citations and cited the references properly, that I haven't falsified and/or fabricated research data and results of the study and that I have abided by the principles of the scientific research and ethics during my Thesis Study under the title of Recycling of ZnS from Wastes and its Utilization as an Electrode Materials in Supercapacitors supervised by my supervisors, Assist. Prof. Dr. Burak BİROL and Assoc. Prof. Dr. Metin GENÇTEN. In the case of a discovery of false statement, I am to acknowledge any legal consequence.

Ozan AYDİN
Signature

This study was supported by the YTÜ Scientific Research Projects, Project ID: FBA-2022-5008.

To my family.

ACKNOWLEDGEMENTS

First and foremost, I would like to thank to my dear supervisors Assist. Prof. Dr. Burak BİROL and Assoc. Prof. Dr. Metin GENÇTEN for their continuous guidance, support and encouragement.

I would like to thank to my laboratory partners, colleagues and friends Res. Assist. Sezgin YAŞA, Res. Assist. Ayşegül BİLEN and Utku HATİPOĞLU for their assistance and support throughout my studies.

I also would like to thank to Res. Assist. Oğuler SAZCI and Kamil KUTLU for all their support, motivation and friendship.

Finally, I would express my deepest gratitude to my beloved parents, grandparents and sister, for shaping me into the individual I am today, for their boundless love and unconditional support.

Ozan AYDİN

TABLE OF CONTENTS

LIST OF SYMBOLS viii

LIST OF ABBREVIATIONS ix

LIST OF FIGURES x

LIST OF TABLES xii

ABSTRACT xiii

ÖZET xv

1 INTRODUCTION 1

1.1 Literature Review 1

1.2 Objective of the Thesis 4

1.3 Hypothesis 4

2 SUPERCAPACITORS 5

2.1 Classification of the Supercapacitors 7

2.2 Components of the Supercapacitors 10

3 WASTES OBTAINED FROM STEEL INDUSTRY 14

3.1 Steelmaking Dusts 14

3.2 Recovery of Zinc from Metallurgical Dusts 24

3.3 Comparison of Zinc Recovery Processes 27

4 MATERIALS AND METHODS 28

4.1 Chemicals and Raw Materials 28

4.2 Equipment 28

4.3 Characterization of Raw Materials and Products 29

4.4 Experimental Procedure 30

5 RESULTS AND DISCUSSIONS 36

5.1 Preparation of Raw Materials 36

5.2 Leaching 39

5.3 Precipitation of ZnS 53

5.4 Production of Supercapacitors 62

6 CONCLUSIONS 74

REFERENCES 76

APPENDICES 82

PUBLICATIONS FROM THE THESIS 87

LIST OF SYMBOLS

R_{ct}	Charge Transfer Resistance
C_{dl}	Double-Layer Capacitance
R_s	Solution Resistance
°	Degree

LIST OF ABBREVIATIONS

AAS	Atomic Absorption Spectroscopy
BF	Blast Furnace
BFD	Blast Furnace Dust
BFS	Blast Furnace Sludge
BOF	Basic Oxygen Furnace
BOFD	Basic Oxygen Furnace Dust
CV	Cyclic Voltammetry
CZO	Crude Zinc Oxide
EAF	Electric Arc Furnace
EAFD	Electric Arc Furnace Dust
EDLC	Electrochemical Double-Layer Capacitor
EIS	Electrochemical Impedance Spectroscopy
FC	Ferrochrome
FE-SEM	Field Emission-Scanning Electron Microscopy
FFD	Ferrochrome Flue Dust
GCD	Galvanostatic Charge-Discharge
L-S	Liquid-Solid
LE	Leaching Efficiency
NMP	N-methyl Pyrrolidone
PE	Precipitation Efficiency
PVDF	Polyvinylidene Fluoride
SEM	Scanning Electron Microscopy
XPS	X-Ray Photoelectron Spectroscopy
XRD	X-Ray Diffraction
XRF	X-Ray Fluorescence
EDS	Energy Dispersive Spectroscopy
W	Warburg Impedance
F	Farad
V	Volt
Hz	Hertz

LIST OF FIGURES

Figure 2.1 Comparison of energy storage systems[17]. 6

Figure 2.2 Classification of supercapacitors [19]. 7

Figure 2.3 Traditional capacitor [21].....8

Figure 2.4 Electrical double-layer capacitor [22]. 8

Figure 2.5 Pseudocapacitor [23].....9

Figure 3.1 Steel production processes [30].....15

Figure 3.2 Ferrochrome production process.....22

Figure 3.3 Recovery of steel industry by-products by hydrometallurgical processes [33]. 25

Figure 4.1 Flow chart of the experimental procedure. 30

Figure 4.2 FFD solution, a) before washing, b) after washing.....31

Figure 4.3 Ferrochrome flue dust leaching experiment.....32

Figure 4.4 a) Precipitation experiment setup, b) after precipitation process, c) after liquid-solid separation. 33

Figure 4.5 Flow chart of the supercapacitor production process. 33

Figure 4.6 Film applicator device.....34

Figure 4.7 The image of, a) produced film, b) produced electrodes, c) produced supercapacitor. 35

Figure 4.8 Gamry Interface 1010 Potentiostat-Galvanostat device.....35

Figure 5.1 XRD pattern of FFD. 36

Figure 5.2 XRD pattern of EAFD. 37

Figure 5.3 SEM image of FFD. 38

Figure 5.4 FE-SEM image of EAFD.....38

Figure 5.5 Effect of L-S ratio a) for Zn in H_2SO_4, b) for Zn in HNO_3, c) for Fe in H_2SO_4, d) for Fe in HNO_3, e) for Cr in H_2SO_4, f) for Cr in HNO_3.....40

Figure 5.6 Effect of acid concentration at 20:1 L-S ratio a) for Zn in H_2SO_4, b) for Zn in HNO_3, c) for Fe in H_2SO_4, d) for Fe in HNO_3, e) for Cr in H_2SO_4, f) for Cr in HNO_3. 44

Figure 5.7 Effect of acid concentration at 10:1 L-S ratio a) for Zn in H_2SO_4, b) for Zn in HNO_3, c) for Fe in H_2SO_4, d) for Fe in HNO_3, e) for Cr in H_2SO_4, f) for Cr in HNO_3. 46

Figure 5.8 Effect of leaching duration a) for Zn in H_2SO_4, b) for Zn in HNO_3, ...49

Figure 5.9 EAF leaching results.....52

Figure 5.10 XRD pattern of the sulfuric acid precipitation sample. 54

Figure 5.11 Effect of Zn concentration on precipitation. 55
Figure 5.12 Effect of Na_2S concentration on precipitation. 57
Figure 5.13 XRD pattern of FC-ZnS sample. 58
Figure 5.14 XRD pattern of EAF-ZnS sample. 58
Figure 5.15 XPS spectra of a) FC-Zn2p, b) FC-S2p, c) EAF-Zn2p, d) EAF-S2p. ..59
Figure 5.16 SEM images a) FC-ZnS, b) EAF-ZnS..... 60
Figure 5.17 SEM-EDS mapping results of a) FC-ZnS, b) EAF-ZnS. 60
Figure 5.18 SEM-EDS spectra of a) FC-ZnS, b) EAF-ZnS..... 61
Figure 5.19 Particle size distributions of a) FC-ZnS, b) EAF-ZnS. 61
Figure 5.20 FE-SEM image of the FC2 sample. 62
Figure 5.21 EDS elemental mapping of FC2 sample. 63
Figure 5.22 FE-SEM image of the EAF2 sample. 63
Figure 5.23 EDS elemental mapping of EAF2 sample. 64
Figure 5.24 Determination of the potential range. 65
Figure 5.25 Cyclic voltammograms obtained at different scan rates a) FC2, b) FC3, and c) FC4. 66
Figure 5.26 Cyclic voltammograms obtained at different scan rates for EAF2. 67
Figure 5.27 Capacity retention ratios of a) FC2, b) FC3, and c) FC4. 68
Figure 5.28 Capacity retention ratio of EAF2. 69
Figure 5.29 GCD curves of a) FC2, b) FC3, and c) FC4 and d) EAF2 at different current densities. 70
Figure 5.30 Nyquist plots of a) FC2, b) FC3, c) FC4. 71
Figure 5.31 Equivalent circuit [85]. 72

LIST OF TABLES

Table 3.1 Chemical compositions of steelmaking dusts [30]. 14

Table 3.2 High carbon ferrochrome producing countries and their production quantities (tons/year) [52]. 23

Table 3.3 Pyrometallurgical recovery processes [46]. 24

Table 3.4 Comparison of leaching agents [46]. 26

Table 4.1 Chemicals and raw materials used in the present study. 28

Table 4.2 Equipment utilized in the present study. 29

Table 4.3 Characterization instrument used in the present study. 29

Table 4.4 Anode and cathode compositions. 34

Table 5.1 Chemical compositions of FFD and EAFD. 37

Table 5.2 Leaching parameters of the optimum solutions. 52

Table 5.3 FFD precipitation experiment results. 54

Table 5.3 FFD precipitation experiment results (continued) 55

Table 5.4 Specific capacitance values of the supercapacitors. 67

Table 5.5 EIS fitting results 72

ABSTRACT

Recycling of ZnS from Wastes and its Utilization as an Electrode Material in Supercapacitors

Ozan AYDIN

Department of Metallurgical and Materials Engineering
Master of Science Thesis

Supervisor: Assist. Prof. Dr. Burak BİROL
Co- supervisor: Assoc. Prof. Dr. Metin GENÇTEN

Ferrochrome and electric arc furnace flue dusts, that are among the wastes generated in the metallurgy industry, contain valuable metal oxides as well as compounds that are harmful to the environment and human health, making recycling of these wastes essential from both an economic and environmental perspective. Additionally, it is known that the utilization of metal sulfides as electrode materials in the new generation energy storage systems has been intensively investigated in recent years. The aim of the study is to develop an efficient hydrometallurgical process to generate ZnS with high purity from flue dusts and to use the generated ZnS as an electrode material in asymmetric type coin cell supercapacitors. In the scope of the study, leaching experiments were conducted at varying liquid-solid ratios, acid concentrations and durations with sulfuric acid and nitric acid solutions. Four optimum parameters were determined to recover Zn from these solutions selectively. By addition of sodium sulfide to optimum solutions, it was ensured that, Zn ions in the solutions were precipitated as ZnS. After determination of the optimal parameters for precipitation, it was revealed that ZnS can be recovered from the leach solutions with an efficiency of about 99%. The electrochemical behavior of the asymmetric

type coin cell supercapacitors produced with the obtained ZnS from ferrochrome flue dust and electric arc furnace dust wastes were investigated in a two-electrode system at a scanning rate of 10 mVs^{-1}, and the specific capacitance of 1723.57 Fg^{-1} and 1293.94 Fg^{-1} was achieved, respectively. Additionally, it has been determined that the supercapacitors retain 92.82% and 79.33% of their capacity in the end of 1000 cycles, respectively. Obtained results demonstrate that, ZnS may be recovered from flue dusts effectively and the utilization of the recovered ZnS to be used as electrode materials in supercapacitor applications is promising.
Keywords: Recycling, hydrometallurgy, flue dust, energy storage, supercapacitor.

ÖZET

Atıklardan ZnS'ün Geri Dönüşümü ve Süperkapasitörlerde Elektrot Malzemesi Olarak Kullanımının Araştırılması

Ozan AYDIN

Metalurji ve Malzeme Mühendisliği Anabilim Dalı
Yüksek Lisans Tezi

Danışman: Dr. Öğr. Üyesi Burak BİROL
Eş-Danışman: Doç. Dr. Metin GENÇTEN

Metalurji sektöründe oluşan atıklardan ferrokrom ve elektrik ark fırını baca tozlarının içeriğinde değerli metal oksitlerin yanı sıra çevre ve insan sağlığına zararlı bileşenlerin de bulunması, bu atıkların geri dönüştürülmesini hem çevresel hem de ekonomik açıdan zorunlu kılmaktadır. Ayrıca, metal sülfürlerin yeni nesil enerji depolama sistemlerinden süperkapasitör uygulamalarında elektrot malzemesi olarak kullanımının son yıllarda yoğun şekilde araştırıldığı bilinmektedir. Bu çalışmada baca tozlarının uygun bir hidrometalurjik proses ile geri dönüştürülerek ZnS formunda yüksek verim ve saflıkta geri kazanılması ve kazanılan bu bileşiğin asimetrik düğme pil tipi süperkapasitörlerde elektrot malzemesi olarak kullanılması amaçlanmıştır. Çalışma kapsamında ham maddelere sülfürik asit ve nitrik asit çözeltileri ile farklı sıvı-katı oranları, asit konsantrasyonları ve sürelerde liç işlemleri uygulanmış ve Zn'nin bu çözeltilerden seçilimli olarak geri kazanılabilmesi için dört farklı optimum liç parametresi belirlenmiştir. Belirlenen parametrelerde hazırlanan çözeltilere sodyum sülfür ilavesi ile çözeltideki Zn iyonlarının ZnS formunda çöktürülmesi sağlanmıştır. Çöktürme için optimum parametrelerin tespit edilmesiyle ZnS'in liç çözeltilerinden yaklaşık %99 verimle geri kazanılabileceği belirlenmiştir. Ferrokrom baca tozu ve elektrik ark fırını tozu atıklarından elde edilen ZnS ile üretilen asimetrik düğme pil tipi süperkapasitörlerin elektrokimyasal davranışları

iki elektrotlu sistemde incelenmiş, 10 mVs^{-1} tarama hızında sırasıyla 1723,57 Fg^{-1} ve 1293,94 spesifik kapasitans değerleri elde edilmiştir. Ayrıca süperkapasitörlerin kapasitesilerini 1000 döngü sonunda sırasıyla %92,82 ve %79,33 oranında koruduğu belirlenmiştir. Elde edilen sonuçlar, ZnS'ün baca tozu atıklarından etkin ve verimli bir şekilde geri kazanılabileceğini ve süperkapasitör uygulamalarında elektrot malzemesi olarak kullanılma potansiyelinin yüksek olduğunu göstermektedir.

Anahtar Kelimeler: Geri dönüşüm, hidrometalurji, baca tozu, enerji depolama, süperkapasitör.

1 INTRODUCTION

1.1 Literature Review

Due to the rapid increase in the world population, the expanding global economy, the depletion of carbon-based fossil fuels and the environmental damage these fuels cause, the importance of alternative energy sources is growing by the day, and there has been substantial development in renewable energy technologies. As a result of these advances, there is an increased demand to store the high energy that can be acquired from renewable energy sources. Electrochemical energy storage devices, such as rechargeable batteries and supercapacitors, have been developed in response to this demand. The main goal of the energy storage studies is to store energy conveniently and rapidly with high capacity and to utilise the stored energy for an extended period of time. Supercapacitors, which were developed for all of these purposes, stand out as a new technology with significant advantages such as high power densities, long cycle numbers, very fast charge/discharge times, low weight, and no negative environmental effects, and are particularly used in portable electronic devices where fast and intense power transfer is required.

The physical and electrochemical properties of the electrode materials utilized are the most critical factors determining the performance of the supercapacitors. The use of metal sulphides as electrode material in pseudocapacitors has attracted intense interest of researchers in recent years due to their high abundance in nature, low cost, high theoretical capacitance and unique electrochemical properties [1].

ZnS is one of the most important II-VI semiconductor materials, having a band gap of 3.5-3.8 eV. ZnS is a prospective material in the field of energy storage due to its high ion availability and charge storage capabilities, high electrical conductivity, low diffusion resistance, rapid electron transfer, and environmental friendliness [2].

Rose et al. (2020) used ZnS microspheres and Ni-doped ZnS microspheres as supercapacitor electrode material. The specific capacitance of the ZnS supercapacitor at a scanning rate of 5 mVs^{-1} was determined as 216.2 Fg^{-1} and the specific capacitance of the Ni-doped supercapacitor was determined as 261.5 Fg^{-1} respectively [2].

Wei et al. (2018) used ZnS/C_3N_4 composite as supercapacitor electrode material. They achieved a specific capacitance of 497 Fg^{-1} at a current density of 1 Ag^{-1} and 80.4% capacity in 1000 cycles at 5 Ag^{-1} current density [3].

Hou et al. (2017) used ultrathin ZnS nanosheet/carbon nanotube composite as supercapacitor electrode material. They obtained a specific capacitance value of 159.6 Fg^{-1} at a current density of 1 Ag^{-1} [4].

Sarma et al. (2015) produced a ZnS electrode deposited on TiO_2 nanotube. The specific capacitance of the supercapacitor at a scanning rate of 20 mVs^{-1} was determined as 226 Fg^{-1} [5].

According to the literature, usage of ZnS as a supercapacitor electrode material has been widely studied in recent years, and high specific capacitance values were attained with these systems. However, when the studies in the literature are examined, it is encountered that ZnS used in these studies were obtained from commercially available sources.

Disposal of the flue dusts generated in metallurgy industry as landfills not only consumes vast amounts of land but also causes severe environmental damage. Furthermore, its fine-grained particulates are spread easily by wind and pose a threat to human health.

Many studies have been carried out in the literature on the recycling of zinc from flue dusts and significant values have been reached in terms of recycling efficiency in these studies.

Strobos et al. (2004) reported that the optimal sulfuric acid concentration to recover zinc from baghouse dusts generated in ferrochrome production is 336 g/L and the acid/dust ratio is 56. They determined that the ratio of dissolved Zn was 71.2%, that of dissolved Al was 1.8%, and that of dissolved Fe was 0.1%.

Furthermore, it was mentioned that temperature and time had a substantial impact on the Zn recovery [6].

Kukurugya et al. (2015) determined that the optimum sulfuric acid concentration for recovery was 1 M, the L:S ratio was 50 and the temperature was 80 °C, and the dissolved Zn ratio was 87% under these conditions. When L:S ratio was 10 and H_2SO_4 concentration was 1 M, they leached out approximately 50% of zinc without any significant iron dissolution [7].

Cruells et al. (1992) determined that the optimum sulfuric acid concentration for the recovery was 1 M, the liquid/solid ratio was 10 and the duration was 3 hours, and the dissolved Zn ratio was 80% under these conditions. It was also stated that the temperature did not have a significant effect on the Zn recovery [8].

Havlik et al. (2006) determined that the optimum sulfuric acid concentration for the recovery was 0.5 M, the temperature was 70-90°C, and the dissolved Zn ratio was 75% under these conditions. It was also stated that the decrease in the liquid/solid ratio adversely affected the Zn recovery [9].

Miki et al. (2016) found that the dissolved Zn ratio approaches 100% under conditions where the ammonium chloride concentration is 2 M, the temperature is 70°C, and the time is 2 hours. However, 20% of Ca is also dissolved under these conditions [10].

Oustadakis et al. (2010) determined that the optimum sulfuric acid concentration for the recovery is 1.5 M, the liquid/solid ratio is 10 and the temperature is 60°C, and the dissolved Zn ratio is 80% and the Fe ratio is 45% under these conditions [11].

Shawabkeh et al. (2010) determined that the optimum sulfuric acid concentration for the recovery was 0.1 M, the temperature was 50°C, the duration was 10-20 minutes, the stirring rate was 900 rpm, and the dissolved Zn ratio was 72% under these conditions [12].

Yatim et al. (2021) determined that, zinc may be recovered about 99.37% efficiency via sulphide precipitation [13].

Chen et al. (2018) determined that, precipitation efficiency of 99.89% of zinc was achieved at 735 mg/L sulfide concentration [14].

1.2 Objective of the Thesis

Objective of the study is to recycle the ferrochrome flue dust and electric arc furnace dust wastes generated in the metallurgy industry to obtain ZnS with low cost and high purity, and to use the obtained ZnS as an electrode material in asymmetric type hybrid supercapacitors.

1.3 Hypothesis

With the methods developed for the production of zinc from primary sources, zinc is mostly obtained in the form of ZnO and extra processes are required to obtain ZnS from these products. Furthermore, primary sources of zinc are known to be depleted. This makes it important to obtain value-added products with the zinc recovered from secondary sources. Numerous studies on the zinc recovery from zinc-containing wastes via pyrometallurgical and hydrometallurgical processes have been conducted in the literature and significant values have been attained in terms of recycling ratio. However, these methods are focused to recover zinc from these wastes in metallic or oxide form. Since it is known that leaching of zinc and its precipitation in sulfide form from acidic solutions is achievable, it is possible to obtain ZnS from ferrochrome flue dusts and electric arc furnace dusts through a hydrometallurgical process.

Due to its high ion availability, charge storage capability, high electrical conductivity, low diffusion resistance, rapid electron transfer, and environmental friendliness; ZnS is a promising material to be used as an electrode material in energy storage devices.

2
SUPERCAPACITORS

Due to limited fossil fuel resources, increasing fuel costs, pollution, geopolitical issues, global warming, a growing population, and technological advancement, humanity faces an energy crisis. Reducing these concerns is an increasingly crucial objective that might be attained by the development of alternative sources of energy and energy storage mechanisms. Consequently, there has lately been an increase in interest in energy storage systems with high power and energy densities [15].

Considering the particular energy density and specific power density of various energy storage systems makes it possible to compare their performances. Although fuel cells and batteries offer good energy densities, it is evident from the Figure 2.1 that, they are unsuitable for applications requiring a quick depletion. In contrast, ordinary capacitors with less energy density cannot supply a constant energy. However, supercapacitors can fill the gap between capacitors and batteries, making them appropriate for a variety of applications, including transportation, consumer electronics, military, power backups, medical field and among others. Supercapacitors have received considerable interest in applications where high specific power, exceptional cycling life, and rapid charging/discharging rates are particularly required, thanks to their superior electrochemical characteristics [16].

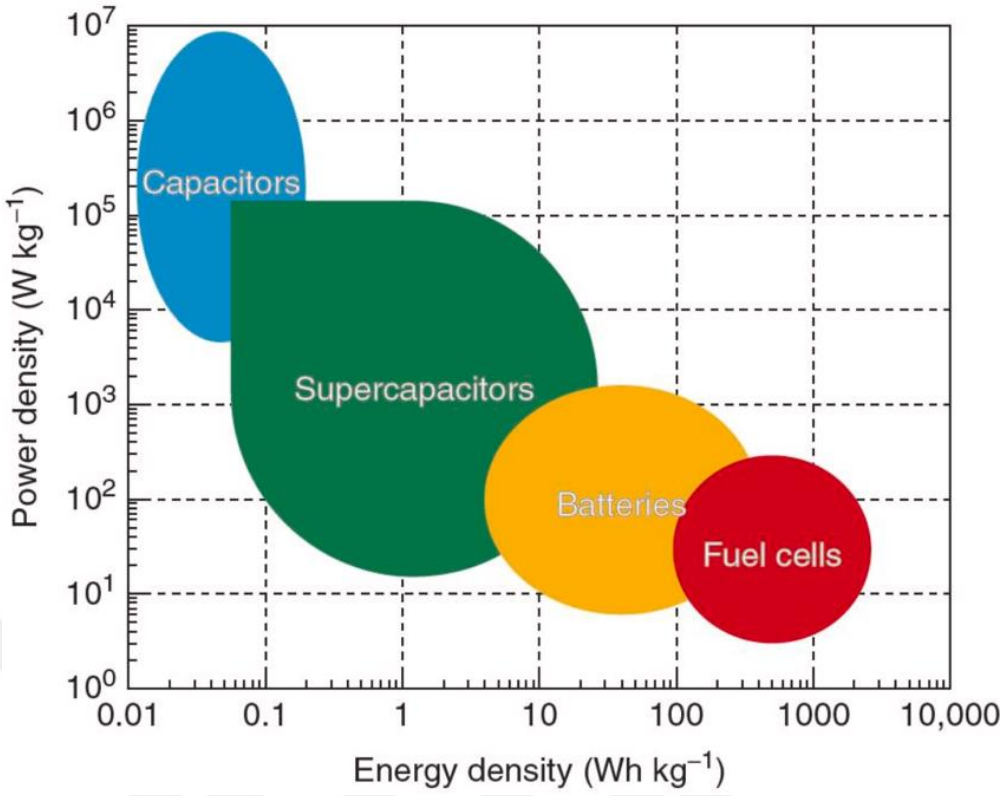


Figure 2.1 Comparison of energy storage systems[17].

The majority of the supercapacitors have capacities in the thousands of Farads and charge-discharge currents in the 10-100 of Amperes range. The key advantage of supercapacitors in terms of application is the extraordinary current that they can work with. Because of this property, supercapacitors bridge the gap between batteries and conventional capacitors [18].

Although supercapacitors produce 100-1000 of times more power per unit volume than batteries, they are not able to hold the same charge amounts. This makes supercapacitors appropriate for applications that demand power bursts but do not require a high energy storage capacity. In order to decoupling the characteristics of an energy storage system, supercapacitors can be added to battery-based energy storage systems, so enhancing the sizing of the energy storage system while meeting its power and energy requirements and possibly extending its lifetime. Currently, supercapacitors are largely utilized in hybrid electric vehicles, electrical equipment such as UPS and RAM in personal computers. Another application area is energy harvesting systems, such as wind turbines or solar panels where supercapacitors supplement traditional batteries [15], [18].

2.1 Classification of the Supercapacitors

Despite the fact that supercapacitors appear to act in the same way to conventional capacitors and batteries, there are substantial differences between their operating mechanisms. Based on the method of charge storage they employ, supercapacitors may be categorized as: electrical double-layer capacitors, pseudocapacitors, and hybrid capacitors, as demonstrated in Figure 2.2.

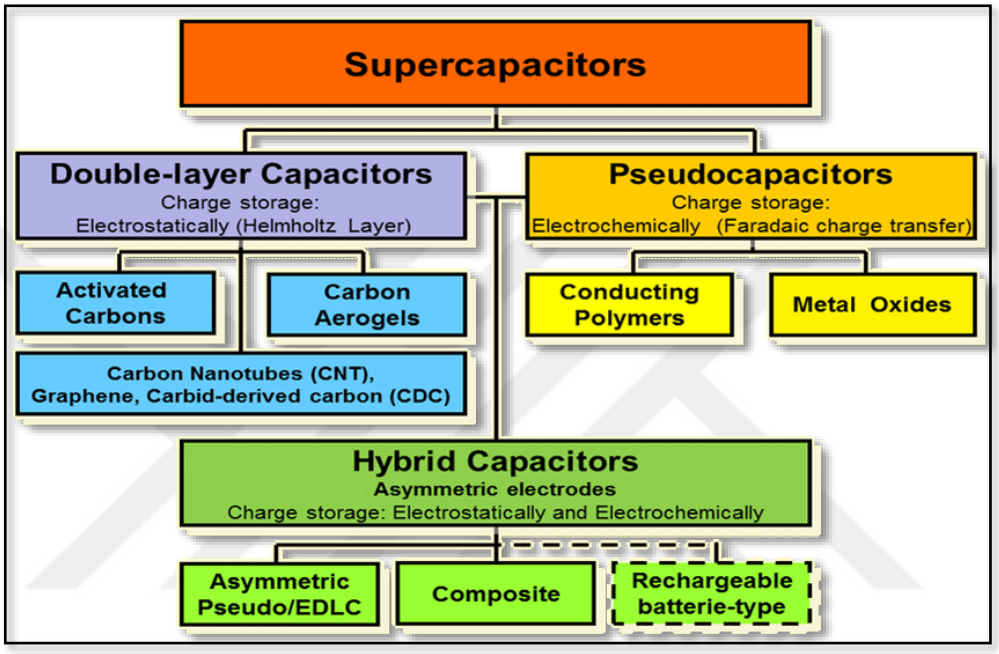


Figure 2.2 Classification of supercapacitors [19].

2.1.1 Electrical Double-Layer Capacitors (EDLC)

Ions are physically adsorbed from electrolyte to the electrode surface in EDLC as opposed to traditional capacitors, which are presented in Figure 2.3 and have two plates separated from each other by a dielectric substance in which the charges are deposited [20].

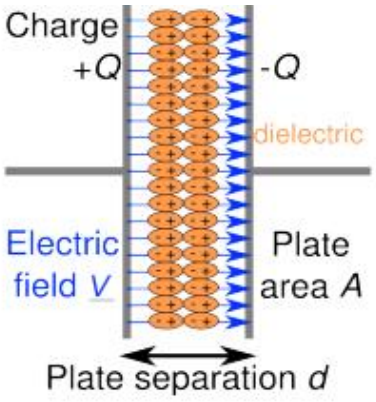


Figure 2.3 Traditional capacitor [21].

On the contrary, they go through a non-Faradaic process in which no charge transfer occurs; instead, Ionic or electrical charges persist at the surface of the electrode, which is presented in Figure 2.4.

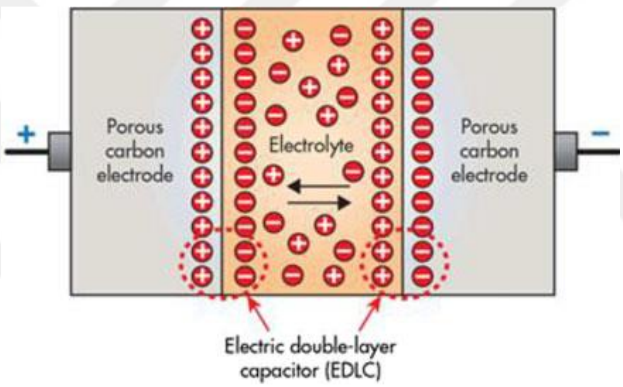


Figure 2.4 Electrical double-layer capacitor [22].

In this instance, electrolyte ions stick to the electrode by electrostatic attraction. During the charging process, when a potential is applied to the electrodes, a Helmholtz double-layer is produced on each electrode, whereas only a single layer is seen in traditional capacitors. Double-layer is composed of polarized ions on the surface of the electrode and dissolved ions from the electrolyte, which have been separated by a monolayer known as the Helmholtz plane. This monolayer may be thought of as a molecular dielectric or separator compared to the dielectric material in traditional capacitors. The wide surface area of the electrodes and the thickness of the Helmholtz layer are crucial in achieving an extraordinarily high capacity in EDLC [18], [20].

2.1.2 Pseudocapacitors

Although they are analogous to the working mechanism of batteries, the absence of phase change processes distinguishes pseudocapacitors from them. Intermittently, pseudocapacitors perform rapid reversible redox reactions at the electrode surface involving electron transfer with electrolyte ions (Figure 2.5). Pseudocapacitors solely use surface-level redox processes to store charge, which is a Faradaic process. They usually provide higher storage capacity than EDLCs thanks to this redox process. They include the transmission of charge through the double layer, indicating that they are fundamentally non-electrostatic. In comparison to batteries, the charging and discharging processes are simpler and more rapid since they just involve transfer of the charges at the electrode-electrolyte interface, without any chemical or phase transition reaction [20].

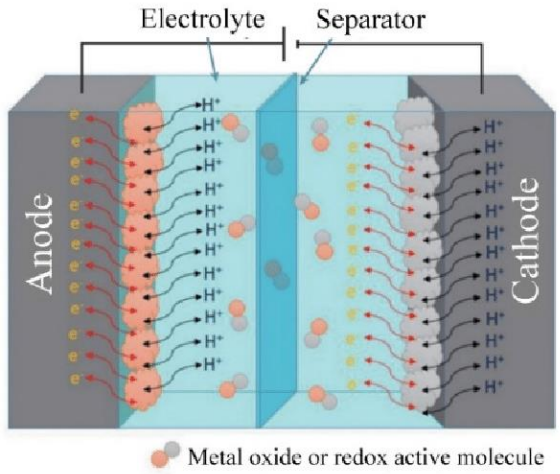


Figure 2.5 Pseudocapacitor [23].

2.1.3 Hybrid Supercapacitors

Many studies are currently being undertaken on the combining of these previous two systems in a single capacitor, referred to as hybrid capacitors. Hybrid capacitors, as their name implies, store charges in both electrostatic and electrochemical way, combining the benefits of both. Typically, they have a phenomenal working capacity and produce more capacitance than a single EDLC or pseudocapacitor. Hybrid capacitors can be symmetric or asymmetric depending on the cell design. The symmetric assembly is made up of the same sort of

electrode components as the asymmetric assembly, which is made up of dissimilar electrodes [20].

2.2 Components of the Supercapacitors

2.2.1 Electrodes

Generally, in supercapacitors, electrodes consist of a thin layer of active materials bonded to a current collector. Appropriate selection and adjustment of electrodes can have a major impact on the performance of the supercapacitors [20]. Supercapacitor electrodes must provide [17], [24];

- high specific surface area, porosity and electrical conductivity,
- long cycling stability,
- adequate chemical, mechanical and thermal stability,
- sufficient surface wettability,
- low cost,
- eco-friendliness.

As electrodes, EDLCs tend to require materials high with conductivity and large surface area. Several carbonaceous materials such as graphite, carbon nanotubes, graphene and activated carbon compounds serve this function satisfactorily. In addition, carbonaceous materials are abundant and have low manufacturing costs, have a controllable morphology, and may be post-treated to adjust their structures and chemical or mechanical characteristics for varied applications. Recently, there is a growing interest in investigating the various morphologies of carbonaceous materials, and it has been observed that nanoscale particle sizes with unique morphologies result in unquestionably superior performance [17], [20], [24].

For pseudocapacitors, due to one of its characteristics, quick reversible redox reactions, which result in high specific capacitances and long operating cycles, conducting polymers and metal oxides are the most often used electrode materials. [25]. Nonetheless, metal sulfides have lately attracted a great deal of attention as electrode materials due to their exceptional electrochemical characteristics, low cost, high availability, and large theoretical capacitances.

The electrochemical characteristics of metal sulfides can be modified by adjusting their morphologies, structures, and chemical compositions. As a result, the techniques of synthesis to produce metal sulfides with required characteristics were developed, to enhance the energy storage capacities of supercapacitors [1].

2.2.2 Electrolytes

The electrolyte is one of the essential components of supercapacitors, since it provides ionic conductivity and facilitates charge adjustment on each electrode. The state of the electrode-electrolyte interface and the structure of active materials have a significant impact on the interaction between the electrolyte and electrodes. Electrolyte type is crucial for the safety and performance of supercapacitive devices. Liquid electrolytes may be classified further as aqueous electrolytes, organic electrolytes, and ionic liquids [26].

2.2.2.1 Aqueous Electrolytes

When compared to organic electrolytes and ionic liquids, which require purifying procedures, aqueous electrolytes have been utilized widely due to their laboratory portability. Aqueous electrolytes have more conductivity than ionic and organic electrolytes, which is advantageous for decreasing the equivalent series resistance and improving the power delivery of supercapacitor [27]. Aqueous electrolytes are affordable and may be handled simply in the laboratory without the need for special conditions, considerably simplifying production and assembly operations [26].

2.2.2.2. Organic Electrolytes

Organic electrolytes for supercapacitors are typically consist of organic solvents dissolved in conducting salts. Devices using organic electrolytes are gaining significant attention due to their high voltage window. Since organic electrolytes include molecules of much larger dimensions than those of aqueous electrolytes, they demand electrodes with much larger pore sizes, which increases their resistance. Also, when compared to aqueous electrolytes, organic electrolytes usually have a greater cost, a lower specific capacitance, worse conductivity, and safety issues about toxicity, flammability and volatility. Moreover, an organic

electrolyte necessitates complex purification and assembly operations in a carefully regulated environment to remove any remaining impurities, which can result in significant performance degradation and substantial self-discharge difficulties [26].

2.2.2.3 Ionic Liquids

Ionic liquids are salts consisting of ions (organic/inorganic anions and organic cations) with melting temperatures less than 100 °C [26]. Because of their distinct structures and properties, ionic liquids have recently sparked considerable interest as alternate electrolytes for supercapacitors. Ionic liquids often have various potential benefits, including strong, chemical, electrochemical and thermal stability, non-flammability and low volatility. In addition, the physical and chemical properties of ionic liquids are highly modifiable thanks to their vast diversity of cation and anion combinations. This attribute tenability of ionic liquids is particularly interesting for supercapacitor electrolytes since the electrolyte compositions can be altered or customized to fulfil certain requirements of supercapacitive performance [27].

2.2.3 Separator

Ion passage between electrodes is enabled by separators with high porosity, which also insulate the electrodes from each other to prevent self-discharging. To achieve high energy and power densities, such separators should have strong ionic conductivity. Furthermore, during the full operating potential range, separator is ought to be chemically inert and should not participate in the electrochemical interaction between electrode and electrolyte. Also, they should be able to resist any heat generated during the process while also providing great wettability for electrolytes. Additionally, they must be non-flammable and have a strong tolerance to volume fluctuations.

Materials that can be utilized as separators in supercapacitors fall into three categories as; cellulose (paper), fiberglass fabrics, and polymers. Among them, the usage of polymer separators appears to be particularly promising when

considering chemical and mechanical resistance, affordability, accessibility, and processing simplicity [20].

2.2.4 Current Collector

Purpose of the current collector is to capture electrons and transmit them to an external load. To achieve that, they must be electrically conductive and have a low contact resistance. Additionally, they should be chemically and thermally stable, thin, flexible, and inexpensive. The choice of current collector is mostly dependent on the electrolyte and electrodes employed. For aqueous electrolytes, many metal-based materials, such as nickel and copper foils or foams may be used, whereas corrosion-resistant metals are required for strong acid electrolytes. In contrast, non-aqueous electrolyte-based supercapacitors frequently utilize aluminum current collectors [20].

3
WASTES OBTAINED FROM STEEL INDUSTRY

3.1 Steelmaking Dusts

Every year, large quantities of steelmaking dust are generated by steel factories. Dusts containing less than 1% zinc can be recycled into the iron and steelmaking processes. However, blast furnace dust (BFD), basic oxygen furnace dust (BOFD) and electric arc furnace dust (EAFD), cannot be reintroduced to ironmaking process due to the presence of Zn, K and Na as stated in Table 3.1[28].

The majority of high-zinc-content flue dusts are disposed as landfill, which not only consumes lots of space but also has a negative impact on the environment [29].

Additionally, the presence of heavy metals and the radioactive components threatens local water safety. Furthermore, the fine particulates spread easily by wind, reducing visibility while also posing a significant threat to human health [30].

Table 3.1 Chemical compositions of steelmaking dusts [30].

	Fe	C	Zn	Mg	Alkali metals
BFD	23.4 - 35.6	18.5 - 33.0	1.2 - 3.4	0.5 - 1.1	0.4 - 1.9
BOFD	50.0 - 80.0	-	1.7 - 9.4	0.4 - 2.2	-
EAFD	29.0 - 48.6	0.4 - 3.0	3.8 - 27.0	0.4 - 2.2	1.2 - 2.7

As seen in Figure 3.1, the steel manufacturing process generates several types of dusts from equipment such as the sintering machine, BF, BOF and EAF. Dusts with low Zn and alkali concentrations, such as BF gravity dust ash and iron oxide scale,

may be directly employed in the sintering and returned to the ironmaking process. Dusts having a low Zn concentration and a high alkali content, such as electrostatic precipitator ash from the sintering process, can be utilized as a raw material for the manufacturing of potassium salt. In addition, returning dust with a moderate or relatively high Zn concentration, such as BF bag ash, converter dust, and EAF dust, as indicated in Table 3.1, to the sintering process would result in cyclic Zn enrichment, which poses a danger to the efficient functioning of the BF [30]. However, these dusts may be recycled with various methods, recovering Zn and other precious metals and elimination of disposal of these dusts as landfills.

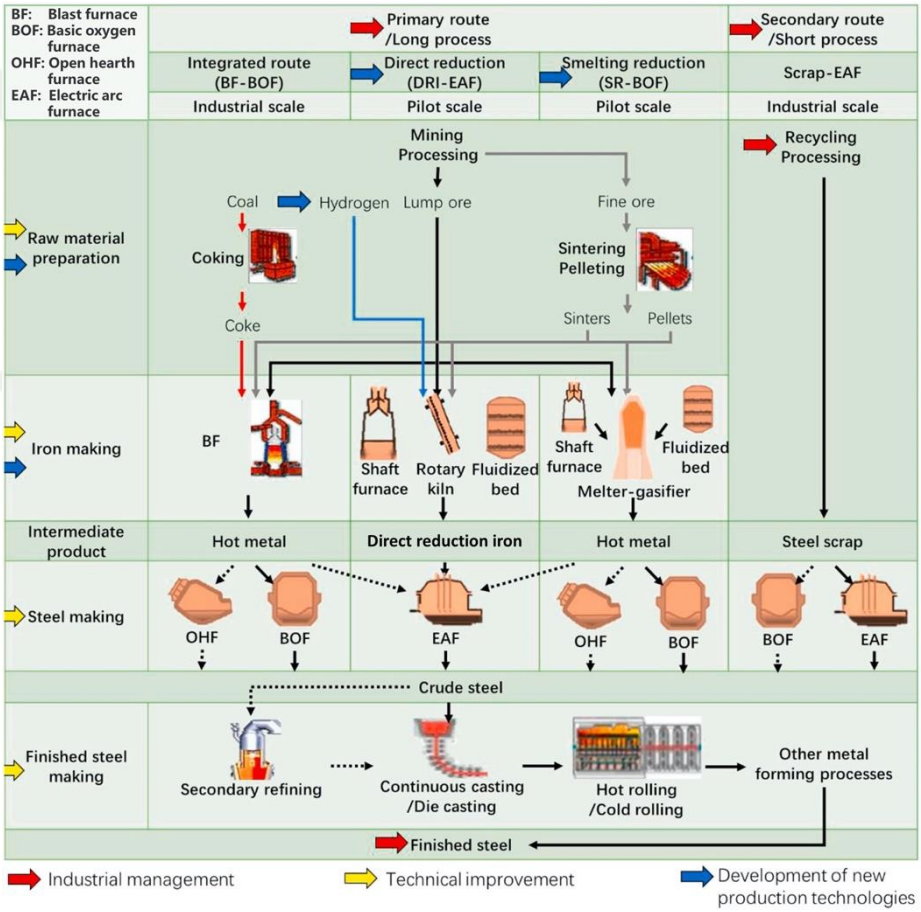


Figure 3.1 Steel production processes [30].

3.1.1 Blast Furnace Dust

Blast furnace dust (BFD) is a solid waste byproduct with a fine grain size, which is created during the ironmaking process. Statistics show that, around 18 kg of BF dust is removed from the off-gas of the BF, for per ton of produced metal. Iron

oxides (25–40%), carbon (about 20% C), and trace amounts of Ca, Al, and Si oxides are the primary components of BF dust. Due to the presence of recyclable components, BFD can be regarded as a valuable resource. However, it is stated that the whole usage rate of BFD is less than 20%. The majority of the dust is deposited or dumped of as solid landfills. In addition to consume a large amount of land, it also pollutes the environment and wastes valuable resources. As a result, it is critical to investigate an effective and clean treatment technique for using this dust to recycle important components [29].

Zn is a trace element in BF raw materials. It generally enters the BF as oxides or sulfides. Zn compounds are reduced easily in a reducing environment at high temperatures, then evaporate at high temperatures due to their low melting point. Evaporated Zn enters the flue gas and ascends proportionally [30].

The ferrous agglomerates charged in BF ironmaking can be of various forms, including lump ore, sinter or pellets. Mechanically and chemically generated particles leave the furnace through the top-gas, despite the type of charged agglomerate. The top-gas is passed through a gas cleaner, producing a coarser fraction referred to as BFD and a cleansed, finer fraction referred to as blast furnace sludge (BFS). There are various methods of recycling these wastes depending on how the BF is operated. The BFD is typically mixed into the sinter at integrated steel plant that run a sinter plant, where it is then recycled back into the BF. Using pellets, BFD can be recycled back into the BF using cold-bonded agglomerates and injection through the tuyeres. Regardless of ferrous burden agglomerate, the obstacles to recycle the dust and sludge back to the BF are comparable due to zinc's nature. The primary zinc source in the BF is the top gas. Recycling all BFD and BFS back to the BF would result in zinc accumulation [31].

To permit the recycling of BF sludge into the furnace, a zinc bleed must be implemented. By dezincing the BFS, a zinc-depleted percentage may be recycled, hence amount of waste sent to landfills is reduced. During the sintering process, a portion of the zinc content is lost when recycling zinc-containing wastes [32]. Therefore, while running pellets on the BF, recycling the BF dust via cold-bonded

agglomerates and injection, zinc removal requirements from BF sludge are more stringent than when operating on sinter [31].

Due to advancements in coke and sinter characteristics as well as improved blast furnace control, generation of BFD and BFS are being decreased [33]. In 2006, the average output of primary dusts was determined as 11.4 kg per ton of hot metal, whereas the average production of secondary sludges was determined as 8.9 kg per ton of hot metal [34].

3.1.2 Basic Oxygen Furnace Dust

According to World Steel Association, 70% of the steel production was conducted with Basic Oxygen Furnaces (BOF) in 2013. BOF produce a significant amount of BOF off gas solid wastes as well as steel, which are removed from BOF vessels by BOF off gas and recovered by BOF off gas cleaning equipment. BOF produce off gas solid wastes at unexpectedly variable rates, ranging 3.7 to 31 kg per ton of liquid steel, depending on operational parameters, such as raw ingredients and steel grades (International Iron and Steel Institute, 1994)

The average rate of solid waste formation from BOF off gas is about 18 kg/tL (American Iron and Steel Institute, 2001). BOF off gas is abundant in Fe, MgO, and CaO, and might be recycled back to the iron and steelmaking processes to replace expensive iron ores, dolomite or limestone. Due to the usage of Zn-containing scrap in the BOF process, however, BOF dust and sludge frequently contain Zn. Zn concentrations are often too high to recycle in the BF, also too low to use as a secondary source for Zn production. For modern BF, per ton of hot metal, Zn loading limits are generally set at 100 to 150 g. Excess Zn loadings may damage the refractory materials, reducing operational life of BF. Furthermore, large Zn input into BF may cause operational challenges, reducing effectivity. As a result, determining how to economically remove Zn from BOF off gas dust and sludge has become a vital step in preserving the dust and sludge's recyclability [35].

Before-process separation, post-process separation, and in-process separation, respectively, are the three basic methodologies for removing zinc from BOF off gas solid wastes[36].

Before-process separation is intended to remove zinc entry into the BOF process so that the BOF off gas solid wastes are not contaminated with Zn and the BOF off gas solid wastes may be completely recycled in the BF process without confronting zinc difficulties. This technique relies heavily on the increasingly scarce supply of affordable zinc-free steel scrap [37].

Post-process separation is the process of separating zinc from BOF off gas after the wastes have reached the ground state. Numerous systems have been analyzed and evaluated, including carbonaceous thermal reduction separation with rotary kilns [38], rotary hearth furnaces [30], electric arc furnaces [39], shaft furnaces [40] and multiple hearth furnaces [41]. Acidic leaching has also been investigated for the Zn separation from BOF off gas [42],[43]. Post-process separation often necessitates a big capital investment, a high operational cost, and extra environmental precautions. Therefore, this process is not an effective technique.

The objective of in-process separation is the extraction of Zn from the BOF off gas while the BOF off gas is being collected. In-process separation provides various benefits, including the possibility to employ extra energy from the process without needing a significant quantity of additional energy, the capability to separate undesirable constituents from solid wastes by implanting or replacing separation equipment and procedures without the requirement for a stand-alone separation facility, as well as the elimination of the need for extra environmental precautions. Two or more separators must be placed in sequence in a BOF off gas cleaning system to permit in-process separation of Zn from BOF off gas. The Zn content of BOF off gas solid waste collected by primary dust collectors is lower than that of final dust collectors. As a result, in the off gas cleaning process, BOF off gas solid wastes are sorted into lower-zinc and higher-zinc sections. Lower-zinc portions of BOF off gas solid wastes could be recycled in the sintering BF ironmaking process if the zinc content of the solid wastes is sufficiently low, and higher-zinc sections might be recycled in zinc recovery facilities if the zinc content of the wastes is reasonably high. In-process separation provides the following advantages; energy usage is minimized or non-existent, capital investment and operational costs are reduced, no additional environmental protection is required compared to separation before-process and after-process separation.

3.1.3 Electric Arc Furnace Dust

Electric Arc Furnace (EAF) is a popular alternative to the traditional BOF production process for carbon and alloy steels. Approximately 30 percent of crude steel is produced using EAF by melting scrap.

Per ton of steel produced in an EAF, around 15–25 kg of fine EAFD is formed. EAFD is considered as a hazardous waste, because of the generation of the leachable heavy metal compounds in the process, such as Pb and Cd, During the operation of EAF, dust is produced as a result of the vaporization of molten iron with non-ferrous metals, the bursting of CO bubbles, and the outflow and dragging of particulates from the liquid metal bath, slag, and other materials in the oven [44].

During in the melting of scrap, volatile compounds are expelled and collected in the off-gas cleaning system together with particulates [45].

During the metal fusing, EAF may reach temperatures as high as 1600°C, and several charge components, including iron, zinc, and lead are volatilized and enter the vapor phase. When vapor is cooled down and collected, a significant quantity of dust is being formed [11].

Composition of the EAFD is determined by the used scrap type and other raw materials. Because of the presence of many scrap types with varying components, the EAFD composition has become incredibly complex and varied. Iron and zinc are the most abundant elements in the EAFD, with potassium, manganese, silicon, cadmium, chlorine and lead being less common. Calcium is another important component in EAFD. In practice, its content remains constant and precisely controllable as it is charged to the furnace as a flux. [46].

Because of its very poor solubility, and especially since the vapor pressure of zinc is higher than vapor pressure of iron at steelmaking temperatures, most of the Zn is lost to dust and fume when scrap is employed in the furnace. Vapor Zn with other gaseous or particulate created during steel-making processes is taken from the furnace, resulting in the formation of compounds such as ZnO and $ZnFe_2O_4$.

The proportion of zinc in the EAFD ranges from 7 to 40 percent, depending on the ratio of galvanized waste utilized [47]–[49].

The annual global production of EAFD is expected to be approximately 3.7 million tons. Europe's vegetation produces between 500,000 and 900,000 tons of dust annually [50]. According to Worldsteel Association, more than 1.6 billion tons of steel were produced globally in 2013, with EAF producing about 30% of this total.

Due to its physical and chemical qualities, the EAFD was classified as hazardous waste in accordance with the European Waste Catalogue (EWC 2002) when the concentration of hazardous compounds exceeded a predetermined level. EAFD is categorized as a hazardous waste by the EPA; therefore, it must be incorporated with care. As a dangerous waste, it is disposed in part at appropriate, regulation-mandated trash sites or used as a secondary source in the manufacturing of Zn, Fe, Pb, etc. Due to the mobility of toxic components, disposal of these industrial solid wastes might pose a threat to the environment.

3.1.4 Ferrochromium Flue Dust

There is a correlation between the amount of ferrochrome that has been generated over the years and the amount of stainless steel that has been produced. Both the production of stainless steel and ferrochrome on a global scale have demonstrated a trend toward steady growth over the past four years. According to ICDA, ferrochrome produced in the globe in 2018 was mostly utilized in the stainless steel sector [51].

Ferrochromium is classified into three types based on its carbon content: high, medium, and low. The ranges of composition for both carbon and chromium have been set by ISO 5448. Aside from these, there are also ferrosilicochrome (FeSiCr), ultra-low carbon FeCr, and nitrided ferrochromium grades (FeCrN) [51].

Low-carbon ferrochrome grades (0.25% to 0.50% C) are mostly utilized to manufacture corrosion-resistant superferritic steels [51].

Medium-carbon ferrochrome also serves as a product of interest in the foundry and steelmaking industries, when refining capacity is restricted but a low silicon content is sought [51].

High carbon ferrochrome is a class of alloys with chromium contents ranging from 60% to 70% and carbon contents ranging from 4% to 6%. The silicon concentration of traditional high carbon ferrochrome is typically less than 2%. High carbon ferrochrome is a feedstock used in the production of value-added commodities like stainless steel. Due to variations in the ores found in different geographic areas, which have an effect on certain alloy components, it does not have a singular specification. Additionally, certain alloy components are impacted by the smelting method used. The type of reductant employed will also have an effect on specific components. As a result, producers typically have their own standards instead of a global standard specification, which depends on their unique method and collection of raw materials [51].

Carbothermic reduction of chromite ore in submerged arc furnaces is the most widely used conventional process in the world, for the production of ferrochrome. By developing a recipe that will give the necessary target metal composition using the carbothermic process, crushed and screened chromite is charged to metallurgical coke and quartzite, exposed to melting, and maximum chromite reduction is ensured.

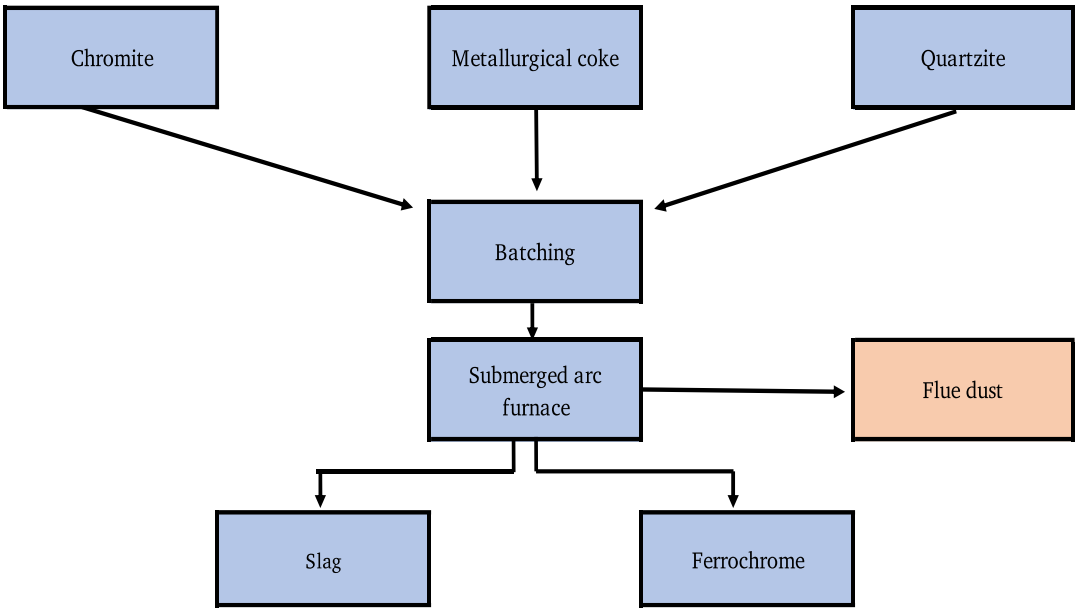


Figure 3.2 Ferrochrome production process.

The arc that the electrodes create provides the heat needed for the reactions to form. Fundamental reduction reactions are given in Eq 3.1-3.3 [52].

$$Cr_2O_3 + 3C = 2Cr + 3CO + \Delta H_1 \quad (3.1)$$

$$FeO + C = Fe + CO + \Delta H_2 \quad (3.2)$$

$$SiO_2 + 2C = Si + CO + \Delta H_3 \quad (3.3)$$

A ferrochrome alloy made of Cr, Fe, C, and Si is produced as a result of the carbothermic processes that take place. The resulting alloy is cooled by pouring it into molds, followed by crushing and screening, before being sold in the specified order sizes (10 mm - 50 mm) or in the specifications required by the client [52].

Due to air infiltration into the furnace during the smelting process, CO-rich off-gas penetrates through the furnace bed and is inevitably ignited on top of the furnace bed. The off-gas is then collected and cleansed using bag filters before being discharged into the atmosphere [53]. Off-gas cleaning is accomplished by first feeding off-gas through a cyclone or drop-out box, which separates coarse debris from the off-gas. This debris can be recycled or disposed. The off-gas then flows through a baghouse where purpose-built bag filters gather the dry fine dusts

[54]. The captured dust is immediately treated with water to minimize dry dust spills or wind dispersion [55].

The majority of ferrochrome alloys are produced worldwide in the Republic of South Africa. Following the South African Republic are, in that order, Japan, India, Sweden, and Brazil [56].

High carbon ferrochrome is produced in Turkey in facilities with a capacity of 150,000 tons annually in Elazığ and 12,000 tons in Balıkesir. Low carbon ferrochrome is produced with a capacity of 10,000 tons annually in Antalya. The combined annual ore consumption of the three facilities ranges between 450,000 and 500,000 tons/year. According to ICDA, Table 3.2 details the countries that produce high carbon ferrochrome and their respective production levels [52].

Table 3.2 High carbon ferrochrome producing countries and their production quantities (tons/year) [52].

	Country	**2016**	**2017**	**2018**	**2019**
1	China	4.224.217	4.994.400	5.282.876	6.021.900
2	South Africa	3.585.378	3.761.054	4.020.390	3.634.073
3	Kazakhstan	1.208.356	1.361.881	1.435.528	1.556.753
4	India	1.059.729	1.305.847	1.299.935	1.280.767
5	Finland	471.116	416.284	492.772	510.899
6	Zimbabwe	30.819	82.325	198.022	192.985
7	Sweden	77.032	108.028	100.011	125.589
8	Brazil	115.396	133.515	135.805	107.097
9	**Turkey**	77.328	77.545	96.100	83.000
10	Russia	130.231	128.486	88.839	70.200

3.2 Recovery of Zinc from Metallurgical Dusts

To recover and utilize valuable metals from metallurgical dusts, numerous treatment strategies have been devised. Two methods for handling metallurgical dusts are pyrometallurgical and hydrometallurgical processes [30].

3.2.1 Pyrometallurgical Processes

Current approaches for processing steelmaking dust are predominately based on pyrometallurgical processes and involve principally the reduction of ZnO in the dust at high temperatures and subsequent oxidation of Zn in the gas phase. [57]. Most of these systems employ rotary kilns, plasma, and flame reactors. These procedures involve reducing agents and high temperatures to generate crude zinc oxide (CZO) [11].

Table 3.3 Pyrometallurgical recovery processes [46].

Process	Furnace type	Temp. (°C)	Products	Max cap. (kt/year)	Remarks	Ref.
Waelz kiln	Rotary kiln	1050-1100	CZO and iron slag	500	Process more than 75% of the dusts produced in steel plants worldwide	[58], [59]
Rotary Hearth Furnace	Rotary hearth furnace	1250-1300	CZO and direct reduced iron (DRI)	300	Promising, yet difficult to treat high zinc dust.	[60], [61]
PRIMUS	Multiple hearth furnace	1000-1150	CZO and DRI	100	Highly energy efficient but extensive corrosion of furnace refractory	[61]–[63]
Sub merged Plasma	Plasma reactor	1400–1600	CZO, liquid iron and slag	40–60	The process may generate high temperature even at low oxygen levels	[64], [65]
OXYCUP	Cupola furnace	1450–1600	CZO, pig iron and slag	200	Limited reduction low metallization of composite pellets/briquettes	[65], [66]
Coke-packed Bed	Shaft furnace	1500–1600	CZO, liquid iron and slag	10–15	Control of temperature and CO_2/CO ratio at the top of the coke bed is essential to avoid zinc sticking and accretion formation on the wall	[61], [62], [67]
Ausmelt	Top submerged lance	1250–1350	CZO, liquid iron and slag	100	Sealed reactor helps to arrest fugitive gas to value-added products. Complex bed operations restrain its flexibility	[68], [69]
ESRF	Electric arc furnace	1400–1600	CZO, liquid iron and slag	36	Operating cost is high	[70]

3.2.2 Hydrometallurgical Processes

Typical hydrometallurgical procedures involve leaching of steelmaking dusts and extraction of the metal of interest in metallic or compound form from the solution [57].

Unwanted species may be also dissolved in the solution with the metal of interest during hydrometallurgical processing. These contaminants may be eliminated using procedures such as selective precipitation, cementation, electrolysis, ion exchange and solvent extraction [71].

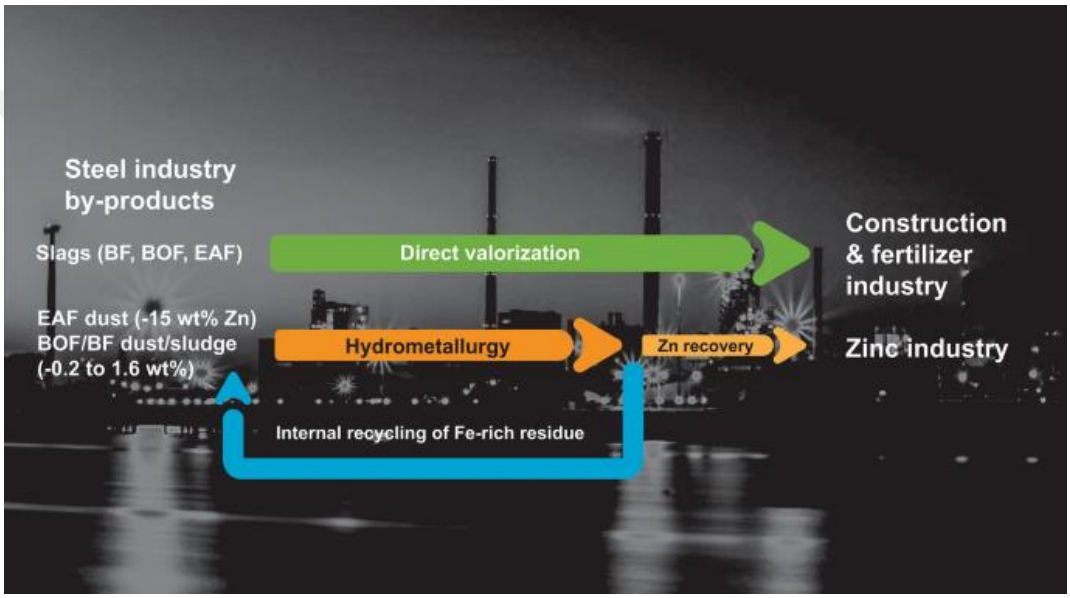


Figure 3.3 Recovery of steel industry by-products by hydrometallurgical processes [33].

The most challenging issue in hydrometallurgical operations of steelmaking dusts is maximizing zinc recovery while inhibiting iron from being extracted into the solution. Since zinc appears in dust in the form of ZnO and $ZnFe_2O_4$, the main issue is separating it from the $ZnFe_2O_4$ and transferring it into the solution. If the zinc is mostly in the form of ZnO, higher leaching efficiency may be achieved. However, if zinc is mostly bonded in $ZnFe_2O_4$ form which is a relatively stable phase, then zinc recovery may be limited [72].

So far, the majority of research on the leaching processes has focused on the employment of acidic and alkaline leaching agents. Reactions take place in the hydrometallurgical Zn recovery processes are given in Eq. 3.4–3.7.

$$ZnO + H_2SO_4 = ZnSO_4 + H_2O \quad (3.4)$$

$$ZnO + 2HNO_3 = Zn(NO_3)_2 + H_2O \quad (3.5)$$

$$ZnO + NaOH = Na_2ZnO_2 + H_2O \quad (3.6)$$

$$ZnO + 2NH_4Cl = ZnCl_2 + 2NH_3 + H_2O \quad (3.7)$$

The benefits of acidic leaching include rapid dissolving, low cost, availability, the ability to use low concentrations and a well-known electrolysis procedure to generate metallic zinc, with acid regeneration. The main disadvantage of acidic leachates, on the other hand, is its low selectivity to the elements present in the dusts. This pertains particularly to iron, which can have a substantially larger concentration, resulting in a high consumption of the leachates and the requirement to purification of the leach solution from significant amounts of iron, which is both complex and challenging. Additionally, pH must be regulated to prevent hydrolysis and zinc hydroxide precipitation [57].

The primary benefit of utilizing an alkaline leachate is its selectivity for zinc over iron, which removes the complicated and costly iron removal process. Also, to extract lead from zinc, which can be employed as an extra intermediate product and raw material during the recovery of metal is feasible. Therefore, the use of alkalines as a leaching agent appears to be a feasible alternative for the treatment of steelmaking dust, despite the fact that alkaline leaching agents have some drawbacks. The most significant are the need for a high concentration to achieve considerable zinc leaching efficiency, the increased cost, and the difficulty in recovery of the solution.[57]

Table 3.4 Comparison of leaching agents [46].

	Acidic leaching	Alkaline leaching
Advantages	Rapid dissolving kinetics Availability Low cost Ability to be used in low concentrations	Selectivity towards the other metals
Disadvantages	Lack of selectivity towards the other metals pH must be regulated	High concentrations are required High cost Recovery from the solution is difficult

3.3 Comparison of Zinc Recovery Processes

Pyrometallurgical processes are being used extensively to recover zinc from metallurgical dusts. Nevertheless, these processes are plagued by high energy use and the generation of undesirable byproducts. Hydrometallurgical methods, on the other hand, still have promise for the future and may provide numerous benefits which are given below, [11]

- They require less capital investment, which makes them more affordable for small businesses [33].
- The operating expenses are much lower, since less energy is required [33].
- They are often more selective, so they can be more efficient [33].
- Hydrometallurgical processes produce nearly zero air pollution, which makes them environment-friendly.
- Leaching produces an iron-bearing material that can be recycled and used again in the production of steel.

In spite of these benefits, the recovery of steelmaking dusts by hydrometallurgical processes is still hampered by issues associated with the high zinc leaching rate and efficient extraction from the solution [57].

4
MATERIALS AND METHODS

4.1 Chemicals and Raw Materials

Chemicals and raw materials used in the study and their qualifications are listed in Table 4.1.

Table 4.1 Chemicals and raw materials used in the present study.

Name	Formula	Brand	Grade (%)
Ferrochrome flue dust	-	Eti Krom	-
Electric arc furnace dust	-	Çolakoğlu	-
Sulphuric acid	H_2SO_4	Sigma-Aldrich	95-98
Nitric acid	HNO_3	Sigma-Aldrich	65
Sodium sulphide	Na_2S	Sigma-Aldrich	60
Sodium hydroxide	NaOH	Merck	98
Potassium hydroxide	KOH	Merck	85
Graphite	C	Sigma-Aldrich	99.9
Carbon black	C	Sigma-Aldrich	99.9
PVDF	$(CH_2CF_2)_n$	Sigma-Aldrich	99.9
NMP	C_5H_9NO	Sigma-Aldrich	99

4.2 Equipment

Purposes of usage and brand information of equipment used in the study are given in Table 4.2.

Table 4.2 Equipment utilized in the present study.

Name	Brand	Purpose
Ball mill	-	Homogenization of raw materials
Magnetic stirrer (10 position)	Weightlab	Leaching of dusts Precipitation of ZnS
Oven	Ecocell	Drying
Centrifuge	Elektro-mag	Separation of nano powders
pH meter	Hanna	Determination of pH of solutions
Film applicator device	Defnelab	Preparation of electrodes
Hydraulic coin cell sealing device	Defnelab	Preparation of coin cells

4.3 Characterization of Raw Materials and Products

Chemical, physical and electrochemical characterization instruments used to analyze raw materials and products are summarized in Table 4.3.

Table 4.3 Characterization instrument used in the present study.

	Analysis	Device
Chemical	XRD	PANalytical X'pert Pro
	XRF	Panalytical Epsilon4
	XPS	Specs-Flex
	AAS	Perkin-Elmer AA800
Physical	SEM	Zeiss EVO LS 10
	Mastersizer	Malvern Hydro 2000MU
Electrochemical	CV	Gamry Interface 1010
	GCD	
	EIS	

4.4 Experimental Procedure

The study carried out within the scope of the thesis is structured under four main headings as;

- Preparation of raw materials
- Leaching
- Precipitation of ZnS
- Production of supercapacitors, and flow chart of the detailed procedure is given in Figure 4.1.

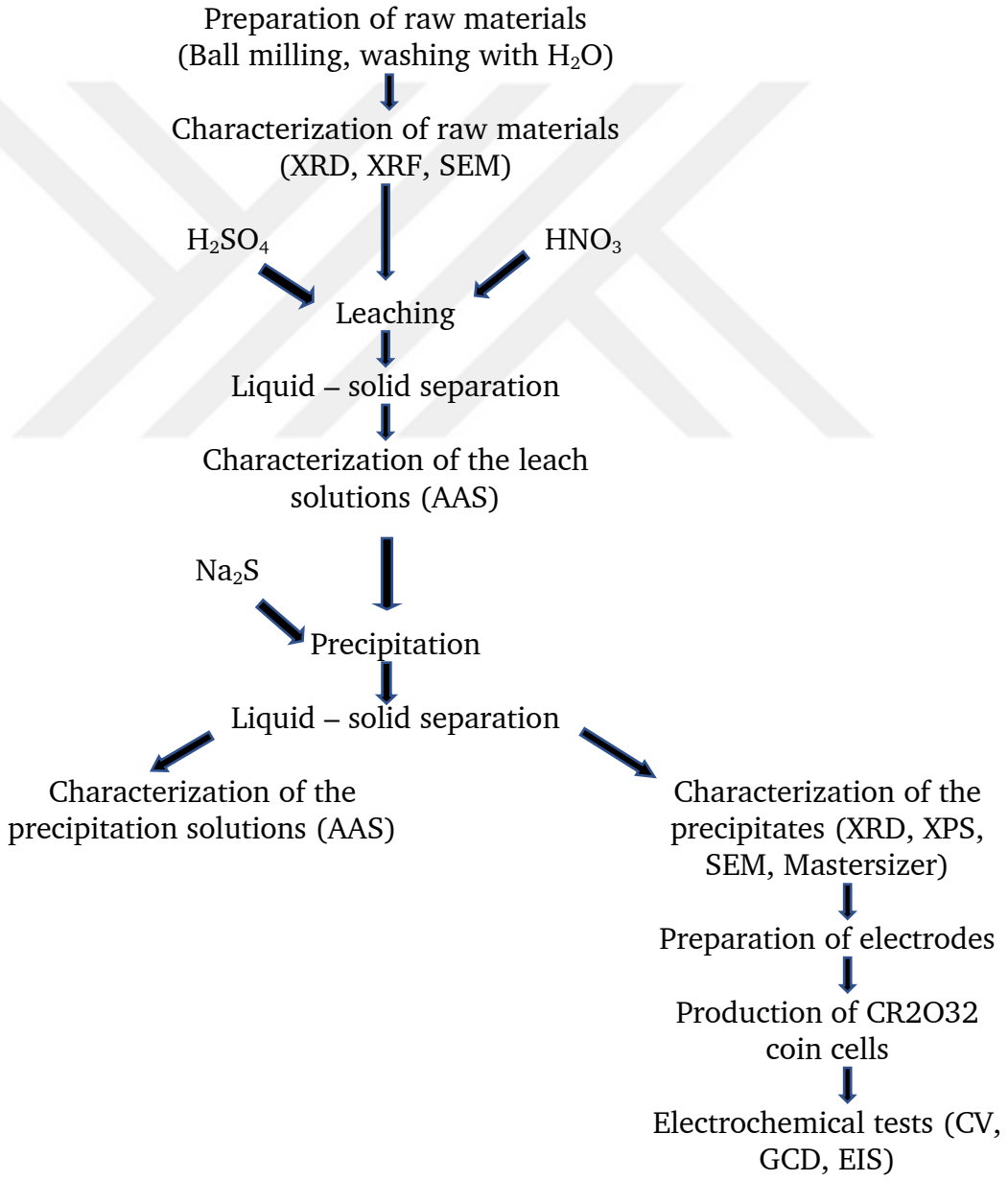


Figure 4.1 Flow chart of the experimental procedure.

4.4.1. Preparation of Raw Materials

In order to obtain homogeneous raw materials, ferrochrome flue dust (FFD) and electric arc furnace dust (EAFD) obtained from Eti Krom and Çolakoğlu respectively, were grinded in a ball mill for 30 minutes. Ground dusts were washed with deionized water at 100-1 liquid-solid (LS) ratio. Washed dusts were dried at 105 °C for 24 hours. Characterization of the prepared raw materials was carried out by XRD, XRF and SEM analyses.

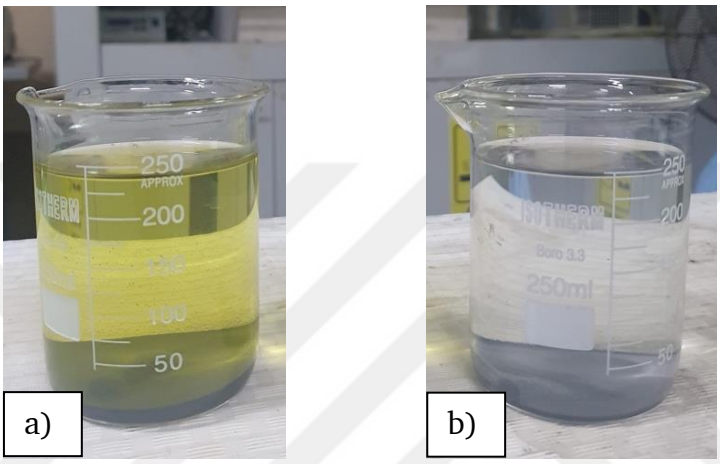


Figure 4.2 FFD solution, a) before washing, b) after washing.

4.4.2. Leaching

Prepared FFD and EAFD powders were leached with sulphuric acid and nitric acid solutions with various concentrations (0.05 to 1M) and LS ratios (10-1 to 100-1) for 15 to 90 minutes. Undissolved particulates were removed from solutions by a vacuum pump using quantitative filter papers. Chemical characterization of the leach solutions was carried out with AAS. Leaching efficiencies (LE) of the solutions were determined from Eq 4.1, where m_l is the mass of dissolved metal ions after leaching and m_{max} is the initial weight of the metal. Characterization results were examined, and optimum parameters were determined for selective leaching of ZnO from each raw material.

$$LE = \frac{m_l}{m_0} \times 100 \qquad (4.2)$$

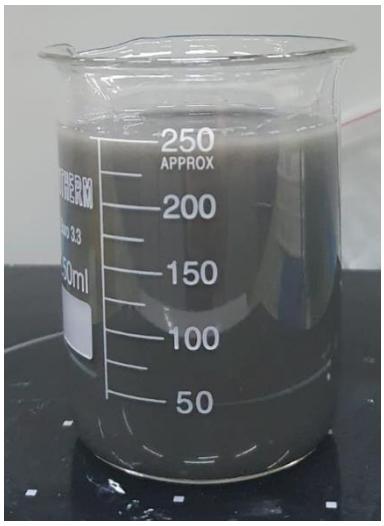


Figure 4.3 Ferrochrome flue dust leaching experiment.

4.4.3. Precipitation of ZnS

Precipitation process is conducted to solutions with optimum parameters, where maximum selective zinc dissolutions are achieved.

Sodium sulfide solutions with various concentrations (1:1-1:3 zinc to sodium sulfide molar ratio) were prepared. Leach solutions were added to sodium sulfide solutions with the rate of 0,25 mLs^{-1} at 600 rpm stirring rate at room temperature. With the utilization of 3M HNO_3 and 3M NaOH solutions, pH of the mixture was kept between 4 and 6, through the precipitation process. Final mixtures were stirred at 150 rpm for 15 minutes at room temperature. Chemical characterization of the precipitation solutions was carried out with AAS. Precipitation efficiencies (PE) were determined from Eq 4.2 where m_p is the mass of dissolved metal ions after precipitation.

$$PE = (1 - \frac{m_p}{m_l}) \times 100 \qquad (4.2)$$

Characterization of produced precipitates was carried out with XRD, XPS, SEM and Mastersizer analyses.

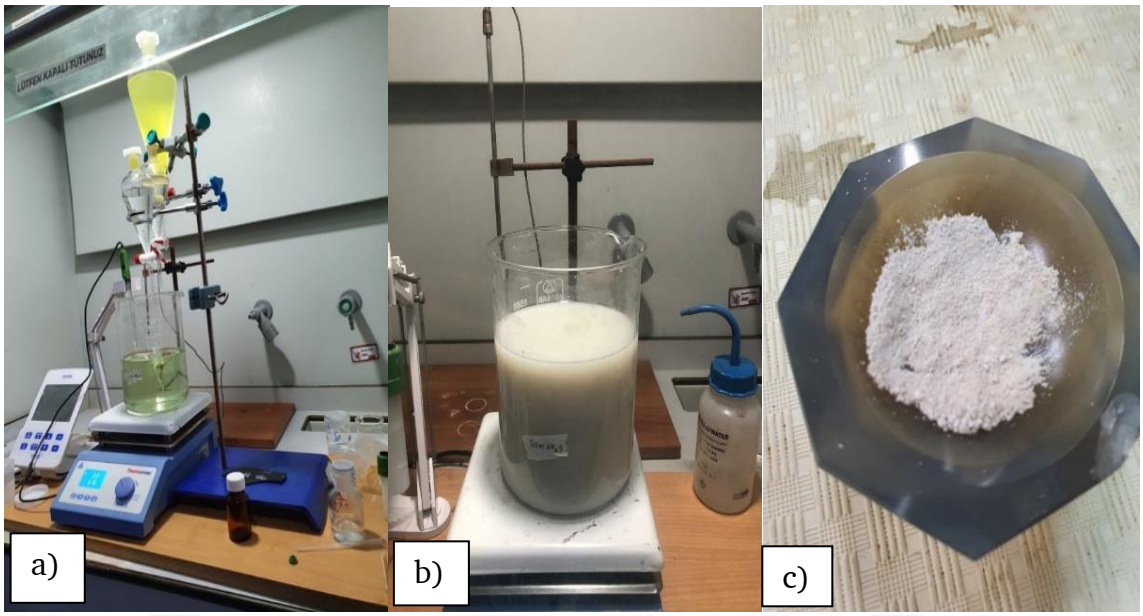


Figure 4.4 a) Precipitation experiment setup, b) after precipitation process, c) after liquid-solid separation.

4.4.4. Production of Supercapacitors

In the scope of the study, asymmetric type hybrid supercapacitors were produced. Active substances for electrodes were prepared by utilization of the produced ZnS from FFD and EAFD with carbon black with various compositions for anode and graphite for cathode. Flow chart of the supercapacitor production process is demonstrated in Figure 4.5.

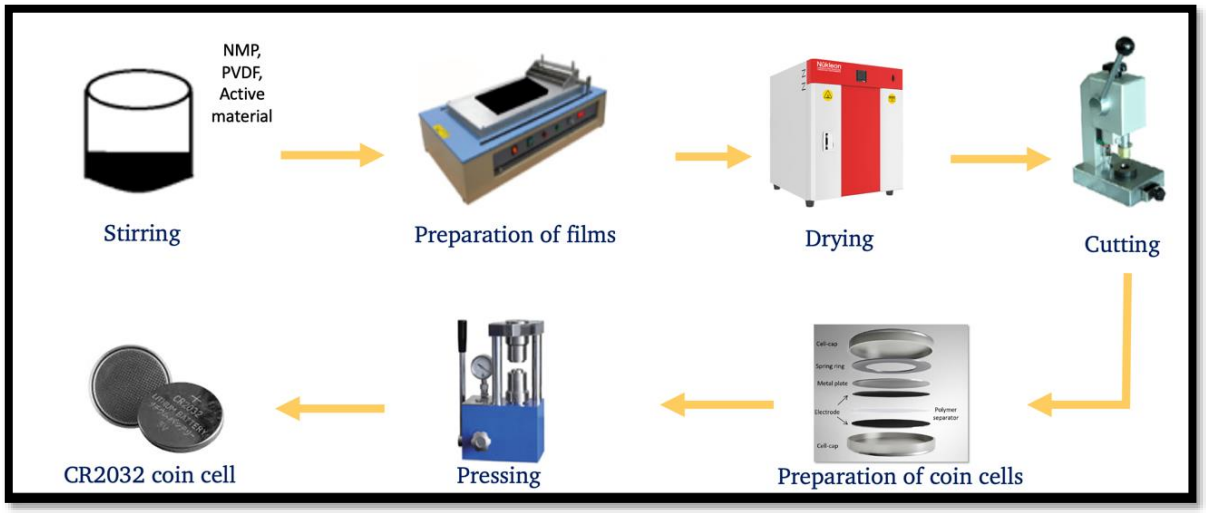


Figure 4.5 Flow chart of the supercapacitor production process.

Compositions of the prepared active substances are given in Table 4.4.

Table 4.4 Anode and cathode compositions.

	Anode (g)	**ZnS (g)**	**Carbon black (g)**	**PVDF (g)**
1	0.50	0.40	0	0.10
2	0.50	0.35	0.05	0.10
3	0.50	0.30	0.10	0.10
4	0.50	0.30	0.15	0.05
	Cathode (g)	**ZnS (g)**	**Graphite (g)**	**PVDF (g)**
	0.50	0	0.40	0.10

PVDF (Polyvinylidene fluoride) was used as a binder for these mixtures. The binder was dissolved in 1.5 mL of NMP (N-methyl pyrrolidone) at 300 rpm stirring rate for 5 minutes, then the active substance was added to the system and mixed with a stirring rate of 750 rpm for 15 minutes. To produce films, prepared mixtures were applied at a thickness of 200 microns through graphite foils, using a film applicator device which is presented in Figure 4.6. The films were dried at 60° C for 6 hours, then cut with a diameter of 16 mm to be inserted into the CR2032 type coin cell.

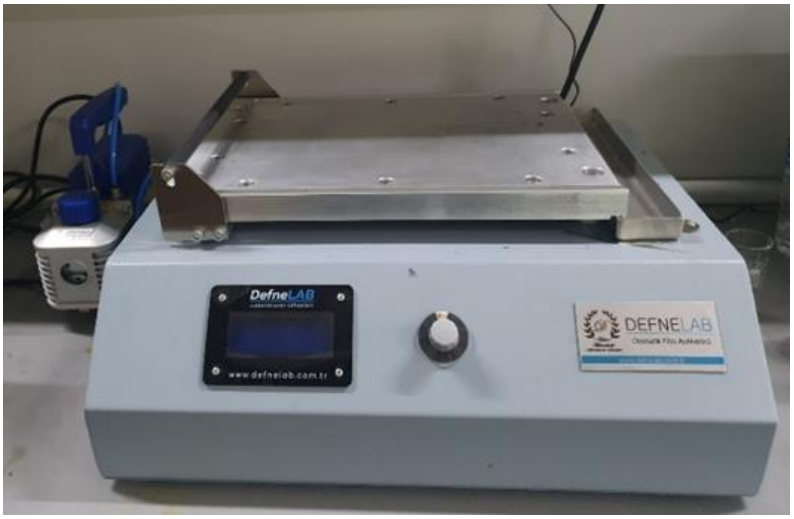


Figure 4.6 Film applicator device.

Produced film and cut electrodes are presented in Figure 4.7a and Figure 4.7b respectively.



Figure 4.7 The image of, a) produced film, b) produced electrodes, c) produced supercapacitor.

The homogeneity of the produced films was determined by SEM analyses. The weights of the electrodes were determined by weighing the empty and coated weights of the foils. The prepared electrodes were separated using a Whatman type separator with a thickness of 25 micrometers. 1 mL of 2 M potassium hydroxide solution was supplied to the system as electrolyte and the coin cell system was sealed under pressure. Electrochemical characterization of the produced supercapacitors was carried out with Cyclic Voltammetry (CV), Galvanostatic Charge-Discharge (GCD) and Electrochemical Impedance Spectroscopy (EIS) analyses by Gamry Interface 1010 Potentiostat-Galvanostat device which is shown in Figure 4.8.

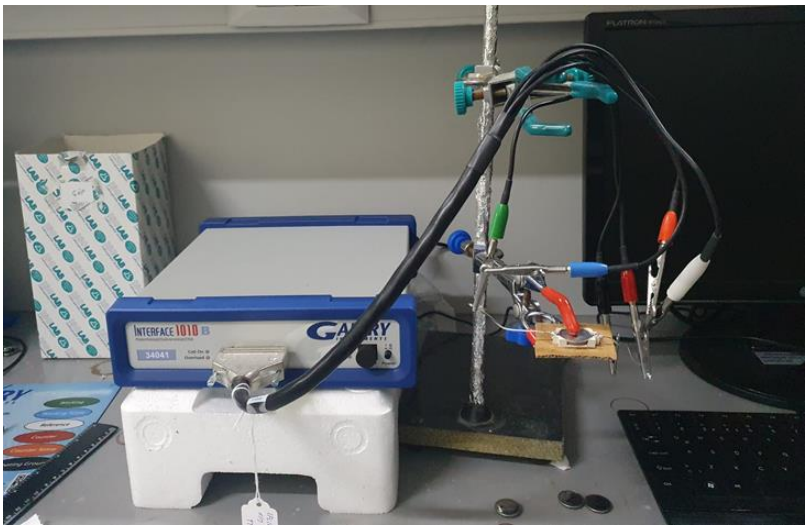


Figure 4.8 Gamry Interface 1010 Potentiostat-Galvanostat device.

5
RESULTS AND DISCUSSIONS

5.1 Preparation of Raw Materials

Chemical and physical characterization of the raw materials were carried out with XRD, XRF, AAS and SEM-EDS analyses.

The XRD analyses were done with the measuring range from 1 to 90° 2θ using a step size of 1°/minutes. XRD pattern of the FFD sample is presented in Figure 5.1.

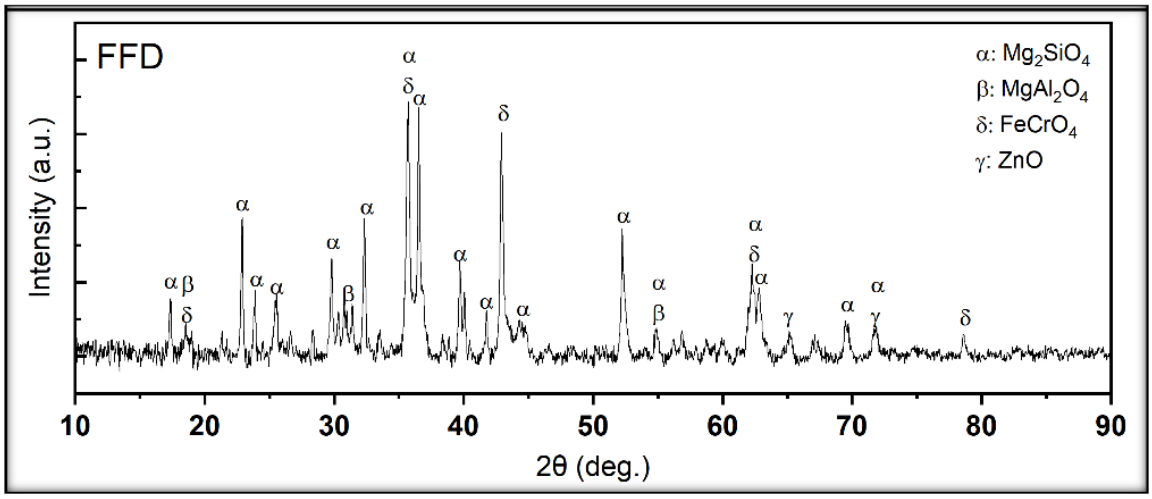


Figure 5.1 XRD pattern of FFD.

The major crystalline phases contained in the sample were determined as Mg_2SiO_4 (ICSD: 00-004-0769), $MgAl_2O_4$ (ICSD: 00-002-1084), $FeCrO_4$ (ICSD: 01-089-2618) and ZnO (ICSD: 01-079-0208) based on the characteristic peak intensity positions.

XRD pattern of the EAFD sample is presented in Figure 5.2.

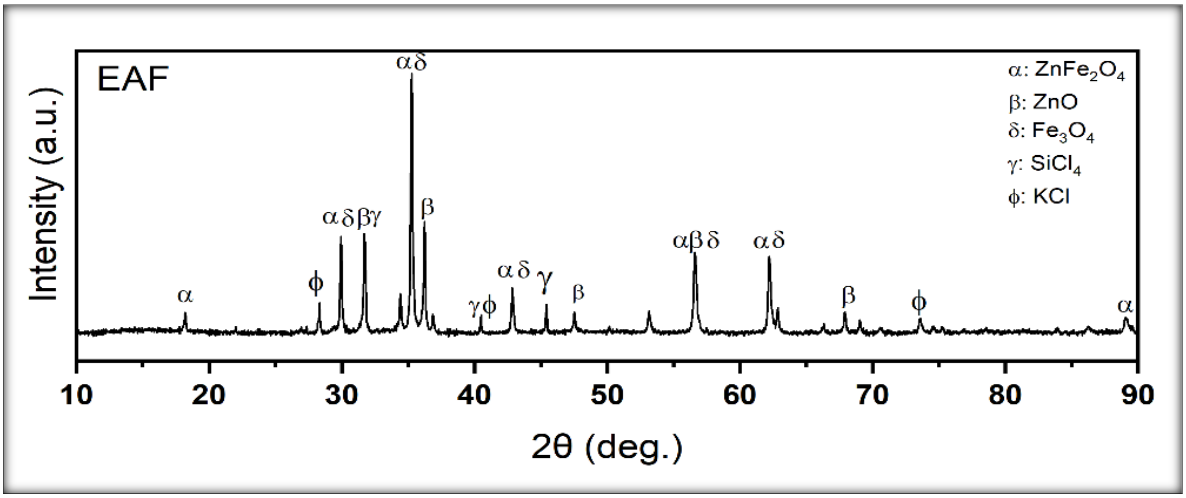


Figure 5.2 XRD pattern of EAFD.

The major crystalline phases contained in the sample were determined as $ZnFe_2O_4$ (ICSD: 081206), ZnO (ICSD: 034477), Fe_3O_4 (ICSD: 020596), $SiCl_4$ (PDF: 00-010-0220) and KCl (PDF: 00-041-1476).

Elemental compositions of the raw materials were determined by the XRF analyses. XRF analysis results are presented in Table 5.1.

Table 5.1 Chemical compositions of FFD and EAFD.

Element	Zn	Fe	Cr	Mn	Si	Mg	Al	Ca	K	Pb	Cu	P
FFD	6.36	1.30	0.62	1.05	29.59	39.82	7.71	0.548	6.69	-	-	-
EAFD	43.40	36.94	0.55	3.15	2.35	1.65	0.55	6.10	0.32	3.41	0.38	2.35

Zn percentages of the FFD and EAFD samples were determined as 6.36% and 43.40 % respectively.

The morphological characteristic and microanalyses of the different phases in the FFD and EAFD samples were investigated by SEM.

SEM image of the FFD is presented in Figure 5.3. It was observed that the sample exhibit a non-uniform structure. The grains were predominantly spherical and frequently aggregated.

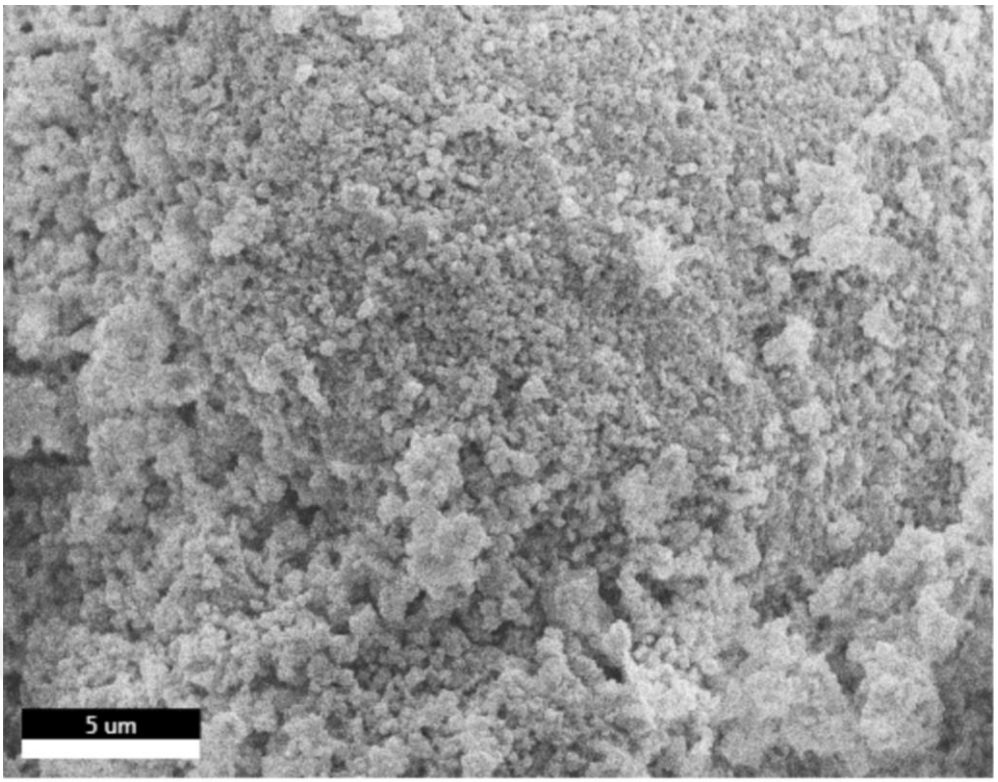


Figure 5.3 SEM image of FFD.

SEM image of the EAFD is presented in Figure 5.4. Similar with FFD sample, a non-uniform structure and predominantly spherical particles were observed.

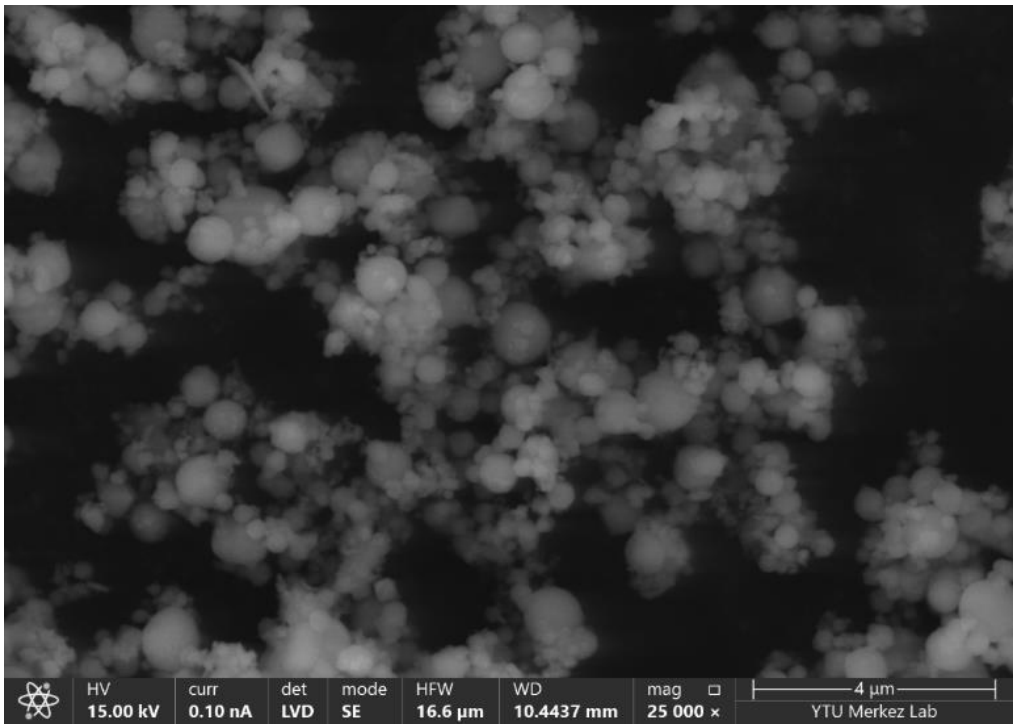


Figure 5.4 FE-SEM image of EAFD.

5.2 Leaching

It is expected that, the solutions obtained during the leaching processes will contain zinc, iron and chromium ions, which are all 3A group cations. The main aim of the leaching experiments was to obtain a Zn solution with the highest purity and minimum dissolution amount of Fe and Cr. During leaching experiments, sulfuric acid and nitric acid solutions were used and the effects of L-S ratio, acid concentration, and leaching duration were investigated by determination of the LE of Zn, Fe and Cr for each solution. Dissolution of ZnO in sulfuric acid and nitric acid mediums was achieved as a result of the reactions given in Eq 5.1 and Eq 5.2 respectively.

$$ZnO + H_2SO_4 = ZnSO_4 + H_2O \quad (5.1)$$

$$ZnO + 2HNO_3 = Zn(NO_3)_2 + H_2O \quad (5.2)$$

In the previous studies it was concluded that zinc could effectively be leached from baghouse dusts, relative to iron. Although the rate of zinc dissolution is not significantly affected by temperature, the rate of iron dissolution is, which means that working at room temperature is required to obtain both a high zinc extraction rate and a low iron dissolution rate [73].

All leaching experiments were done at room temperature. The results of all leaching experiments are presented in Appendices.

5.2.1. Effect of L-S Ratio

Effect of L-S ratio was investigated for five different acid concentrations, 0.05, 0.1, 0.25, 0.5 and 1 M respectively. Leaching experiments were carried out at four different L-S ratios which were 100:1, 50:1, 20:1 and 10:1 for both sulfuric acid and nitric acid solutions. To determine the effect of L-S ratio, all experiments were performed for 60 minutes. The results of the experiments are given in Figure 5.5.

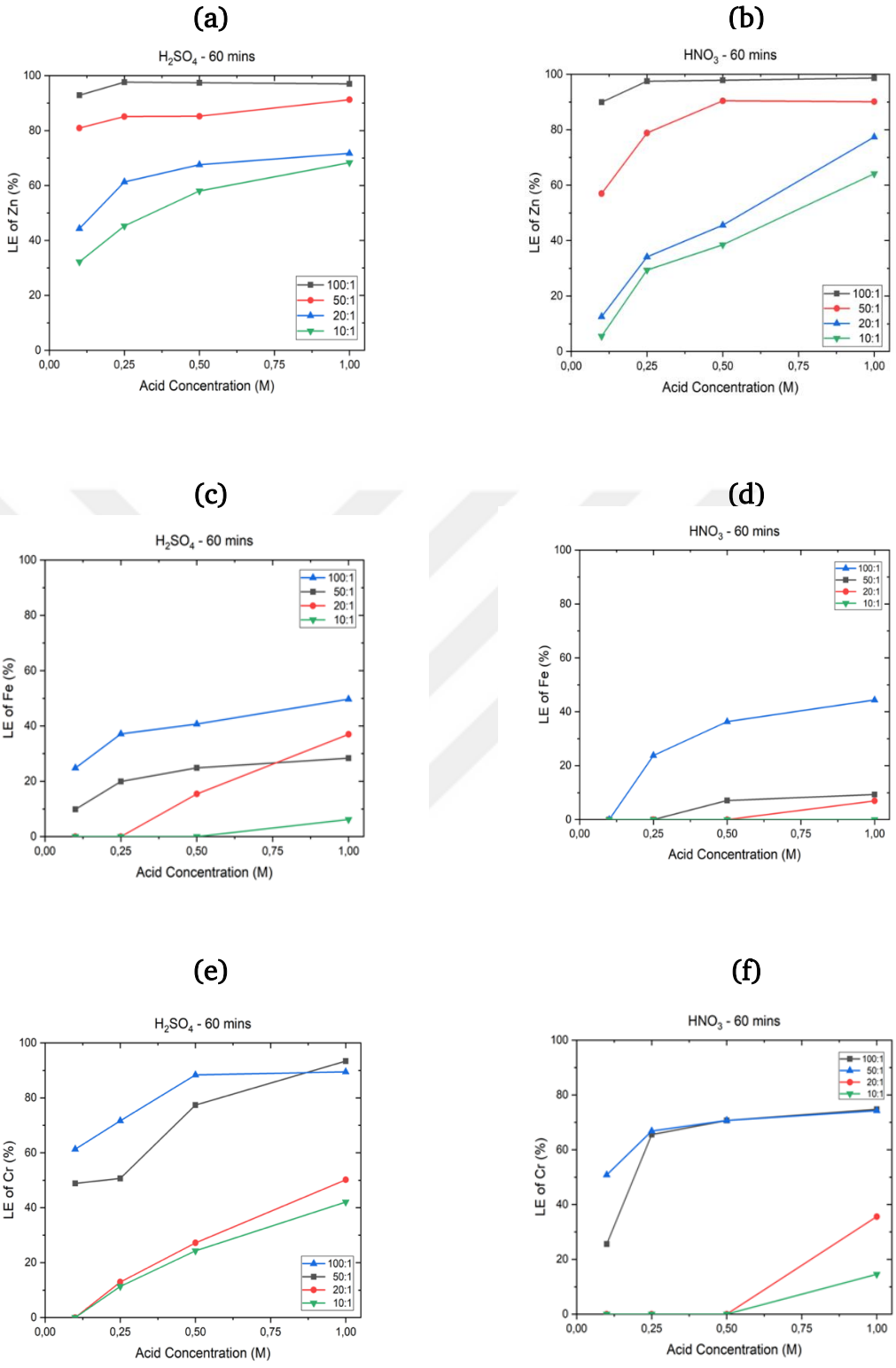


Figure 5.5 Effect of L-S ratio a) for Zn in H_2SO_4, b) for Zn in HNO_3, c) for Fe in H_2SO_4, d) for Fe in HNO_3, e) for Cr in H_2SO_4, f) for Cr in HNO_3.

In the leaching experiments performed at 100:1 L-S ratio at 0.05, 0.1, 0.25, 0.5 and 1 M sulfuric acid concentrations, the LE of Zn was determined to be 80.75%, 92.91% 97.66%, 97.44% and 97.01%, while LE of Fe was determined to be 9.86%, 24.81%, 37.13%, 40.68% and 49.69% and LE of Cr was determined to be 39.16%, 61.33%, 71.68%, 88.35 and 89.48%, respectively.

In the leaching experiments performed in the same L-S ratio at 0.05, 0.1, 0.25, 0.5 and 1 M nitric acid concentrations, the LE of Zn was determined to be 76.87%, 89.94% 97.55%, 97.86% and 98.65%, while LE of Fe was determined to be 0.00%, 0.00%, 23.81%, 36.36% and 44.38% and LE of Cr was determined to be 36.73%, 50.81%, 66.83%, 87.70 and 82.04% respectively.

In 50:1 L-S ratio at 0.05, 0.1, 0.25, 0.5 and 1 M sulfuric acid concentrations, the LE of Zn was determined to be 70.99%, 80.94% 84.01%, 85.24% and 91.27%, while LE of Fe was determined to be 0.00%, 9.86%, 19.95%, 24.88%, and 28.35% and LE of Cr was determined to be 35.52%, 48.87%, 50.65%, 77.35 and 93.37% respectively.

In the same L-S ratio at 0.05, 0.1, 0.25, 0.5 and 1 M nitric acid concentrations, the LE of Zn was determined to be 53.47%, 57.00%, 78.84%, 83.27% and 90.13. Fe was determined to do not dissolve until 0.25 M. For 0.5 and 1 M nitric acid concentrations LE of Fe was determined to be 7.09% and 9.32%, respectively. LE of Cr was determined to be 17.15%, 25.57%, 65.53%, 70.71 and 74.76% respectively.

For the 20:1 L-S ratio at 0.1, 0.25, 0.5 and 1 M sulfuric acid concentrations, the LE of Zn was determined to be 44.34% 61.32%, 67.61% and 71.70%. Fe was determined to do not dissolve until 0.25 M. For 0.5 and 1 M sulfuric acid concentrations LE of Fe was determined to be 15.41% and 36.98%, respectively. Cr was determined to do not dissolve until 0.1 M. For 0.25, 0.5 and 1 M sulfuric acid concentrations LE of Cr was determined to be 12.94%, 16.18 and 50.16% respectively.

For the same L-S ratio at 0.1, 0.25, 0.5 and 1 M nitric acid concentrations, the LE of Zn was determined to be 12.58%, 34.12% 45.60 and 77.36%. Fe was determined to do not dissolve until 0.5 M. For 1 M nitric acid concentration LE of

Fe was determined to be 6.93%. Cr was determined to do not dissolve until 0.5 M. For 1 M nitric acid concentration, LE of Cr was determined to be 2.08%.

In the leaching experiments conducted in 10:1 L-S ratio at 0.1, 0.25, 0.5 and 1 M sulfuric acid concentrations, the LE of Zn was determined to be 32.23% 45.28%, 58.02% and 68.30%. Fe was determined to do not dissolve until 0.5 M. For 1 M sulfuric acid concentration LE of Fe was determined to be 6.16%. Cr was determined to do not dissolve until 0.1 M. For 0.25, 0.5 and 1 M sulfuric acid concentrations LE of Cr was determined to be 1.07%, 2.29 and 3.97%, respectively.

In the leaching experiments conducted in the same L-S ratio at 0.1, 0.25, 0.5 and 1 M nitric acid concentrations, the LE of Zn was determined to be 5.50%, 29.40% 38.52 and 64.15%. Fe was determined to do not dissolve. Cr was determined to not dissolve until 0.5 M. For 1 M nitric acid concentration LE of Cr was determined to be 1.38%.

Kukurugya et al. (2015) determined that the L:S ratio is one of the defining parameters for determination of optimal acid content in the leaching solution [7].

The leaching efficiencies of Zn, Fe, and Cr were observed to rise with increasing L-S ratio for each acid concentration in both sulfuric acid and nitric acid solutions.

In the sulfuric acid medium, at a 10:1 L-S ratio, with increasing acid concentration Zn can be recovered with the efficiency of 68.30%. This amount reaches to 71.70% at 20:1 ratio, 91.27% at 50:1 ratio and 97.1% at 100:1 ratio. In nitric acid medium these amounts were determined as 64.15%, 77.36%, 90.13% and 98.65% respectively.

Fe can be recovered with the efficiency of 6.16% in the sulfuric acid medium, at a 10:1 L-S ratio. This amount reaches to 36.98% at 20:1 ratio, 28.35% at 50:1 ratio and 49.69% at 100:1 ratio. These amounts were determined as 0.00%, 6.93%, 9.32% and 44.38% for the nitric acid medium, respectively.

In the sulfuric acid medium, at a 10:1 L-S ratio Cr can be recovered with the efficiency of 3.97%. This amount reaches to 50.16% at 20:1 ratio, 93.37% at 50:1

ratio and 89.48% at 100:1 ratio. In nitric acid medium these amounts were determined as 1.38%, 2.08%, 74.76% and 82.04% respectively.

5.2.2. Effect of Acid Concentration

Effect of acid concentration was investigated at two different L-S ratios, 20:1 and 10:1 respectively. Leaching experiments were carried out at four different acid concentrations which were 0,1 0,25 0,5 and 1 M for both sulfuric acid and nitric acid solutions. To determine the effect of acid concentration, all experiments were done at 60 minutes.

Variation of LE of Zn, Fe and Cr at 20:1 L-S ratio with different acid concentrations are presented in Figure 5.6.

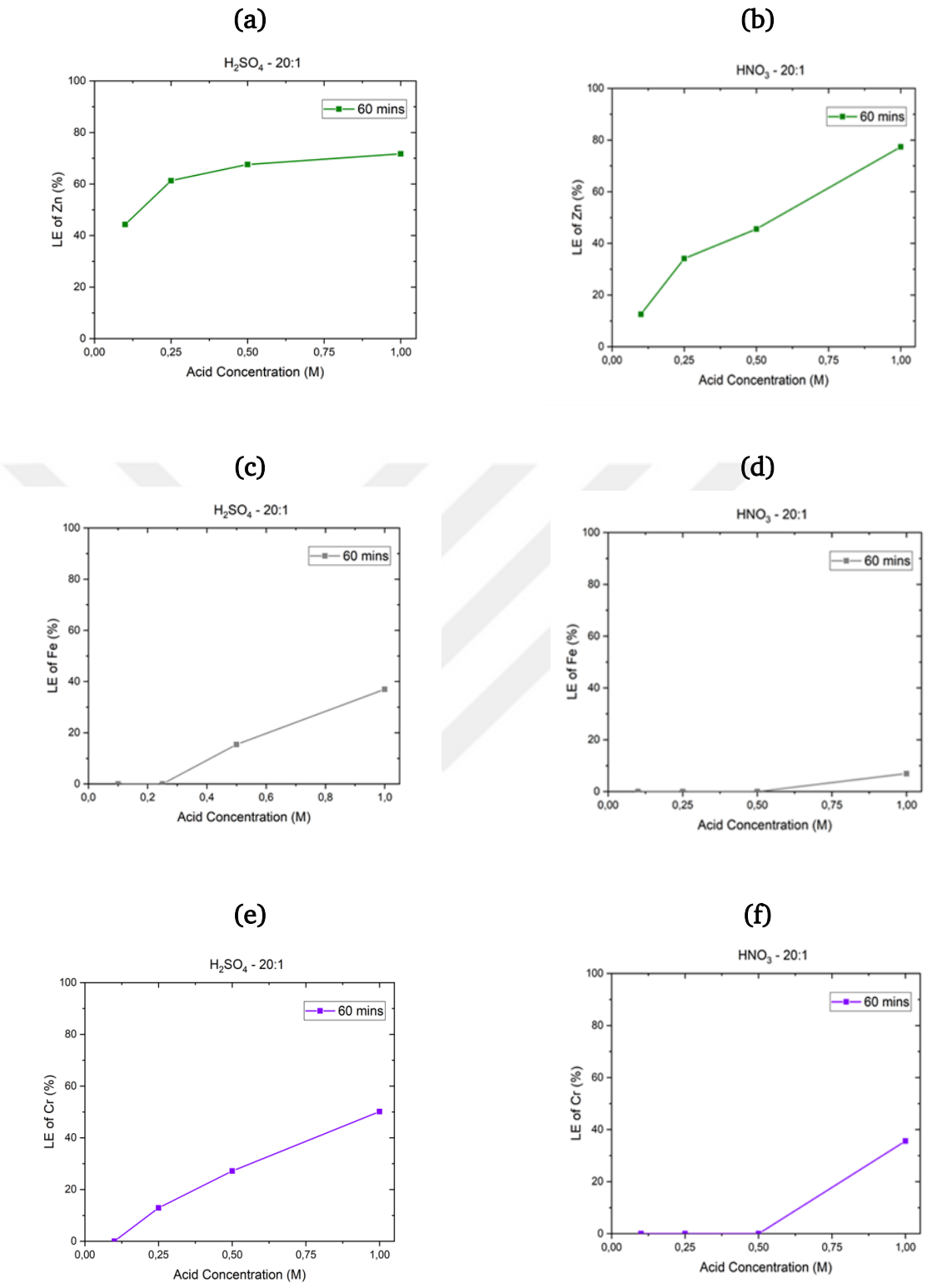


Figure 5.6 Effect of acid concentration at 20:1 L-S ratio a) for Zn in H_2SO_4, b) for Zn in HNO_3, c) for Fe in H_2SO_4, d) for Fe in HNO_3, e) for Cr in H_2SO_4, f) for Cr in HNO_3.

In the leaching experiments performed in 0.1 M sulfuric acid concentration, LE of Zn was determined to be 44.34%. Fe and Cr were determined to do not dissolve. In the leaching experiments performed in same nitric acid concentration, the LE of Zn was determined to be 12.58%. Fe and Cr were determined to do not dissolve.

For the in 0.25 M sulfuric acid concentration LE of Zn and Cr was determined to be 61.32% and 12.94%, respectively and Fe was determined to do not dissolve. For the same nitric acid concentration, the LE of Zn was determined to be 34.12%. Fe and Cr were determined to do not dissolve.

In the leaching experiments conducted in 0.5 M sulfuric acid concentration LE of Zn, Fe and Cr was determined to be 67.61%, 15.41% and 24.27%, respectively. In the experiments conducted in same nitric acid concentration, the LE of Zn was determined to be 45.60%. Fe and Cr were determined to do not dissolve.

In the leaching experiments performed in 1 M sulfuric acid concentration LE of Zn, Fe and Cr was determined to be 71.70%, 36.98% and 42.07%, respectively. In the leaching experiments performed in same nitric acid concentration, the LE of Zn, Fe and Cr was determined to be 77.36%, 6.93% and 35.60%, respectively.

Variation of LE of Zn, Fe and Cr at 10:1 L-S ratio with different acid concentrations are presented in Figure 5.7.

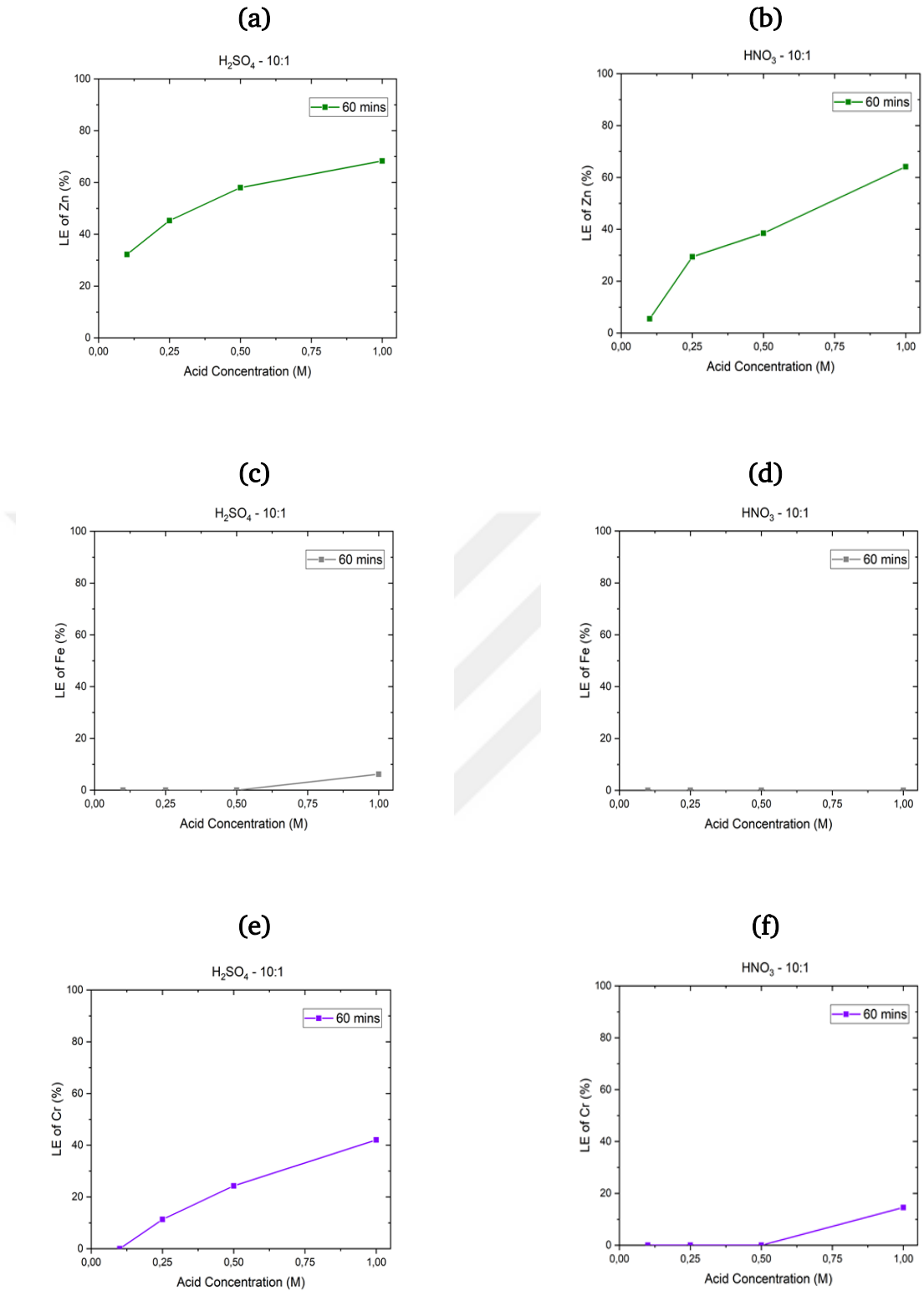


Figure 5.7 Effect of acid concentration at 10:1 L-S ratio a) for Zn in H_2SO_4, b) for Zn in HNO_3, c) for Fe in H_2SO_4, d) for Fe in HNO_3, e) for Cr in H_2SO_4, f) for Cr in HNO_3.

In the leaching experiments performed in 0.1 M sulfuric acid concentration, LE of Zn was determined to be 32.23%. Fe and Cr were determined to do not dissolve. the LE of Zn was determined to be 5.50%. Fe and Cr were determined to do not dissolve.

LE of Zn and Cr was determined to be 45.28% and 11.33%, respectively and Fe was determined to do not dissolve in the leaching experiments performed in 0.25 M sulfuric acid concentration. For the same nitric acid concentration, the LE of Zn was determined to be 29.40%. Fe and Cr were determined to do not dissolve.

For the 0.5 M sulfuric acid concentration, LE of Zn and Cr was determined to be 58.02% and 24.27%, respectively and Fe was determined to do not dissolve. For the same nitric acid concentration, the LE of Zn was determined to be 38.52%. Fe and Cr were determined to do not dissolve.

In the 1 M sulfuric acid leaching experiments, LE of Zn, Fe and Cr was determined to be 68.30%, 6.16% and 16.18%, respectively. For the nitric acid concentration, the LE of Zn, Fe and Cr was determined to be 64.15%, 0.00% and 14.56%, respectively.

Abdel-Aal et al. (2000) suggested that the higher the acid concentration, the better LE for zinc [74]. However, Habashi (1993) determined that, as the LE increases with increasing acid concentration, the dissolution of unwanted minerals and reagent consumption also increase [75].

Although the leaching efficiency of Zn for a 20:1 L-S ratio increases with increasing acid concentration in the sulfuric acid environment, Cr and Fe begin to dissolve at 0.25 M and 0.5 M, respectively. However, at a concentration of 0.1 M sulfuric acid, it was determined that Zn could be selectively recovered with the efficiency of 44.34%. In the nitric acid medium, it was determined that Fe and Cr did not dissolve at concentrations up to 0.5 M, whereas Zn could be recovered selectively with a 45.60% efficiency.

Similarly, for 10:1 L-S ratio Cr and Fe begin to dissolve at 0.25 M and 0.5 M, respectively. However, at a concentration of 0.1 M sulfuric acid, it was determined that Zn could be selectively recovered with the efficiency of 32.23%. In the nitric acid environment, it was observed that Fe does not dissolve in the determined

experimental parameters while Cr began to dissolve at concentrations above 0.5 M. It was determined that Zn could be selectively recovered at 0.5 M concentration with an efficiency of 38.52%.

5.2.3. Effect of Leaching Duration

Effect of leaching duration was investigated for five different acid concentrations which were 0,05, 0,1 0,25 0,5 and 1 M for both sulfuric acid and nitric acid solutions. Leaching experiments were carried out at four different durations 15, 30, 60 and 90 minutes respectively. To determine the effect of leaching duration, all experiments were done at 50:1 L-S ratio.

Variation of LE of Zn, Fe and Cr with different durations are given in Figure 5.8.

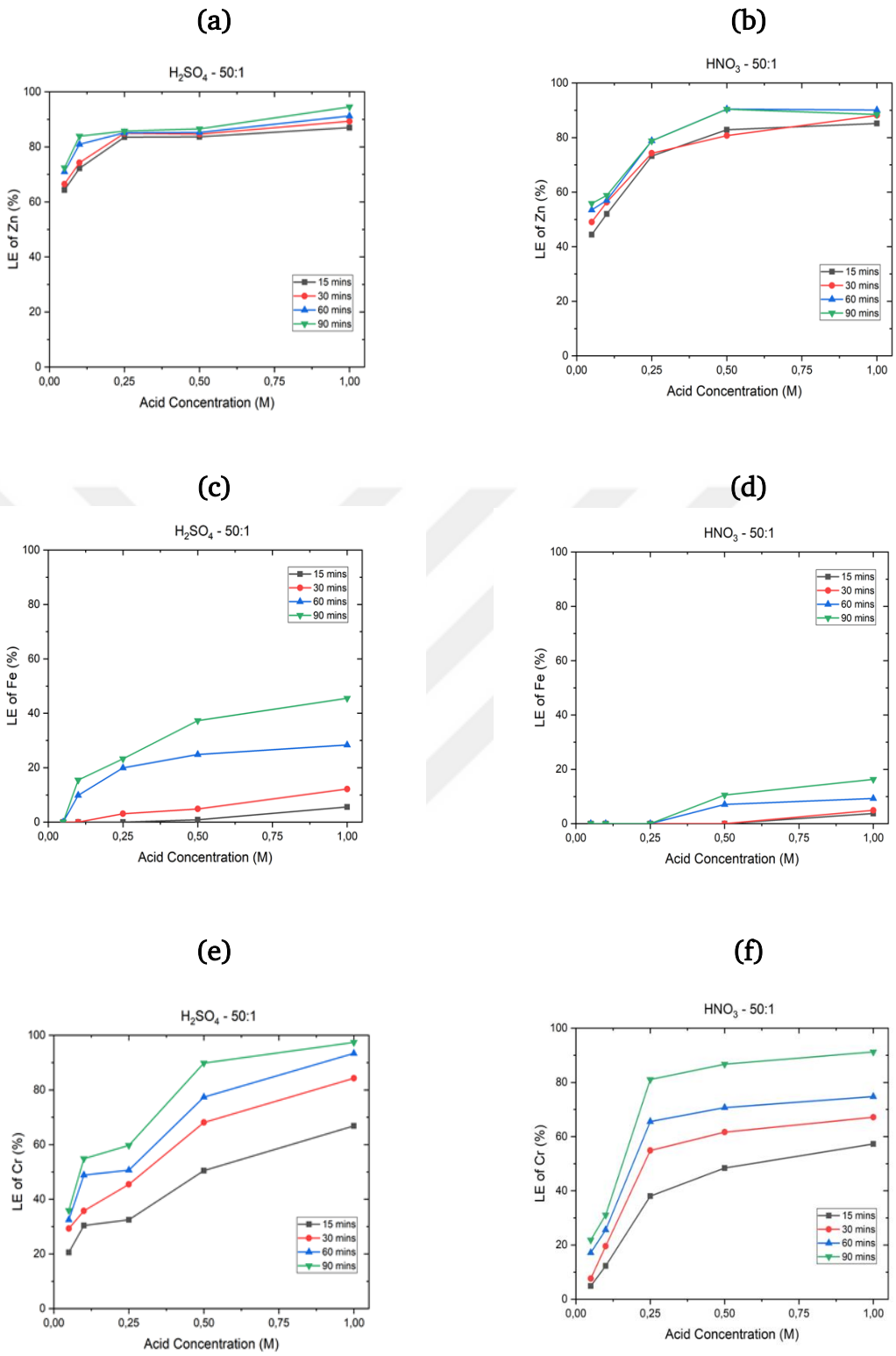


Figure 5.8 Effect of leaching duration a) for Zn in H_2SO_4, b) for Zn in HNO_3, c) for Fe in H_2SO_4, d) for Fe in HNO_3, e) for Cr in H_2SO_4, f) for Cr in HNO_3.

In the leaching experiments performed in 15 minutes at 0.05, 0.1, 0.25, 0.5 and 1 M sulfuric acid concentrations, the LE of Zn was determined to be 64.34%, 72.22% 83.55%, 83.68% and 87.00%. while LE of Fe was determined to be 0.00%, 0.00%, 0.00%, 0.85% and 5.55% and LE of Cr was determined to be 20.55%, 30.42%, 32.52%, 50.49 and 66.83%, respectively. In the leaching experiments performed in same duration at 0.05, 0.1, 0.25, 0.5 and 1 M nitric acid concentrations, the LE of Zn was determined to be 44.43%, 52.00%, 73.27%, 82.89% and 85.19%, while LE of Fe was determined to be 0.00%, 0.00%, 0.00%, 0.00% and 3.78% and LE of Cr was determined to be 4.85%, 12.30%, 38.03%, 48.38 and 57.28%, respectively.

For 30 minutes at 0.05, 0.1, 0.25, 0.5 and 1 M sulfuric acid concentrations, the LE of Zn was determined to be 66.49%, 74.26% 81.95%, 80.63% and 84.29%, while LE of Fe was determined to be 0.00%, 0.00%, 3.08%, 4.85% and 12.17% and LE of Cr was determined to be 29.29%, 35.76%, 45.47%, 68.12 and 84.30%, respectively. For the same duration at 0.05, 0.1, 0.25, 0.5 and 1 M nitric acid concentrations, the LE of Zn was determined to be 49.07%, 56.31% 74.29%, 80.74% and 88.14%, while LE of Fe was determined to be 0.00%, 0.00%, 0.00%, 0.00% and 4.93% and LE of Cr was determined to be 7.61%, 19.58%, 54.85%, 61.65 and 67.15% respectively.

For the 60 minutes leaching experiments at 0.05, 0.1, 0.25, 0.5 and 1 M sulfuric acid concentrations, the LE of Zn was determined to be 70.99%, 80.94% 84.01%, 85.24% and 91.27%, while LE of Fe was determined to be 0.00%, 9.86%, 19.95%, 24.88% and 28.35% and LE of Cr was determined to be 32.52%, 48.87%, 50.65%, 77.35 and 93.37%, respectively. For the same duration at 0.05, 0.1, 0.25, 0.5 and 1 M nitric acid concentrations, the LE of Zn was determined to be 53.47%, 57.00% 78.84%, 83.27% and 90.13%, while LE of Fe was determined to be 0.00%, 0.00%, 0.00%, 7.09% and 9.32% and LE of Cr was determined to be 17.15%, 25.57%, 65.53%, 70.71 and 74.76% respectively.

In the leaching experiments conducted in 90 minutes at 0.05, 0.1, 0.25, 0.5 and 1 M sulfuric acid concentrations, the LE of Zn was determined to be 72.37%, 83.90% 85.25%, 85.55% and 94.53%, while LE of Fe was determined to be 0.00%, 15.49%, 23.27%, 37.29% and 45.53% and LE of Cr was determined to be 35.92%,

54.85%, 59.71%, 89.81 and 97.41% respectively. In the leaching experiments conducted in same duration at 0.05, 0.1, 0.25, 0.5 and 1 M nitric acid concentrations, the LE of Zn was determined to be 55.90%, 58.84% 78.77%, 90.42% and 88.47%, while LE of Fe was determined to be 0.00%, 0.00%, 0.00%, 10.55% and 16.33% and LE of Cr was determined to be 21.84%, 31.07%, 81.07%, 86.73 and 91.26% respectively.

Kukurugya et al. (2015) determined that, leaching of zinc is a fairly rapid process. All zinc that might possible to dissolve, will do so within 15 minutes. They also determined that, the kinetics of iron leaching into solution are slower compared to zinc [7].

It was observed that the leaching time has no significant effect on Zn recovery in sulfuric acid and nitric acid environments, and that the Zn leaching efficiency does not alter significantly after 15 minutes for each acid concentration investigated within the scope of the study. It was determined that Fe exhibits no significant dissolution during the first 30 minutes in both acidic environments, and Fe recovery began after 60 minutes. It is clearly apparent that the Cr recovery is significantly dependent on the duration of leaching in both acid media, and that the Cr recovery increases with increasing duration for each acid concentration investigated within the scope of the study.

In general, it has been determined that sulfuric acid solutions typically yield higher Zn leaching efficiencies than nitric acid solutions. However, since leaching efficiencies of Fe and Cr are also greater in sulfuric acid solutions, it is determined that, nitric acid is more appropriate for selective recovery of Zn from ferrochrome flue dusts. The determined optimum solution parameters to conduct precipitation experiments are given in Table 5.2.

Table 5.2 Leaching parameters of the optimum solutions.

Sample #	L-S Ratio	Acid Conc. (M)	Leach Time (min)	LE of Zn (%)	Zn Conc. (*10^{-3}) (M)	LE of Fe (%)	Fe Conc. (*10^{-3}) (M)	LE of Cr (%)	Cr Conc. (*10^{-3}) (M)
1	100:1	0.05	60	76.87	7.7	0.00	0.00	36.73	0.36
2	50:1	0.25	5	70.71	13.8	0.00	0.00	21.36	0.40
3	20:1	1	60	77.36	46.4	0.00	0.00	35.60	2.08
4	10:1	1	60	64.15	63.8	6.93	0.85	14.56	1.38

EAF dusts were leached with nitric acid solutions with various concentrations (0.1-1 M) for 15 minutes. Obtained results are presented in Figure 5.9.

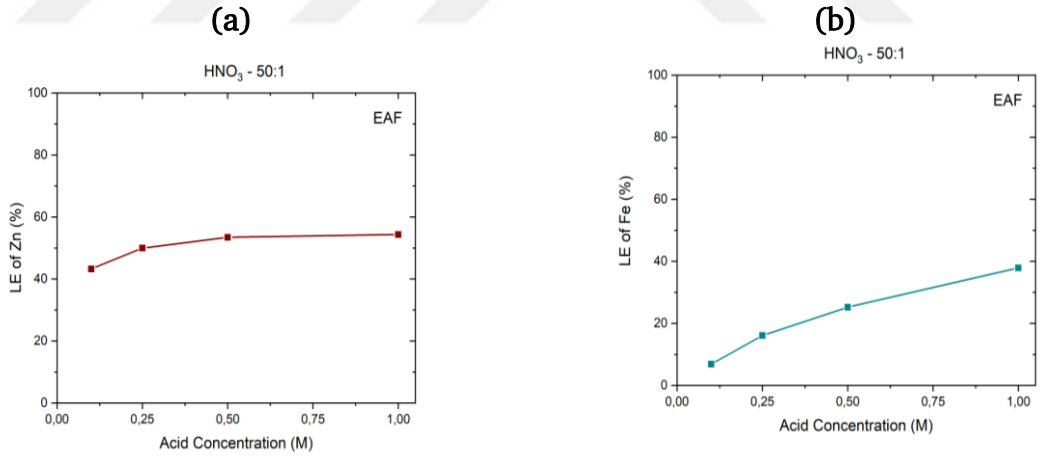


Figure 5.9 EAF leaching results.

In the leaching experiments performed in 15 minutes at 0.1, 0.25, 0.5 and 1 M nitric acid concentrations, the LE of Zn was determined to be 43.27%, 49.98% 53.47% and 54.35%, while LE of Fe was determined to be 2.59%, 6.09%, 9.54%, and 14.35%, respectively.

Optimum acid concentration to conduct precipitation process was selected as 0.1 M. In this concentration, dissolved Zn and Fe concentrations were determined to be $56.56x10^{-3}$ and $1.20x10^{-3}$ M respectively.

5.3 Precipitation of ZnS

The main aim of the precipitation experiments was to obtain ZnS powders from the leach solutions with the highest purity while inhibiting the possible precipitation of other possible compounds such as $Zn(OH)_2$ and FeS. From the literature survey, it was determined that, to achieve selective ZnS precipitation with a high efficiency pH of the solution must be maintained in 4-6 range. During precipitation experiments, sodium sulfide solutions were used as the sulphur source and the effects of dissolved zinc ion concentration, and sodium sulfide concentration on the PE were investigated for each solution. All precipitation experiments were carried out at room temperature. Reactions that occur during ZnS precipitation in sulfuric acid media is given in Eq 5.3 and Eq 5.4 respectively.

$$Na_2S_{(aq)} + H_2SO_4 = Na_2SO_{4(aq)} + H_2S_{(g)} \quad (5.3)$$

$$ZnSO_{4(aq)} + H_2S_{(g)} = ZnS_{(s)} + H_2SO_4 \quad (5.4)$$

In the preliminary experiments, it was determined that S_8 was formed as well as ZnS as a result of the precipitation process applied to the sulfuric acid solutions. The reaction take place in the precipitation of S_8 is given in Eq 5.5. XRD pattern of the sulfuric acid precipitation sample is given in Fig 5.10. S_8 peak was identified at 22 ° 2θ degree (PDF code: 00-008-0247).

$$H_2S_{(g)} + H_2SO_4 = S_8 + SO_{2(g)} + 2H_2O \quad (5.5)$$

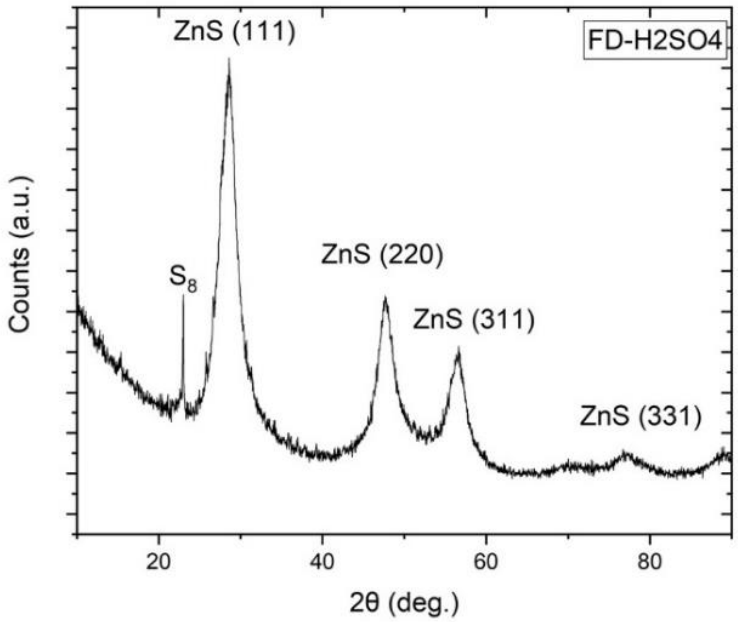


Figure 5.10 XRD pattern of the sulfuric acid precipitation sample.

In addition to S_8 formation in sulfuric acid media, as nitric acid solutions were determined to be more suitable for selective recovery of Zn as a result of leaching experiments, precipitation experiments were carried out with nitric acid leach solutions. Reactions that occur during ZnS precipitation in nitric acid media is given in Eq 5.6 and Eq 5.7 respectively.

$$Na_2S_{aq} + HNO_3 = H_2S_{(g)} + NaNO_3 \quad (5.6)$$

$$Zn(NO_3)_2 + H_2S_{(g)} = ZnS_{(s)} + HNO_3 \quad (5.7)$$

Results of the FFD precipitation experiments are given in Table 5.3.

Table 5.3 FFD precipitation experiment results.

Sample #	Zn Concentration (*10^{-3} M)	L-S Ratio	Zn:Na_2S Molar Ratio	PE (%)
1	7.7	100:1	1:1	8.42
			1:2	83.72
			1:3	94.98
2	13.8	50:1	1:1	31.48
			1:2	88.48
			1:3	98.06

Table 5.3 FFD precipitation experiment results (continued)

3	46,4	20:1	1:1	74.02
			1:2	93.96
			1:3	98.20
4	63.8	10:1	1:1	95.36
			1:2	97.48
			1:3	98.70

EAFD sample was precipitated with 1:2 Zn-Na_2S molar ratio and 94.24 % PE was achieved.

5.3.1. Effect of Zn Concentration

Effect of the dissolved Zn ion concentration in the leach solutions on the PE of ZnS was investigated for three different Zn-Na_2S molar ratios, 1:1, 1:2 and 1:3 respectively and obtained results are presented in Figure 5.11.

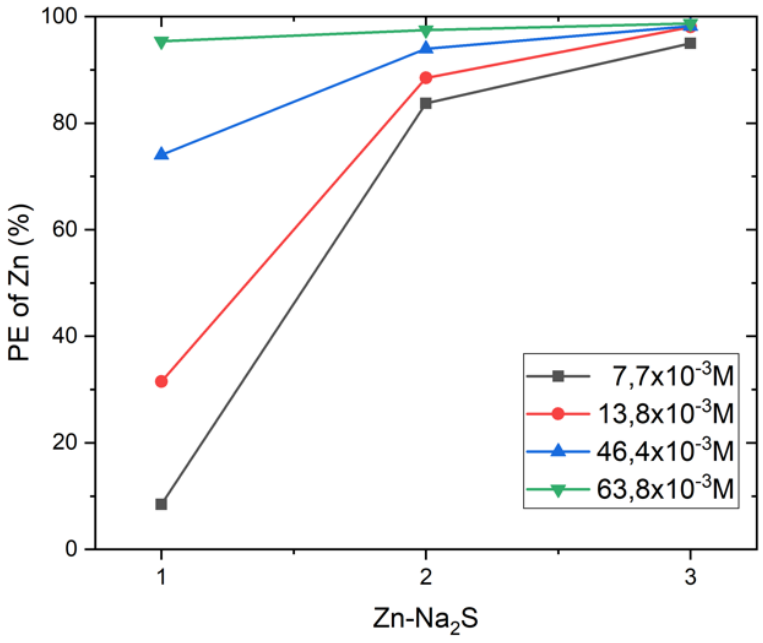


Figure 5.11 Effect of Zn concentration on precipitation.

For the 7.7x10^{-3} M Zn solution, PE of ZnS was determined to be 8.42%, 83.72% and 94.98% for 1:1, 1:2 and 1:3 Zn:Na_2S molar ratios, respectively. When Zn

concentration is increased to $13.8x10^{-3}$ M, PE of ZnS was determined to be 31.48%, 88.48% and 98.06%, respectively. For the $46.4x10^{-3}$ M Zn solution, PE of ZnS is increased to 74.02%, 93.96% and 98.20%, respectively. For the $63.8x10^{-3}$ M solution, PE of ZnS was determined to be 95.36%, 97.48% and 98.70%, respectively.

Mersmann (1999) determined that, supersaturation level of the solution determines the nucleation and growth of particles, according to crystallization theory [76].

Nomura et al. (2000) determined that, zinc sulphide will precipitate when zinc ions are present in the solution with a sufficient concentration. The concentration of zinc sulphide monomer in the solution rises progressively until it reaches a specific critical supersaturation concentration. Then, the nuclei of radius r are generated immediately by homogeneous nucleation. They also determined that, the low precipitant concentrations tend to facilitate particle growth on preexisting solids, whereas high precipitant concentrations result in the rapid creation of new solid particles, which increases particle number while decreasing particle size. [77].

According to experiment results, it was observed that, PE of ZnS is critically dependent on the initial Zn concentration in the solution in a 1:1 Zn:Na_2S molar ratio, and this dependency reduces as the sulphur ratio increases. For an effective precipitation at this ratio, it was determined that the initial Zn ion concentration in the solution should be $50x10^{-3}$ M or higher.

5.3.2. Effect of Na_2S Concentration

Effect of the Na_2S concentration on the PE of ZnS was investigated for four different Zn concentration, $7.7x10^{-3}$ M, $13.8x10^{-3}$ M, $46.4x10^{-3}$ M and $63.8x10^{-3}$ M respectively and presented in Figure 5.12.

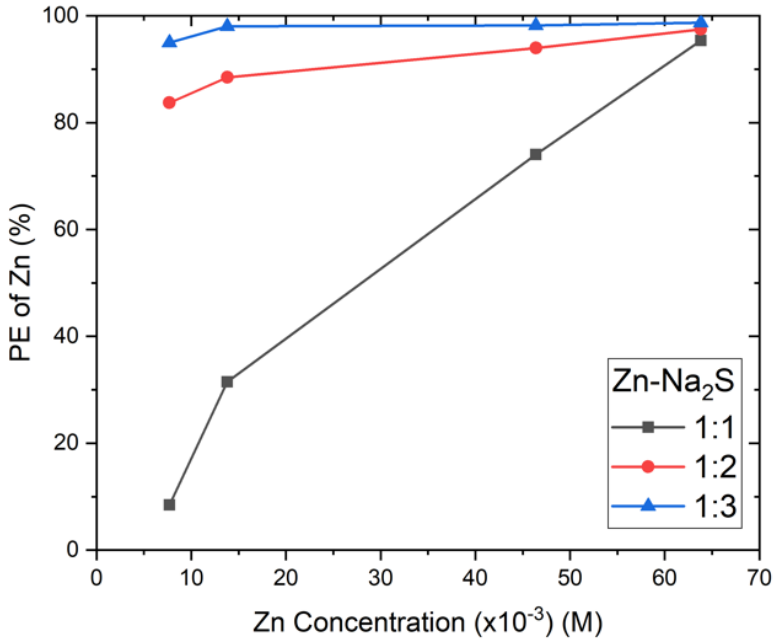


Figure 5.12 Effect of Na_2S concentration on precipitation.

For the 1:1 Zn:Na_2S molar ratio, PE of ZnS was determined to be 8.42%, 31.48% 74.02 and 95.36 with increasing initial Zn concentration, respectively. When the Zn:Na_2S molar ratio is increased 1:2, PE of ZnS was determined to be 83.72%, 88.48% 93.96 and 97.48, respectively. When the Zn:Na_2S molar ratio is reached to 1:3, PE of ZnS was determined as 94.98%, 98.06% 98.20 and 98.70, respectively.

Nomura et al. (2000) observed that, increasing initial sulfide concentration shortens the nucleation time and increases the particle number concentration. [77].

Despite the very low initial Zn concentration in the solution, it has been determined that the precipitation efficiency can reach roughly 95% as the sulfur level increases due to the increasing initial sulfide concentration.

5.3.3. Characterization of the Precipitates

Characterization of produced ZnS particles were conducted by XRD, XPS, SEM and Mastersizer analyses.

XRD pattern of the FC-ZnS sample is presented in Figure 5.13. Characteristic ZnS peaks were identified (JCPDS: 01-080-0020).

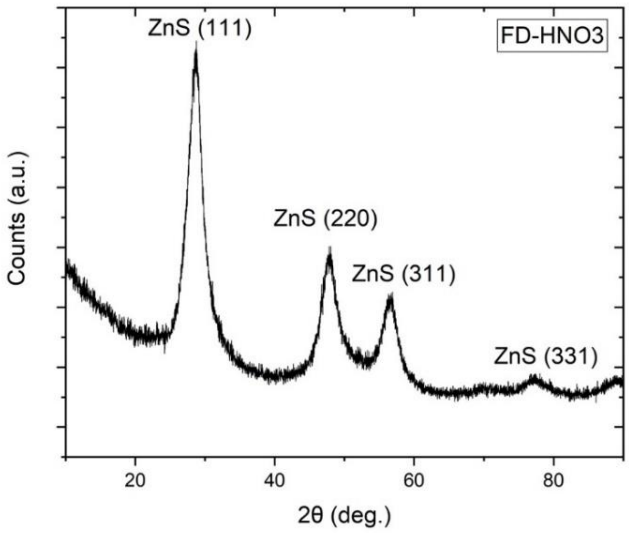


Figure 5.13 XRD pattern of FC-ZnS sample.

XRD pattern of the EAF-ZnS sample is presented in Figure 5.14. Characteristic ZnS peaks were identified (JCPDS: 01-080-0020).

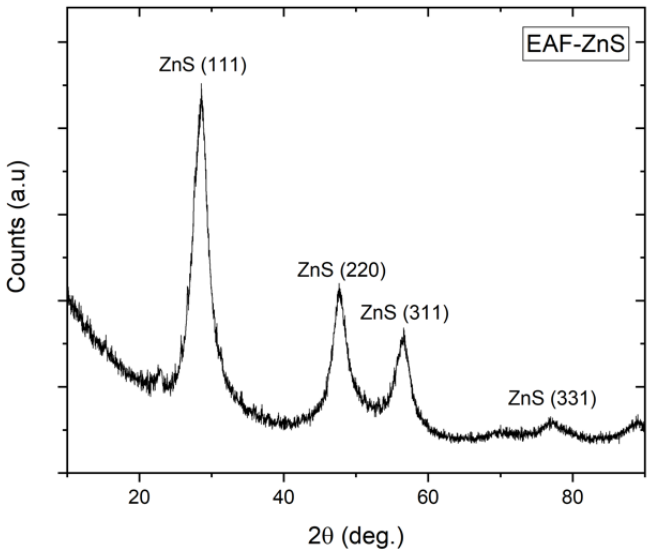


Figure 5.14 XRD pattern of EAF-ZnS sample.

XPS spectra of the FC-ZnS, EAF-ZnS and REF-ZnS samples are presented in Figure 5.15.

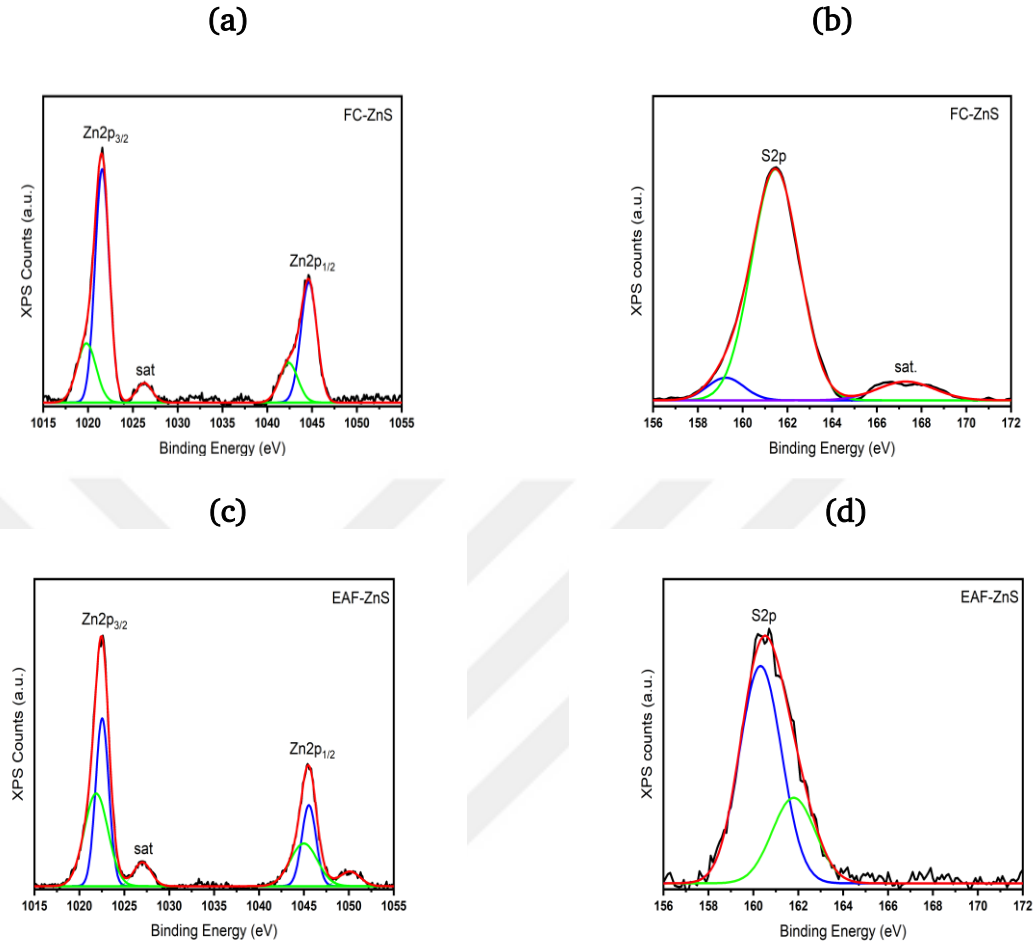


Figure 5.15 XPS spectra of a) FC-Zn2p, b) FC-S2p, c) EAF-Zn2p, d) EAF-S2p.

$Zn2p_{3/2}$, $Zn2p_{1/2}$ and S2p peaks were identified at about 1021.6 eV, 1044.7 eV and 161 eV respectively, for each sample [78].

The morphological characteristics and microanalyses of the FC-ZnS and EAF-ZnS samples were investigated by SEM, which was attached to an Energy-Dispersive X-ray Spectroscopy (EDS) unit for chemical analyses. SEM images of the FC-ZnS and EAF-ZnS samples are presented in Figure 5.16.

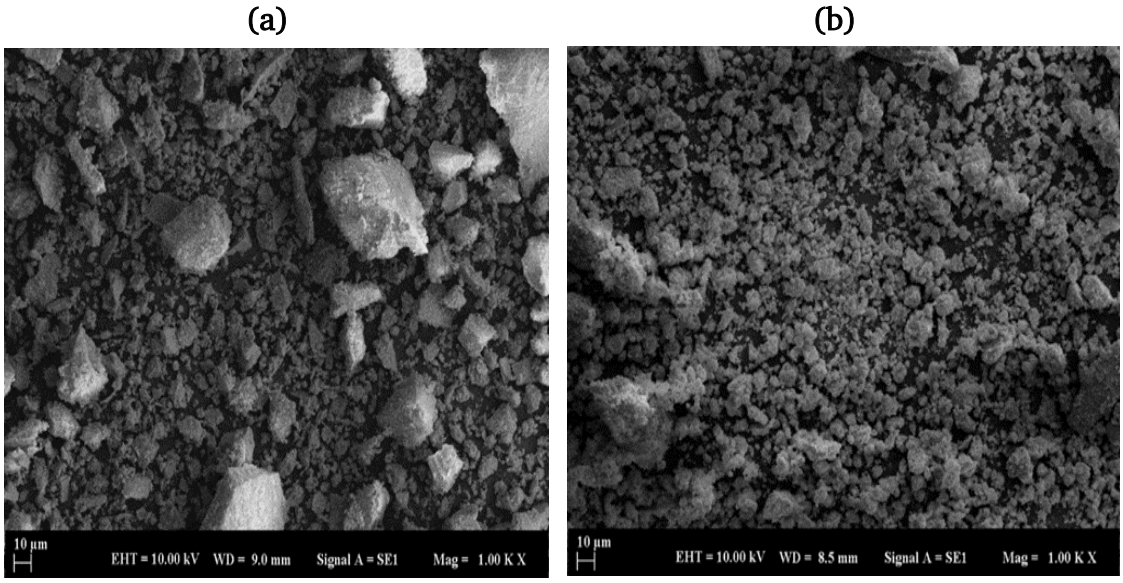


Figure 5.16 SEM images a) FC-ZnS, b) EAF-ZnS.

Spherical and agglomerated particles were observed for both samples. Also, it was observed that, the grain size distribution of EAF-ZnS sample is more homogeneous.

SEM-EDS mapping results of the FC-ZnS and EAF-ZnS samples are presented in Figure 5.17.

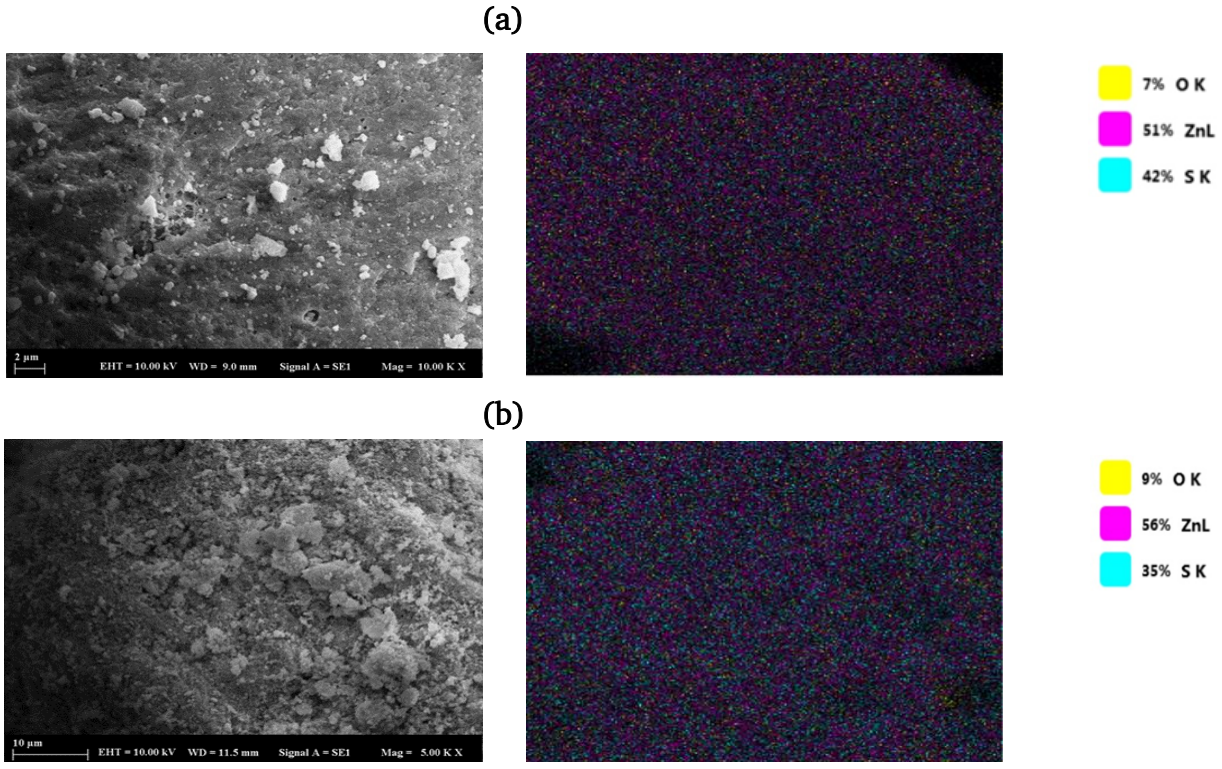
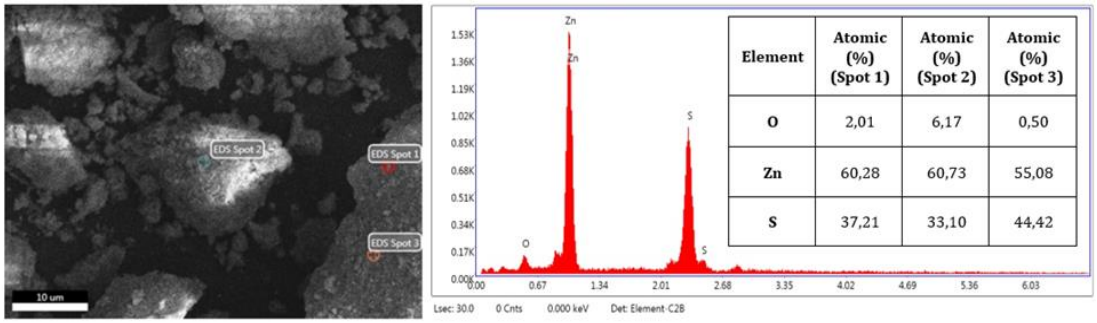


Figure 5.17 SEM-EDS mapping results of a) FC-ZnS, b) EAF-ZnS.

From the mapping results, it was determined that ZnS particles are homogeneously distributed for both samples.

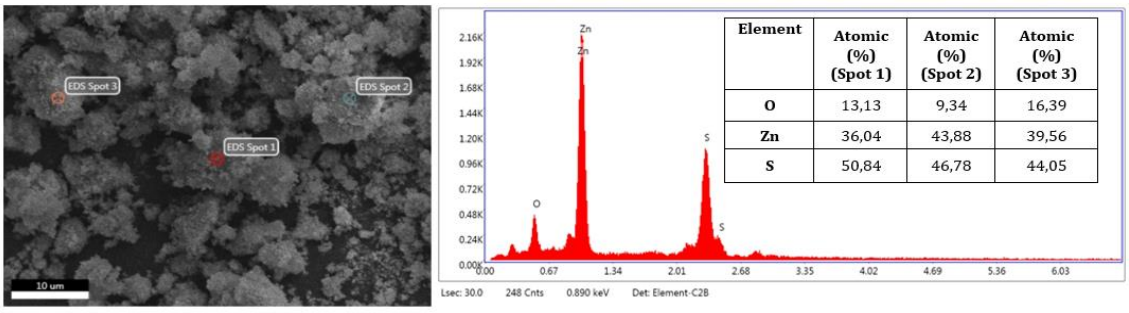
SEM-EDS spectra and elemental composition of the FC-ZnS and EAF-ZnS samples are presented in Figure 5.18.

(a)



Element	Atomic (%) (Spot 1)	Atomic (%) (Spot 2)	Atomic (%) (Spot 3)
O	2,01	6,17	0,50
Zn	60,28	60,73	55,08
S	37,21	33,10	44,42

(b)



Element	Atomic (%) (Spot 1)	Atomic (%) (Spot 2)	Atomic (%) (Spot 3)
O	13,13	9,34	16,39
Zn	36,04	43,88	39,56
S	50,84	46,78	44,05

Figure 5.18 SEM-EDS spectra of a) FC-ZnS, b) EAF-ZnS.

Particle size distribution and the specific surface areas of the samples were determined by Mastersizer analyses and the results are presented in Figure 5.19.

(a) (b)

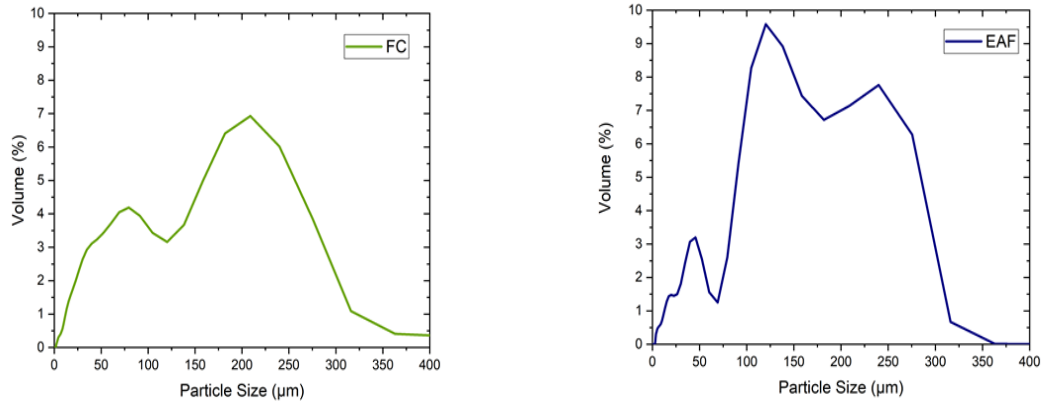


Figure 5.19 Particle size distributions of a) FC-ZnS, b) EAF-ZnS.

It was observed that samples present a heterogeneous distribution of particle size between 50-300 μm. The SEM images confirm the conclusion that the FC-ZnS sample has a larger particle size distribution. Specific surface area of the FC-ZnS and EAF-ZnS samples were determined as 0.141 m^2g^{-1} and 0.132 m^2g^{-1}, respectively.

5.4 Production of Supercapacitors

In the scope of the study, asymmetric type hybrid coin cell supercapacitors were produced by using a mixture of the produced ZnS and carbon black at the anode, graphite at the cathode, and 2 M KOH solution as the electrolyte.

5.4.1. Morphological and Chemical Characterization of the Produced Electrodes

Homogeneity and elemental distribution of the produced electrodes were investigated by FE-SEM analyses.

FE-SEM image of the FC2 sample is presented in Figure 5.20.

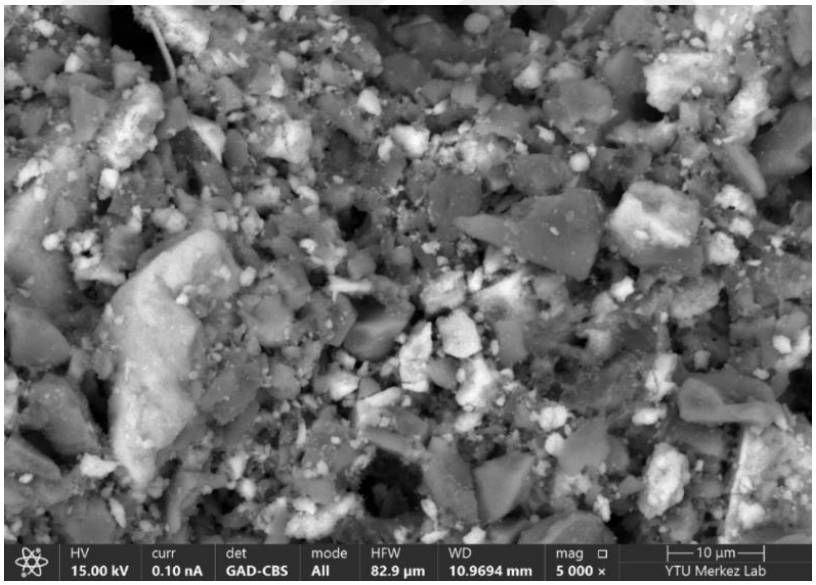


Figure 5.20 FE-SEM image of the FC2 sample.

A non-uniform structure with large particles was observed for FC2 sample.

EDS mapping result of the FC2 sample is presented in Figure 5.21.

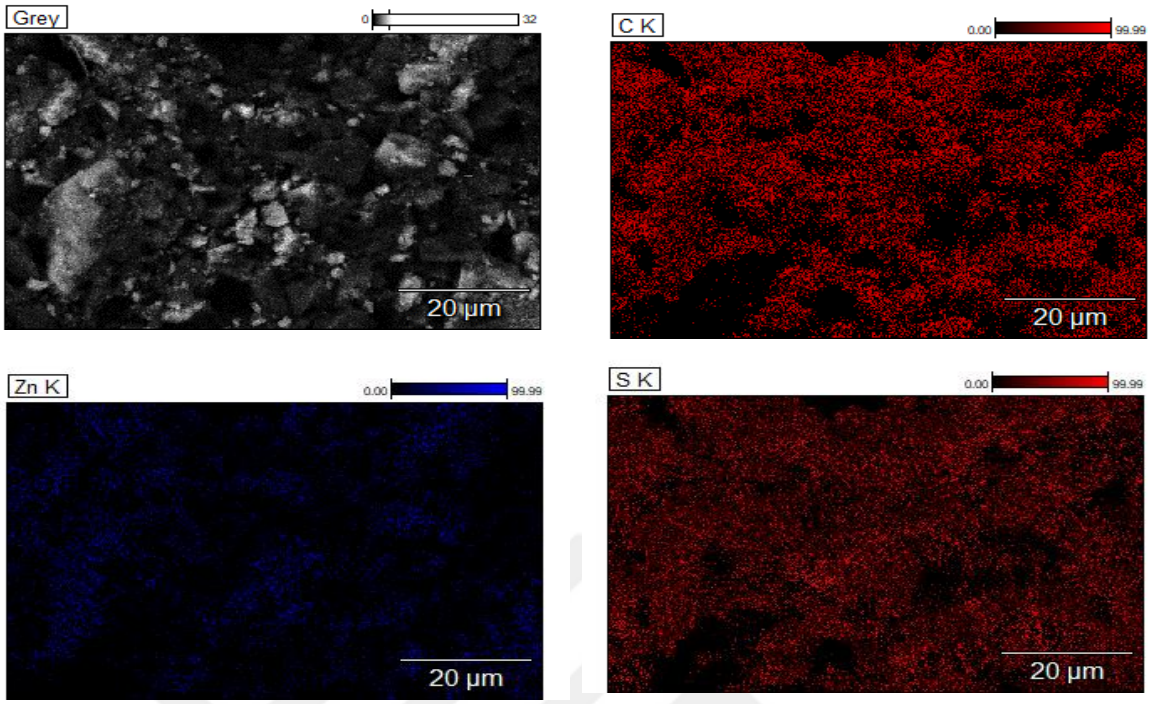


Figure 5.21 EDS elemental mapping of FC2 sample.

From the mapping result, it was determined that ZnS and carbon black particles are homogeneously distributed through the sample.

FE-SEM image of the EAF2 sample is presented in Figure 5.22.

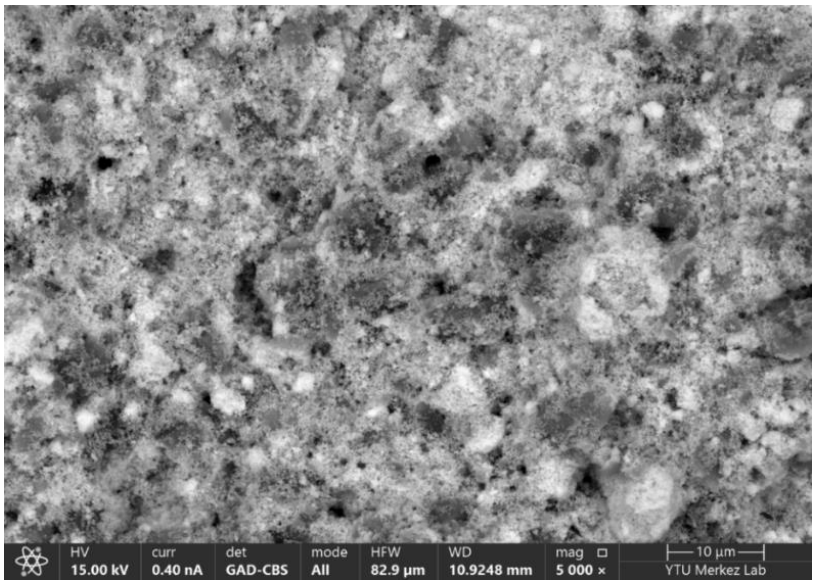


Figure 5.22 FE-SEM image of the EAF2 sample.

For EAF2 sample, a reticulated, and also more homogeneous structure was observed compared to FC2.

EDS mapping result of the EAF2 sample is presented in Figure 5.23.

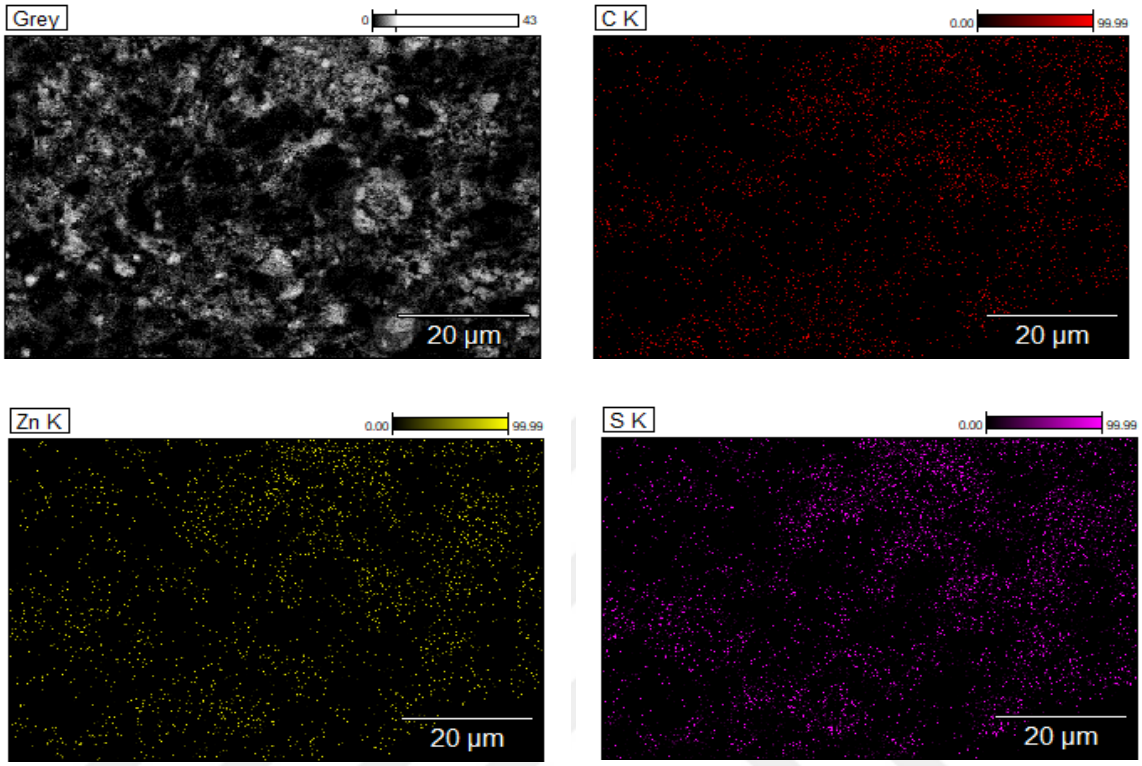


Figure 5.23 EDS elemental mapping of EAF2 sample.

The mapping result confirmed the homogeneous distribution of ZnS and carbon black particles through the sample. Furthermore, it was determined that the sample contains a significant amount of porosity.

Electrochemical characterization of the supercapacitors was determined by the CV, GCD and EIS analyses conducted in two electrode system.

5.4.2. Cyclic Voltammetry

The fundamental capacitive properties of the prepared supercapacitors were investigated with the cyclic voltammetry (CV) analyses. The shapes of the cyclic voltammograms and the obtained current values were directly related to the capacitive properties of the materials [79].

The suitable working potential range of the produced supercapacitors was determined as (-0.6 – 1.2 V) by CV analyses conducted at 100 mVs^{-1} scanning rate.

In this potential range, the highest peak currents and capacitive behaviors were determined in the system. Indeed, there was no gas evolution reactions in the studied potential range. Further electrochemical characterizations in CV was conducted between -0.6 V and 1.2 V. Obtained voltammograms during the determination of the potential range are presented in Figure 5.24.

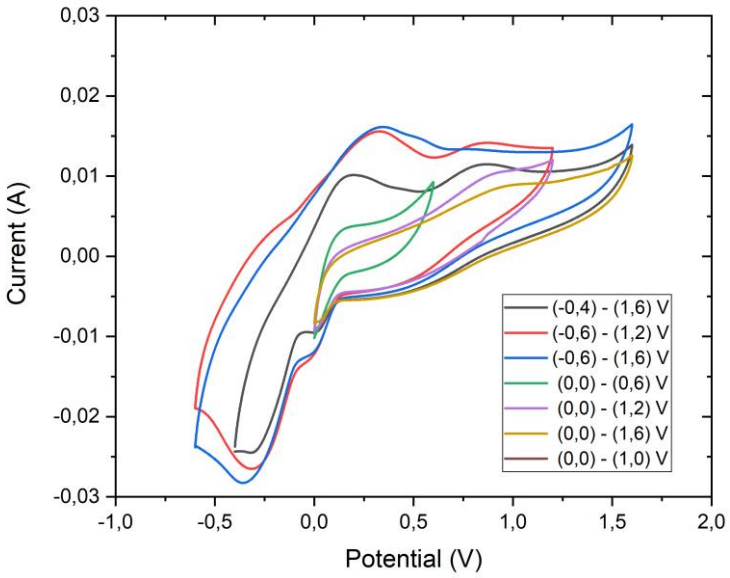


Figure 5.24 Determination of the potential range.

It was observed that, the cyclic voltammograms of the sample did not exhibit a rectangular characteristic, as in the EDLC, which stores energy only using an electrostatic mechanism. This demonstrates that, faradaic (pseudocapacitive) processes are effective in the energy storage mechanism of the sample, which are heavily impacted by ion diffusion and charge transfer limits.

CV analyzes were performed at scanning rates of 10, 20, 40, 50, 60, 80, 100, 200, 300, 400 and 500 mVs^{-1} for FC2, FC3, FC4 compounds in the determined potential range and the obtained voltammograms are presented in Figure 5.25.

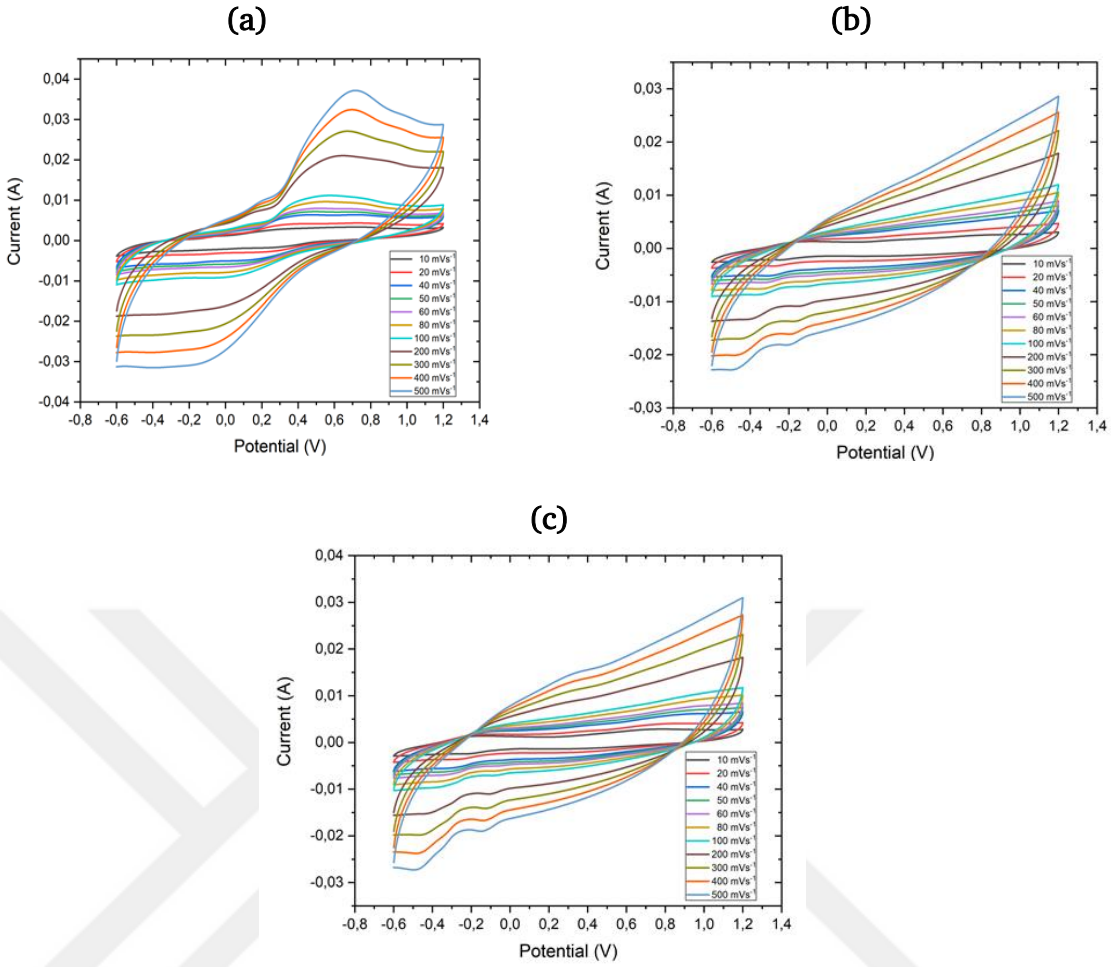


Figure 5.25 Cyclic voltammograms obtained at different scan rates a) FC2, b) FC3, and c) FC4.

The increase in current as a function of increasing scanning speed indicates that the mass transfer in the studied supercapacitors is predominantly diffusion-controlled. The oxidation peak, which was detected in the FC2 sample at a potential of about 0.7V, was not observed in the FC3 and FC4 samples. This is due to the fact that the ZnS ratio, which determines the pseudocapacitive behavior, is lower in the relevant samples. This result also demonstrates that the electrical double layer mechanism is more dominant in the energy storage process of FC3 and FC4 samples which contain higher amount of activated carbon.

CV analyzes were performed at scanning rates of 10, 20, 40, 50, 60, 80, 100, 200, 300, 400 and 500 mVs^{-1} for EAF2 sample in the determined potential range and the obtained voltammograms are presented in Figure 5.26.

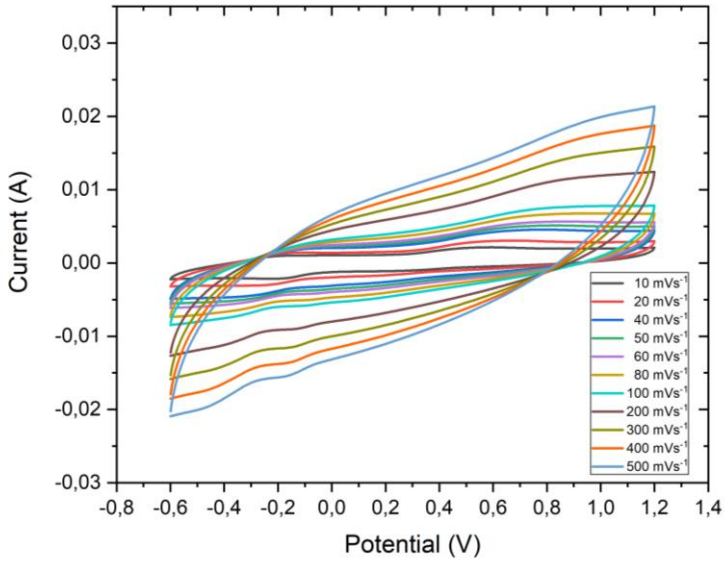


Figure 5.26 Cyclic voltammograms obtained at different scan rates for EAF2.

The specific capacitance values of the supercapacitors were determined for each scanning rate with Eq 5.8 and presented in Table 5.4.

$$C_s = \frac{area\ under\ the\ curve}{\Delta V * scan\ rate * weight\ of\ electrodes} \tag{5.8}$$

Table 5.4 Specific capacitance values of the supercapacitors.

FC2		FC3		FC4		EAF2	
Scan Rate (mVs^{1})	Specific Capacitance (Fg^{-1})	Scan Rate (mVs^{1})	Specific Capacitance (Fg^{-1})	Scan Rate (mVs^{1})	Specific Capacitance (Fg^{-1})	Scan Rate (mVs^{1})	Specific Capacitance (Fg^{-1})
10	1723.57	10	1614.48	10	1557.58	10	1293.94
20	594.61	20	583.50	20	576.09	20	460.43
40	226.85	40	215.07	40	211.78	40	170.36
50	159.19	50	155.96	50	152.79	50	123.23
60	121.55	60	120.26	60	116.78	60	94.56
80	80.81	80	79.71	80	76.60	80	62.54
100	58.86	100	57.95	100	55.19	100	45.19
200	26.21	200	21.18	200	19.39	200	16.21
300	14.24	300	11.62	300	10.29	300	8.81
400	9.22	400	7.55	400	6.52	400	5.71
500	6.57	500	5.39	500	4.55	500	4.06

It was determined that the specific capacitance values of the FC2 sample which contains the highest ZnS amount was greater than other samples for each scanning

rate. Specific capacitance of FC2 is also greater than EAF2 compound, due to its higher specific surface area which is proven by the Mastersizer analysis.

Rose et al. (2020) used ZnS microspheres and Ni-doped ZnS microspheres as supercapacitor electrode material. The specific capacitance of the ZnS supercapacitor at a scanning rate of 5 mVs^{-1} was determined as 216.2 Fg^{-1}[2].

Sarma et al. (2015) produced a ZnS electrode deposited on TiO_2 nanotube. The specific capacitance of the supercapacitor at a scanning rate of 20 mVs^{-1} was determined as 226 Fg^{-1} [5].

Javed et al. (2015) produced a ZnS electrode growing on carbon textile. The specific capacitance of the supercapacitor at a scanning rate of 5 mVs^{-1} was determined as 540 Fg^{-1} [80].

When compared to similar studies in the literature, it was determined that the produced supercapacitors provide greater specific capacitance values.

The capacity retention ratios of the prepared supercapacitors were determined as a result of long cycle CV tests applied at a scanning rate of 200 mVs-1 in the potential range of -0.6 and 1.2 V. Capacity retention ratios of the FC2, FC3 and FC4 supercapacitor samples are presented in Figure 5.27.

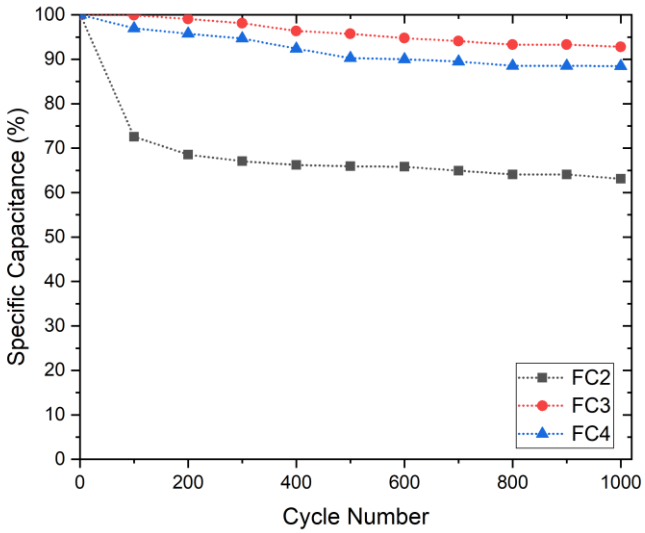


Figure 5.27 Capacity retention ratios of a) FC2, b) FC3, and c) FC4.

It was determined that the FC2 sample was able to maintain 72.52% of its capacity at the end of 100 cycles, and this ratio decreased to 63.10% at the end of 1000 cycles. For FC3 and FC4 samples, these ratios were determined as 92.82% and 88.45% respectively, at the end of 1000 cycles.

Capacity retention ratio of the EAF2 sample is presented in Figure 5.28.

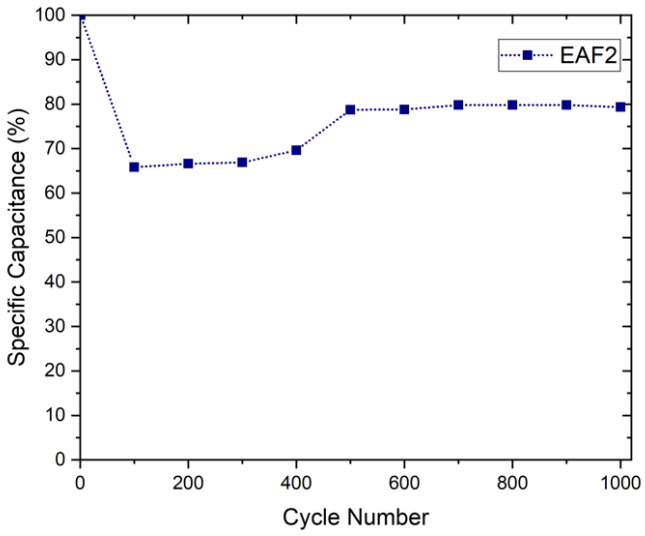


Figure 5.28 Capacity retention ratio of EAF2.

It was determined that the EAF2 sample was able to maintain 79.33% of its capacity at the end of 1000 cycles.

Since mass transfer is diffusion-controlled, as the number of cycles increased, some of the mesoporous sites on the electrodes closed due to redox reactions resulting in surface morphology changes. [79]. As a result of these reactions occurring at random areas on the electrode surface, the fluctuations depicted in Figures 5.27 and 5.28 were observed.

Hussain et al. (2021) used ZnS nanoflakes as supercapacitor electrode material. They achieved a 96% capacity after 2000 cycles at 5 Ag^{-1} current density [81].

Yi et al. (2019) used ZnS nanoparticles as supercapacitor electrode material. They achieved a 93.1% capacity after 10000 cycles at 10 Ag^{-1} current density [82].

Wei et al. (2018) used ZnS/C_3N_4 composite as supercapacitor electrode material. They achieved an 80.4% capacity in 1000 cycles at 5 Ag^{-1} current density [3].

5.4.3. Galvanostatic Charge-Discharge

GCD tests were conducted to FC2, FC3 and FC4 and EAF2 samples at 0.1, 0.5 and 1 Ag^{-1} current densities. Obtained GCD curves are presented in Figure 5.29.

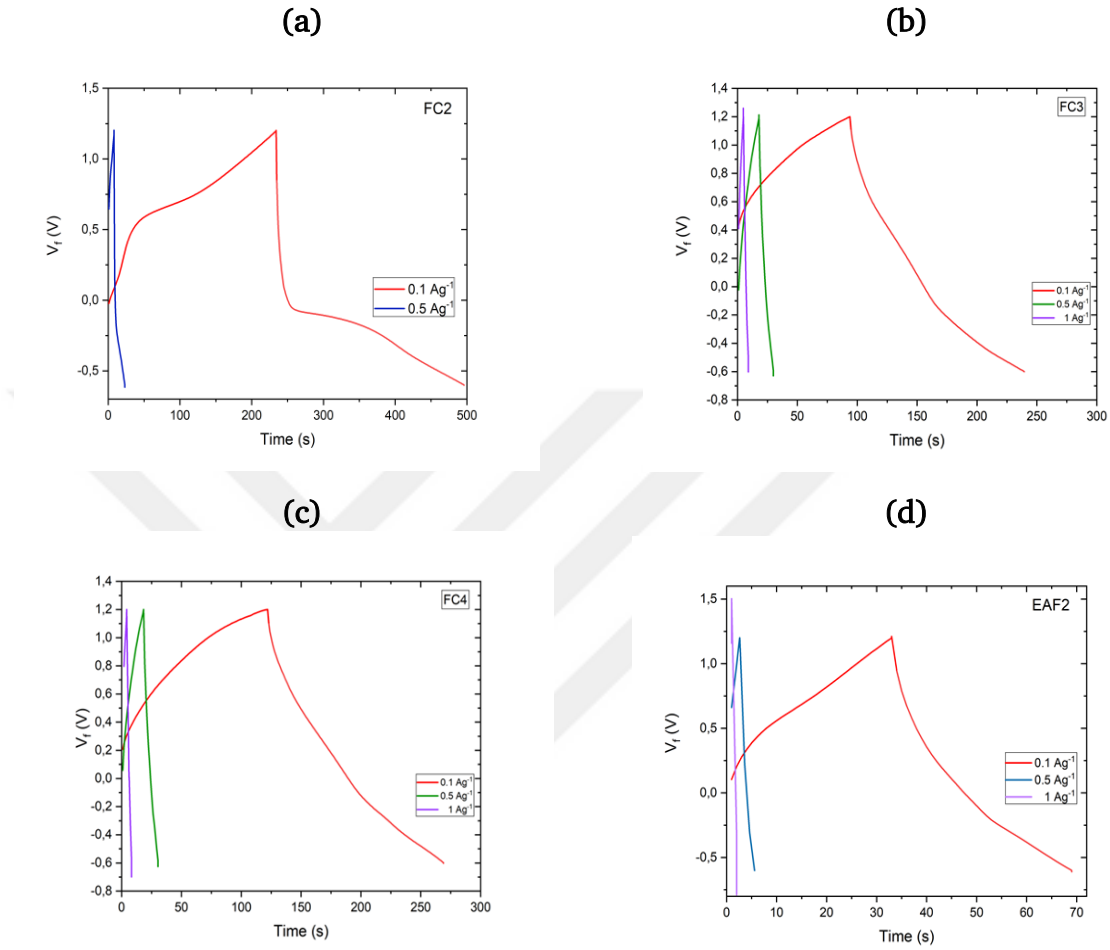


Figure 5.29 GCD curves of a) FC2, b) FC3, and c) FC4 and d) EAF2 at different current densities.

It was determined that charge-discharge period of the FC2 sample is greater than other samples, which indicates a higher specific capacitance value.

5.4.4. Electrochemical Impedance Spectroscopy

To further investigate the capacitive behavior of the FC2, FC3 and FC4 samples, EIS analyses were also carried out over a frequency range from 10 kHz to 10 mHz before and after the long cycle CV tests. Analyses were conducted by the application of 10 mV amplitude AC in 0.01 Hz-100 kHz frequency range. Nyquist plots of FC2, FC3 and FC4 samples are presented in Figure 5.30.

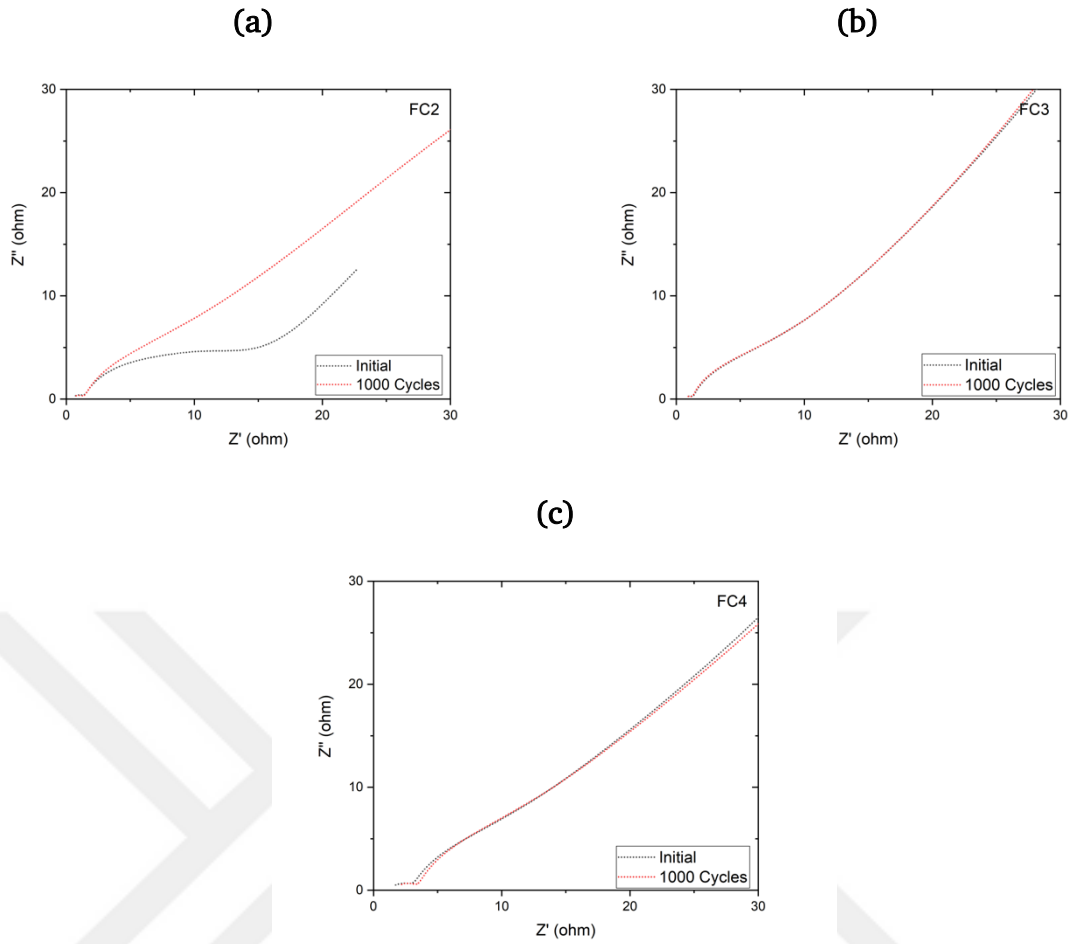


Figure 5.30 Nyquist plots of a) FC2, b) FC3, c) FC4.

In the high frequency region, the intersection of the axes represents the internal resistance (R_s) of the electrode, which consists of the ionic resistance of the electrolyte, the intrinsic resistance of the active substance, and the contact resistance at the interface of the active material and current collector [83]. The semicircular section whose diameter is equal to the charge transfer resistance (R_{ct}) that governs the electron transfer kinetics of the redox reactions. In the low frequency range, the straight line indicates the Warburg impedance (W), which is the diffusive resistance of the electrolyte in the porous structure. [84].

Obtained results were fitted to an equivalent circuit which is presented in Figure 5.31.

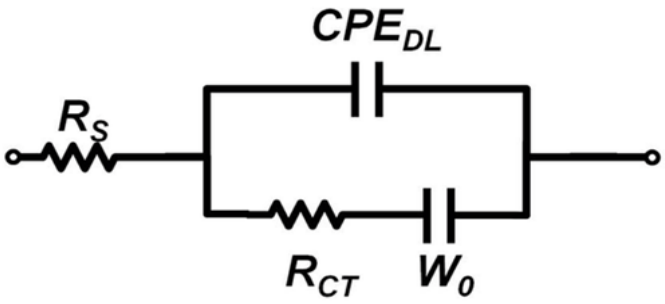


Figure 5.31 Equivalent circuit [85].

From fitting results, R_s, R_{ct}, C_{dl} and W values were determined for each sample and the obtained results are presented in Table 5.5.

Table 5.5 EIS fitting results.

Sample	R_s (Ω)	R_{ct} (Ω)	$C_{dl}*10^{-3}$ (F)	W
FC2 (initial)	0.724	1.289	0.073	0.399
FC2 (after 1000 cycles)	0.778	1.346	0.321	0.235
FC3 (initial)	0.936	1.540	0.449	0.023
FC3 (after 1000 cycles)	0.968	1.593	0.494	0.024
FC4 (initial)	1.725	2.822	0.023	0.021
FC4 (after 1000 cycles)	2.190	3.136	0.411	0.021

Increasing R_{ct} with the increasing cycle number indicates that, the redox reactions were hindered, which results as the decreasing specific capacitance for each sample.

It was also determined that the W, which is correlated with the diffusion of mobile ions to the surface of the electrode, is decreased about 40% at the end of 1000 cycles, for the FC2 sample. This result indicates, the porous sites, where the mobile ions may diffuse, were closed with the increasing cycle number. For the FC3 and

FC4 samples, W value did not exhibit a significant decrease, which yields as a high cyclic stability for these samples.

With the increasing R_{ct}, a decrease in the capacitive behavior might be expected in the FC4 sample. However, the increasing activated carbon amount in the relevant sample facilitated the diffusion and the sample performed a high cyclic stability.

6
CONCLUSIONS

This study aimed to recycle the FFD and EAFD wastes generated in the metallurgy industry to obtain ZnS with high purity and to use the obtained ZnS as an electrode material in coin cell type asymmetric hybrid supercapacitors. For the recovery of ZnS from these wastes, a hydrometallurgical process was conducted.

FFD were treated with sulfuric acid and nitric acid solutions with various liquid-solid ratios (10:1, 20:1, 50:1, 100:1), acid concentrations (0.05, 0.1, 0.25, 0.5 and 1 M) and leaching times (5, 15, 30, 60 and 90 minutes). Leaching efficiency of Zn, Fe and Cr for each solution was determined with AAS analyses. By the evaluation of the leaching results, nitric acid was selected as the optimum leaching medium to achieve a selective Zn recovery.

Four optimum leaching parameters to recover Zn selectively from FFD were determined as followed; 0.05 M HNO_3 solution with 100:1 L-S ratio for 60 minutes, 0.25 M HNO_3 solution with 50:1 L-S ratio for 5 minutes, 1 M HNO_3 solution with 20:1 L-S ratio for 60 minutes and 1 M HNO_3 solution with 10:1 L-S ratio for 60 minutes. Leaching efficiency of Zn for the optimum solutions were determined as 76.87, 70.71, 77.36 and 64.15 % respectively.

EAFD were treated with nitric acid solutions at 0.1, 0.25, 0.5 and 1 M acid concentrations for 15 minutes. Optimum EAFD solution to conduct precipitation process was selected as 0.1 M. In this concentration, leaching efficiency of Zn was determined as 43.27%.

Leach solutions were mixed with Na_2S solutions with various concentrations (1:1, 1:2 and 1:3 Zn-Na_2S molar ratio) to precipitate the dissolved Zn ions as ZnS. It was determined that, when the Zn concentration of the solution reaches a critical amount, it is possible to precipitate the Zn ions as ZnS completely. Also, increasing Na_2S concentration was observed to shorten the nucleation time and increase the precipitation efficiency.

Formation of the ZnS particles was confirmed by the XRD, XPS and SEM-EDS analyses.

Asymmetric type hybrid coin cell supercapacitors were produced by using a mixture of the produced ZnS and carbon black at the anode, graphite at the cathode, and 2 M KOH solution as the electrolyte. For FC2 and EAF2 samples, a specific capacitance of 1723.57 Fg^{-1} and 1293.94 Fg^{-1} was achieved at a scanning rate of 10 mV/s, respectively. Also, it has been determined that the FC3 and EAF2 samples retain 92.82% and 79.33% of their capacity after 1000 cycles, respectively.

When compared to previous studies in the literature, electrochemical characterization results proved that, the ZnS recovered from FFD and EAFD exhibit similar electrochemical characteristics to ZnS produced from commercial sources.

In the future works, it is aimed to further investigate the leaching characteristics of the EAFD. Furthermore, to obtain ZnS from FFD and EAFD with various crystal structures and morphologies by the modification of the precipitation parameters. Also, it is aimed to produce a supercapacitor electrode material from FFD and EAFD, which consists of multiple metal sulfides to achieve better electrochemical properties.

REFERENCES

[1] R. Barik and P. P. Ingole, “Challenges and prospects of metal sulfide materials for supercapacitors,” *Current Opinion in Electrochemistry*, vol. 21. Elsevier B.V., pp. 327–334, Jun. 01, 2020. doi: 10.1016/j.coelec.2020.03.022.

[2] A. Rose, B. Shunmugapriya, T. Maiyalagan, and T. Vijayakumar, “Investigation on the electrochemical properties of hydrothermally synthesized pure and Nickel doped Zinc Sulfide microspheres for supercapacitor electrode applications,” *Journal of Materials Science: Materials in Electronics*, vol. 31, no. 21, pp. 19204–19212, Nov. 2020, doi: 10.1007/s10854-020-04456-7.

[3] B. Wei, H. Liang, R. Wang, D. Zhang, Z. Qi, and Z. Wang, “One-step synthesis of graphitic-C3N4/ZnS composites for enhanced supercapacitor performance,” *Journal of Energy Chemistry*, vol. 27, no. 2, pp. 472–477, Mar. 2018, doi: 10.1016/J.JECHEM.2017.11.015.

[4] X. Hou *et al.*, “Ultrathin ZnS nanosheet/carbon nanotube hybrid electrode for high-performance flexible all-solid-state supercapacitor,” *Nano Res*, vol. 10, no. 8, pp. 2570–2583, Aug. 2017, doi: 10.1007/s12274-017-1459-9.

[5] B. Sarma, R. S. Ray, and M. Misra, “Charge storage in flower-like ZnS electrochemically deposited on TiO2 nanotube,” *Mater Lett*, vol. 139, pp. 77–80, Jan. 2015, doi: 10.1016/j.matlet.2014.09.115.

[6] J. G. Strobos and J. F. C. Friend, “Zinc recovery from baghouse dust generated at ferrochrome foundries,” *Hydrometallurgy*, vol. 74, no. 1–2, pp. 165–171, Aug. 2004, doi: 10.1016/j.hydromet.2004.03.002.

[7] F. Kukurugya, T. Vindt, and T. Havlík, “Behavior of zinc, iron and calcium from electric arc furnace (EAF) dust in hydrometallurgical processing in sulfuric acid solutions: Thermodynamic and kinetic aspects,” *Hydrometallurgy*, vol. 154, 2015, doi: 10.1016/j.hydromet.2015.03.008.

[8] M. Cruells, A. Roca, and C. Núñez, “Electric arc furnace flue dusts: characterization and leaching with sulphuric acid,” *Hydrometallurgy*, vol. 31, no. 3, pp. 213–231, Nov. 1992, doi: 10.1016/0304-386X(92)90119-K.

[9] T. Havlík, B. V. e. Souza, A. M. Bernardes, I. A. H. Schneider, and A. Miškufová, “Hydrometallurgical processing of carbon steel EAF dust,” *J Hazard Mater*, vol. 135, no. 1–3, pp. 311–318, Jul. 2006, doi: 10.1016/j.jhazmat.2005.11.067.

[10] T. Miki, R. Chairaksa-Fujimoto, K. Maruyama, and T. Nagasaka, “Hydrometallurgical extraction of zinc from CaO treated EAF dust in ammonium chloride solution,” *J Hazard Mater*, vol. 302, 2016, doi: 10.1016/j.jhazmat.2015.09.020.

[11] P. Oustadakis, P. E. Tsakiridis, A. Katsiapi, and S. Agatzini-Leonardou, “Hydrometallurgical process for zinc recovery from electric arc furnace dust (EAFD). Part I: Characterization and leaching by diluted sulphuric acid,” *J Hazard Mater*, vol. 179, no. 1–3, pp. 1–7, Jul. 2010, doi: 10.1016/j.jhazmat.2010.01.059.

[12] R. A. Shawabkeh, “Hydrometallurgical extraction of zinc from Jordanian electric arc furnace dust,” *Hydrometallurgy*, vol. 104, no. 1, pp. 61–65, Jul. 2010, doi: 10.1016/j.hydromet.2010.04.014.
[13] S. R. M. Yatim, N. A. Zainuddin, N. S. Mokhtar, H. N. Syahjidan, and S. N. H. Kamsuri, “Competitiveness in removing copper, zinc and chromium trivalent in plating industrial effluent by using hydroxide precipitation versus sulphide precipitation,” *IOP Conf Ser Mater Sci Eng*, vol. 1053, no. 1, p. 012084, Feb. 2021, doi: 10.1088/1757-899x/1053/1/012084.
[14] Q. Chen, Y. Yao, X. Li, J. Lu, J. Zhou, and Z. Huang, “Comparison of heavy metal removals from aqueous solutions by chemical precipitation and characteristics of precipitates,” *Journal of Water Process Engineering*, vol. 26, pp. 289–300, Dec. 2018, doi: 10.1016/j.jwpe.2018.11.003.
[15] A. González, E. Goikolea, J. A. Barrena, and R. Mysyk, “Review on supercapacitors: Technologies and materials,” *Renewable and Sustainable Energy Reviews*, vol. 58. Elsevier Ltd, pp. 1189–1206, May 01, 2016. doi: 10.1016/j.rser.2015.12.249.
[16] M. A. A. Mohd Abdah, N. H. N. Azman, S. Kulandaivalu, and Y. Sulaiman, “Review of the use of transition-metal-oxide and conducting polymer-based fibres for high-performance supercapacitors,” *Materials and Design*, vol. 186. Elsevier Ltd, Jan. 15, 2020. doi: 10.1016/j.matdes.2019.108199.
[17] B. K. Kim, S. Sy, A. Yu, and J. Zhang, “Electrochemical Supercapacitors for Energy Storage and Conversion,” in *Handbook of Clean Energy Systems*, John Wiley & Sons, Ltd, 2015, pp. 1–25. doi: 10.1002/9781118991978.hces112.
[18] J. Libich, J. Máca, J. Vondrák, O. Čech, and M. Sedlaříková, “Supercapacitors: Properties and applications,” *J Energy Storage*, vol. 17, pp. 224–227, Jun. 2018, doi: 10.1016/j.est.2018.03.012.
[19] O. K. Oyeniran and H. Pretoria, “Synthesis and characterization of carbon-based nanostructured material electrodes for designing novel hybrid supercapacitors,” 2018.
[20] A. Pramitha and Y. Raviprakash, “Recent developments and viable approaches for high-performance supercapacitors using transition metal-based electrode materials,” *Journal of Energy Storage*, vol. 49. Elsevier Ltd, May 01, 2022. doi: 10.1016/j.est.2022.104120.
[21] P. Huang Justus-, “On-chip micro-supercapacitors based on nano-structured carbon materials.” [Online]. Available: https://www.researchgate.net/publication/281695897
[22] H. Ahuja, P. S. Dhapola, Rahul, N. G. Sahoo, V. Singh, and P. K. Singh, “Ionic liquid (1-hexyl-3-methylimidazolium iodide)-incorporated biopolymer electrolyte for efficient supercapacitor,” *High Perform Polym*, vol. 32, no. 2, pp. 220–225, Mar. 2020, doi: 10.1177/0954008319897763.
[23] E. Hossain, H. M. R. Faruque, M. S. H. Sunny, N. Mohammad, and N. Nawar, “A comprehensive review on energy storage systems: Types, comparison, current scenario, applications, barriers, and potential solutions, policies, and future prospects,” *Energies*, vol. 13, no. 14. MDPI AG, Jul. 01, 2020. doi: 10.3390/en13143651.

[24] P. Forouzandeh, V. Kumaravel, and S. C. Pillai, “Electrode materials for supercapacitors: A review of recent advances,” *Catalysts*, vol. 10, no. 9. MDPI, pp. 1–73, Sep. 01, 2020. doi: 10.3390/catal10090969.
[25] P. E. Lokhande, U. S. Chavan, and A. Pandey, “Materials and Fabrication Methods for Electrochemical Supercapacitors: Overview,” *Electrochemical Energy Reviews*, vol. 3, no. 1. Springer Science and Business Media B.V., pp. 155–186, Mar. 01, 2020. doi: 10.1007/s41918-019-00057-z.
[26] B. Pal, S. Yang, S. Ramesh, V. Thangadurai, and R. Jose, “Electrolyte selection for supercapacitive devices: A critical review,” *Nanoscale Adv*, vol. 1, no. 10, pp. 3807–3835, 2019, doi: 10.1039/c9na00374f.
[27] C. Zhong, Y. Deng, W. Hu, J. Qiao, L. Zhang, and J. Zhang, “A review of electrolyte materials and compositions for electrochemical supercapacitors,” *Chemical Society Reviews*, vol. 44, no. 21. Royal Society of Chemistry, pp. 7484–7539, Nov. 07, 2015. doi: 10.1039/c5cs00303b.
[28] D. Zhang *et al.*, “Selective leaching of zinc from blast furnace dust with mono-ligand and mixed-ligand complex leaching systems,” *Hydrometallurgy*, vol. 169, pp. 219–228, May 2017, doi: 10.1016/j.hydromet.2017.02.003.
[29] J. Xu, N. Wang, M. Chen, Z. Zhou, and H. Yu, “Comparative investigation on the reduction behavior of blast furnace dust particles during in-flight process in hydrogen-rich and carbon monoxide atmospheres,” *Powder Technol*, vol. 366, pp. 709–721, Apr. 2020, doi: 10.1016/j.powtec.2020.03.025.
[30] Y. Xue, X. Hao, X. Liu, and N. Zhang, “Recovery of Zinc and Iron from Steel Mill Dust—An Overview of Available Technologies,” *Materials*, vol. 15, no. 12. MDPI, Jun. 01, 2022. doi: 10.3390/ma15124127.
[31] A. Andersson, H. Ahmed, J. Rosenkranz, C. Samuelsson, and B. Björkman, “Characterization and upgrading of a low zinc-containing and fine blast furnace sludge - A multi-objective analysis,” *ISIJ International*, vol. 57, no. 2, pp. 262–271, 2017, doi: 10.2355/isijinternational.ISIJINT-2016-512.
[32] C. Lanzerstorfer, B. Bamberger-Strassmayr, and K. Pilz, “Recycling of blast furnace dust in the iron ore sintering process: Investigation of coke breeze substitution and the influence on offgas emissions,” *ISIJ International*, vol. 55, no. 4, pp. 758–764, 2015, doi: 10.2355/isijinternational.55.758.
[33] K. Binnemans, P. T. Jones, Á. Manjón Fernández, and V. Masaguer Torres, “Hydrometallurgical Processes for the Recovery of Metals from Steel Industry By-Products: A Critical Review,” *Journal of Sustainable Metallurgy*, vol. 6, no. 4. Springer Science and Business Media Deutschland GmbH, pp. 505–540, Dec. 01, 2020. doi: 10.1007/s40831-020-00306-2.
[34] World Steel Association, “Steel industry by-products,” 2010.
[35] N. Ma, “Recycling of basic oxygen furnace steelmaking dust by in-process separation of zinc from the dust,” *J Clean Prod*, vol. 112, pp. 4497–4504, 2016, doi: 10.1016/j.jclepro.2015.07.009.
[36] M. Geerdes, H. Toxopeus, and C. van der Vliet, *Modern Blast Furnace Ironmaking: An Introduction*. 2009.
[37] P. J. Koros, “DOE Direct Steelmaking Program and its follow-on Waste Oxide Recycling Program. He was chairman of the AISI Task Force on Degalvanizing Steel.”

[38] Ruetten, “Application of the Waelz Technology on Resource Recycling of Steel Mill Dust,” 2006.
[39] A. Fleischanderl, U. Gennari, and A. Ilie, “Revenue from waste: ZEWA - Metallurgical process for treatment of residues from steel industry and other industrial sectors to generate valuable products,” *Ironmaking and Steelmaking*, vol. 31, no. 6, pp. 444–449, 2004, doi: 10.1179/irs.2004.31.6.444.
[40] Bartels-vonVarnbüler, Peters, and Schueller, “OxiCup process for recycling steel mill waste oxides,” 2002.
[41] “Efficient treatment of steelmaking by-products.”
[42] S. Kelebek, S. Yörük, and B. Davis, “Characterization of basic oxygen furnace dust and zinc removal by acid leaching,” in *Minerals Engineering*, Feb. 2004, vol. 17, no. 2, pp. 285–291. doi: 10.1016/j.mineng.2003.10.030.
[43] Z. H. Trung *et al.*, “Acidic leaching both of zinc and iron from basic oxygen furnace sludge,” *J Hazard Mater*, vol. 192, no. 3, pp. 1100–1107, Sep. 2011, doi: 10.1016/j.jhazmat.2011.06.016.
[44] A. G. Guézennec, J. C. Huber, F. Patisson, P. Sessiecq, J. P. Birat, and D. Ablitzer, “Dust formation in Electric Arc Furnace: Birth of the particles,” in *Powder Technology*, Sep. 2005, vol. 157, no. 1–3, pp. 2–11. doi: 10.1016/j.powtec.2005.05.006.
[45] E. C. Barretta, E. H. Nenniger-, J. Dziewinski, A. Barrett, and E. H. And Dziewinski, “A hydro metallurgical process to treat carbon steel electric arc furnace dust,” 1992.
[46] T. KiranKumar and G. G. Roy, “A Review on Processing of Electric Arc Furnace Dust (EAFD) by Pyro-Metallurgical Processes,” *Transactions of the Indian Institute of Metals*, vol. 75, no. 5. Springer, pp. 1101–1112, May 01, 2022. doi: 10.1007/s12666-021-02465-6.
[47] C. F. Pereira, Y. L. Galiano, M. A. Rodríguez-Piñero, and J. V. Parapar, “Long and short-term performance of a stabilized/solidified electric arc furnace dust,” *J Hazard Mater*, vol. 148, no. 3, pp. 701–707, Sep. 2007, doi: 10.1016/j.jhazmat.2007.03.034.
[48] G. Orhan, “Leaching and cementation of heavy metals from electric arc furnace dust in alkaline medium,” *Hydrometallurgy*, vol. 78, no. 3–4, pp. 236–245, Aug. 2005, doi: 10.1016/j.hydromet.2005.03.002.
[49] G. Salihoglu and V. Pinarli, “Steel foundry electric arc furnace dust management: Stabilization by using lime and Portland cement,” *J Hazard Mater*, vol. 153, no. 3, pp. 1110–1116, May 2008, doi: 10.1016/j.jhazmat.2007.09.066.
[50] J. G. M. S. Machado, F. A. Brehm, C. A. M. Moraes, C. A. dos Santos, A. C. F. Vilela, and J. B. M. da Cunha, “Chemical, physical, structural and morphological characterization of the electric arc furnace dust,” *J Hazard Mater*, vol. 136, no. 3, pp. 953–960, Aug. 2006, doi: 10.1016/j.jhazmat.2006.01.044.
[51] J. Basson and J. Daavittila, “High Carbon Ferrochrome Technology,” in *Handbook of Ferroalloys*, Elsevier, 2013, pp. 317–363. doi: 10.1016/B978-0-08-097753-9.00009-5.
[52] Ö. Fizibilite Raporu, “Elâzığ İli Yüksek Karbonlu Ferrokrom Üretim Tesisi.”

[53] M. Riekkola-Vanhanen, “Finnish expert report on best available techniques in ferrochromium production T h e F i n n i s h E n v i r o n m e n t.”
[54] “Ferrochrome waste management-addressing current gaps SP du Preez orcid.org/ 0000-0001-5214-3693.”
[55] J. P. Beukes, “Treatment of Cr(VI)-containing wastes in the South African ferrochrome industry-review of currently applied methods S,” 2012. [Online]. Available: https://www.researchgate.net/publication/258109609
[56] Ü. Bulut *et al.*, “Ferrokrom ark Fırın Baca Tozunun Çevresel Karakterizasyonu ve Stabilizasyonu,” 2006.
[57] P. Palimakaą, S. Pietrzyk, M. Stępień, K. Ciećko, and I. Nejman, “Zinc recovery from steelmaking dust by hydrometallurgical methods,” *Metals (Basel)*, vol. 8, no. 7, Jul. 2018, doi: 10.3390/met8070547.
[58] K. Mager, U. Meurer, and J. Wirling, “Minimizing Dioxin and Furan Emissions during Zinc Dust Recycle by the Waelz Process.”
[59] N. L. Piret, “EAF dust processing: Rotary hearth a potential substitute for the Waelz kiln?,” *World of Metallurgy - ERZMETALL*, vol. 65, pp. 306–316, 2012.
[60] Y. Kuwauchi and M. Barati, “A mathematical model for carbothermic reduction of dust-carbon composite agglomerates,” *ISIJ International*, vol. 53, no. 6, pp. 1097–1105, 2013, doi: 10.2355/isijinternational.53.1097.
[61] T. Suetens, B. Klaasen, K. van Acker, and B. Blanpain, “Comparison of electric arc furnace dust treatment technologies using exergy efficiency,” *J Clean Prod*, vol. 65, pp. 152–167, Feb. 2014, doi: 10.1016/j.jclepro.2013.09.053.
[62] “Efficient treatment of steelmaking by-products.”
[63] “TMS Partners in Progress,” *JOM*, vol. 66, no. 7, pp. 1119–1121, Jul. 2014, doi: 10.1007/s11837-014-1044-6.
[64] K. Verscheure, M. van Camp, B. Blanpain, P. Wollants, P. Hayes, and E. Jak, “Continuous fuming of zinc-bearing residues: Part I. Model development,” *Metallurgical and Materials Transactions B: Process Metallurgy and Materials Processing Science*, vol. 38, no. 1, pp. 13–20, Feb. 2007, doi: 10.1007/s11663-006-9009-y.
[65] K. Verscheure, M. van Camp, B. Blanpain, P. Wollants, P. Hayes, and E. Jak, “Continuous fuming of zinc-bearing residues: Part II. The submerged-plasma zinc-fuming process,” *Metallurgical and Materials Transactions B: Process Metallurgy and Materials Processing Science*, vol. 38, no. 1, pp. 21–33, Feb. 2007, doi: 10.1007/s11663-006-9010-5.
[66] I. F. Kurunov, “Environmental Aspects of Industrial Technologies for Recycling Sludge and Dust that Contain Iron and Zinc,” 2012.
[67] H. Itaya, H. Katayama, T. Hamada, M. Sato, T. Ushijima, and H. Momokawa, “Advanced Technologies of Iron and Steel, Commemorating the 20th Anniversary of the Technical Research Division,” 1990.
[68] S. Hughes Outotec, M. A. Reuter, S. Hughes, R. Baxter, and A. Kaye, “Ausmelt Technology For Lead and Zinc Processing,” 2008. [Online]. Available: https://www.researchgate.net/publication/270285815

[69] J. Hoang, M. A. Reuter, R. Matusewicz, S. Hughes, and N. Piret, “Top submerged lance direct zinc smelting,” *Miner Eng*, vol. 22, no. 9–10, pp. 742–751, Aug. 2009, doi: 10.1016/j.mineng.2008.12.014.
[70] Z. Peng and J. Y. Hwang, “Microwave-assisted metallurgy,” *International Materials Reviews*, vol. 60, no. 1, pp. 30–63, Jan. 2015, doi: 10.1179/1743280414Y.0000000042.
[71] M. K. Jha, V. Kumar, and R. J. Singh, “Review of hydrometallurgical recovery of zinc from industrial wastes,” *Resour Conserv Recycl*, vol. 33, no. 1, 2001, doi: 10.1016/S0921-3449(00)00095-1.
[72] H. Mordo and ˇ Gan, “Caustic Soda Leach of Electric Arc Furnace Dust.”
[73] B. Asadi Zeydabadi, D. Mowla, M. H. Shariat, and J. Fathi Kalajahi, “Zinc recovery from blast furnace flue dust,” *Hydrometallurgy*, vol. 47, no. 1, pp. 113–125, Nov. 1997, doi: 10.1016/S0304-386X(97)00039-X.
[74] E. A. Abdel-Aal, “Kinetics of sulfuric acid leaching of low-grade zinc silicate ore,” 2000. [Online]. Available: www.elsevier.nlrlocaterhydromet
[75] F. Habashi, *A Textbook of Hydrometallurgy*. 1993.
[76] A. Mersmann, “Crystallization and precipitation,” 1999. [Online]. Available: www.elsevier.com/locate/cep
[77] T. Nomura, Y. Kousaka, M. Alonso, and M. Fukunaga, “Precipitation of zinc sulfide particles from homogeneous solutions,” *J Colloid Interface Sci*, vol. 223, no. 2, pp. 179–184, Mar. 2000, doi: 10.1006/jcis.1999.6444.
[78] J. F. Xu, W. Ji, J. Y. Lin, S. H. Tang, and Y. W. Du, “Preparation of ZnS nanoparticles by ultrasonic radiation method,” 1998.
[79] O. Gorduk, M. Gencten, S. Gorduk, M. Sahin, and Y. Sahin, “Electrochemical fabrication and supercapacitor performances of metallo phthalocyanine/functionalized-multiwalled carbon nanotube/polyaniline modified hybrid electrode materials,” *J Energy Storage*, vol. 33, Jan. 2021, doi: 10.1016/j.est.2020.102049.
[80] M. S. Javed *et al.*, “Flexible full-solid state supercapacitors based on zinc sulfide spheres growing on carbon textile with superior charge storage,” *J Mater Chem A Mater*, vol. 4, no. 2, pp. 667–674, 2015, doi: 10.1039/c5ta08752j.
[81] I. Hussain *et al.*, “Uniform growth of ZnS nanoflakes for high-performance supercapacitor applications,” *J Energy Storage*, vol. 36, Apr. 2021, doi: 10.1016/j.est.2021.102408.
[82] T. F. Yi, Y. Li, Y. M. Li, S. Luo, and Y. G. Liu, “ZnS nanoparticles as the electrode materials for high-performance supercapacitors,” *Solid State Ion*, vol. 343, Dec. 2019, doi: 10.1016/j.ssi.2019.115074.
[83] F. Ran *et al.*, “Super long-life supercapacitor electrode materials based on hierarchical porous hollow carbon microcapsules,” *RSC Adv*, vol. 5, no. 106, pp. 87077–87083, 2015, doi: 10.1039/c5ra15594k.
[84] J. Yang and S. Gunasekaran, “Electrochemically reduced graphene oxide sheets for use in high performance supercapacitors,” *Carbon N Y*, vol. 51, no. 1, pp. 36–44, Jan. 2013, doi: 10.1016/j.carbon.2012.08.003.
[85] W. Wang *et al.*, “Hydrous ruthenium oxide nanoparticles anchored to graphene and carbon nanotube hybrid foam for supercapacitors,” *Sci Rep*, vol. 4, Mar. 2014, doi: 10.1038/srep04452.

APPENDICES

Table 1 FFD, H_2SO_4 leaching results

L-S Ratio	Time (mins)	Acid concentration (M)	LE of Zn (%)	Zn Concentration ($*10^{-3}$) (M)	LE of Fe (%)	Fe Concentration ($*10^{-3}$) (M)	LE of Cr (%)	Cr Concentration ($*10^{-3}$) (M)
100:1	15	0.05	71.26	7.13	0.00	0.00	30.74	0.30
100:1	15	0.1	87.78	8.78	0.00	0.00	39.16	0.38
100:1	15	0.25	88.90	8.89	2.93	0.06	50.81	0.49
100:1	15	0.5	90.72	9.07	6.09	0.12	0.431	69.74
100:1	15	1	94.87	9.49	15.56	0.32	87.06	0.85
100:1	30	0.05	76.64	7.66	0.00	0.00	32.85	0.32
100:1	30	0.1	90.83	9.08	5.47	0.11	56.80	0.55
100:1	30	0.25	94.53	9.45	7.24	0.15	7.24	0.15
100:1	30	0.5	96.01	9.60	9.78	0.20	84.30	0.82
100:1	30	1	96.70	9.67	21.19	0.43	85.92	0.83
100:1	60	0.05	80.75	8.08	9.86	0.20	39.16	0.38
100:1	60	0.1	92.91	9.29	24.81	0.51	61.33	0.60
100:1	60	0.25	97.66	9.77	37.13	0.76	71.68	0.70
100:1	60	0.5	97.44	9.74	40.68	0.83	88.35	0.86
100:1	60	1	97.01	9.70	49.69	1.01	89.48	0.87
100:1	90	0.05	83.68	8.37	15.64	0.32	44.01	0.43
100:1	90	0.1	94.61	9.46	32.13	0.66	76.70	0.75
100:1	90	0.25	98.16	9.82	44.92	0.92	78.96	0.77
100:1	90	0.5	97.36	9.74	54.08	1.10	93.37	0.91
100:1	90	1	99.23	9.92	63.33	1.29	97.41	0.95
50:1	15	0.05	64.34	12.55	0.00	0.00	20.55	0.39
50:1	15	0.1	72.22	14.08	0.00	0.00	30.42	0.58
50:1	15	0.25	83.55	16.29	0.00	0.00	32.52	0.62

Table 1 FFD, H_2SO_4 leaching results (continued)

50:1	15	0.5	83.68	16.32	0.85	0.03	50.49	0.96
50:1	15	1	87.00	16.96	5.55	0.22	66.83	1.27
50:1	30	0.05	66.49	12.97	0.00	0.00	29.29	0.55
50:1	30	0.1	74.26	14.48	0.00	0.00	35.76	0.68
50:1	30	0.25	81.95	15.98	3.08	0.12	45.47	0.86
50:1	30	0.5	80.63	15.72	4.85	0.19	68.12	1.29
50:1	30	1	83.29	16.24	12.17	0.48	84.30	1.60
50:1	60	0.05	70.99	13.84	0.00	0.00	32.52	0.62
50:1	60	0.1	80.94	15.78	9.86	0.39	48.87	0.93
50:1	60	0.25	84.01	16.38	19.95	0.79	50.65	0.96
50:1	60	0.5	85.24	16.62	24.88	0.99	77.35	1.47
50:1	60	1	91.27	17.80	28.35	1.13	93.37	1.77
50:1	90	0.05	72.37	14.11	0.00	0.00	35.92	0.68
50:1	90	0.1	83.90	16.36	15.49	0.62	54.85	1.04
50:1	90	0.25	85.25	16.62	23.27	0.93	59.71	1.13
50:1	90	0.5	85.55	16.68	37.29	1.48	89.81	1.70
50:1	90	1	94.53	18.43	45.53	1.81	97.41	1.85
20:1	60	0.1	44.34	26.60	0.00	0.00	0.00	0.00
20:1	60	0.25	61.32	36.79	0.00	0.00	12.94	0.75
20:1	60	0.5	67.61	40.57	15.41	1.89	16.18	0.94
20:1	60	1	71.70	43.02	36.98	4.53	50.16	2.92
10:1	60	0.1	32.23	31.33	0.00	0.00	0.00	0.00
10:1	60	0.25	45.28	44.02	0.00	0.00	11.33	1.07
10:1	60	0.5	58.02	56.39	0.00	0.00	24.27	2.29
10:1	60	1	68.30	66.39	6.16	0.00	42.07	3.97

Table 2 FFD, HNO_3 leaching results

L-S Ratio	Time (mins)	Acid concentration (M)	LE of Zn (%)	Zn Concentration ($*10^{-3}$) (M)	LE of Fe (%)	Fe Concentration ($*10^{-3}$) (M)	LE of Cr (%)	Cr Concentration ($*10^{-3}$) (M)
100:1	15	0.05	53.00	5.30	0.00	0.00	11.49	0.11
100:1	15	0.1	79.78	7.98	0.00	0.00	40.94	0.40
100:1	15	0.25	99.45	9.95	1.08	0.02	51.29	0.50
100:1	15	0.5	99.07	9.91	2.39	0.05	60.36	0.59
100:1	15	1	99.01	9.90	16.33	0.33	66.34	0.64
100:1	30	0.05	65.08	6.51	0.00	0.00	20.06	0.19
100:1	30	0.1	88.81	8.88	0.00	0.00	45.79	0.44
100:1	30	0.25	97.86	9.79	2.62	0.05	52.75	0.51
100:1	30	0.5	98.63	9.86	8.55	0.17	69.74	0.68
100:1	30	1	98.18	9.82	19.65	0.40	69.74	0.68
100:1	60	0.05	76.87	7.69	0.00	0.00	36.73	0.36
100:1	60	0.1	89.94	8.99	0.00	0.00	50.81	0.49
100:1	60	0.25	97.55	9.76	23.81	0.49	66.83	0.65
100:1	60	0.5	97.86	9.79	36.36	0.74	87.70	0.85
100:1	60	1	98.65	9.87	44.38	0.91	82.04	0.80
100:1	90	0.05	76.31	7.63	0.00	0.00	50.65	0.49
100:1	90	0.1	90.39	9.039	0.00	0.00	63.43	0.62
100:1	90	0.25	99.26	9.93	40.22	0.82	91.10	0.89
100:1	90	0.5	98.03	9.80	55.16	1.13	92.56	0.90
100:1	90	1	98.38	9.84	59.01	1.20	94.01	0.91
50:1	15	0.05	44.43	8.67	0.00	0.00	4.85	0.09
50:1	15	0.1	52.00	10.14	0.00	0.00	12.30	0.23
50:1	15	0.25	73.27	14.29	0.00	0.00	38.03	0.72

Table 2 FFD, HNO_3 leaching results (continued)

50:1	15	0.5	82.89	16.16	0.00	0.00	48.38	0.92
50:1	15	1	85.19	16.61	3.78	0.15	57.28	1.09
50:1	30	0.05	49.07	9.57	0.00	0.00	7.61	0.14
50:1	30	0.1	56.31	10.98	0.00	0.00	19.58	0.37
50:1	30	0.25	74.29	14.49	0.00	0.00	54.85	1.04
50:1	30	0.5	80.74	15.74	0.00	0.00	61.65	1.17
50:1	30	1	88.14	17.19	4.93	0.20	67.15	1.27
50:1	60	0.05	53.47	10.43	0.00	0.00	17.15	0.33
50:1	60	0.1	57.00	11.11	0.00	0.00	25.57	0.48
50:1	60	0.25	78.84	15.37	0.00	0.00	65.53	1.24
50:1	60	0.5	83.27	16.24	7.09	0.28	70.71	1.34
50:1	60	1	90.13	17.58	9.32	0.37	74.76	1.42
50:1	90	0.05	55.90	10,90	0.00	0.00	21.84	0.41
50:1	90	0,1	58.84	11.47	0.00	0.00	31.07	0.59
50:1	90	0.25	78.77	15.36	0.00	0.00	81.07	1.54
50:1	90	0.5	90.42	17.63	10.55	0.42	86.73	1.64
50:1	90	1	88.47	17.25	16.33	0.65	91.26	1.73
20:1	60	0.1	12.58	7.55	0.00	0.00	0.00	0.00
20:1	60	0.25	34.12	20.47	0.00	0.00	0.00	0.00
20:1	60	0.5	45.60	27.36	0.00	0.00	0.00	0.00
20:1	60	1	77.36	46.42	6.93	0.85	35.60	2.08
10:1	60	0.1	5.50	5.35	0.00	0.00	0.00	0.00
10:1	60	0.25	29.40	28.58	0.00	0.00	0.00	0.00
10:1	60	0.5	38.52	37.44	0.00	0.00	0.00	0.00
10:1	60	1	64.15	62.36	0.00	0.00	14.56	1.38

Table 3 EAFD, HNO_3 leaching results

L-S Ratio	Time (mins)	Acid concentration (M)	LE of Zn (%)	Zn Concentration ($*10^{-3}$) (M)	LE of Fe (%)	Fe Concentration ($*10^{-3}$) (M)
50:1	15	0.1	43.27	56.56	2.59	1.20
50:1	15	0.25	49.98	65.32	6.09	2.83
50:1	15	0.5	53.47	69.88	9.54	4.43
50:1	15	1	54.35	71.04	14.35	6.66

PUBLICATIONS FROM THE THESIS

Conference Papers

1. Aydin O., Gencten M., Birol B., "Production of Metal Sulfides From Ferrochrome Flue Dusts and Investigation of Their Electrochemical Properties, IMMC2022 21st International Metallurgy and Materials Congress, 6-8 October 2022, p.119.

Projects

1. Birol B., Gençten M., Aydin O., “Ferrokrom Baca Tozlarından ZnS'ün Geri Kazanılması ve Süperkapasitör Elektrot Malzemesi Olarak Kullanımının Araştırılması, YTÜ BAP, Genel Araştırma Projesi, Proje No: FBA-2022-5008.